# Use of OCT and Oculus Pentacam HR® as

# Aids to Semi-Scleral Contact Lens Fitting

by

Heinz Otchere

A thesis

presented to the University of Waterloo

in fulfillment of the

thesis requirement for the degree of

Master of Science

in

Vision Science

Waterloo, Ontario, Canada, 2013

## AUTHOR'S DECLARATION

I hereby declare that I am the sole author of this thesis. This is a true copy of the thesis, including any required final revisions, as accepted by my examiners.

I understand that my thesis may be made electronically available to the public.

## Abstract

**Purpose**

To determine whether semi-scleral contact lenses (sSCL) can be appropriately fitted using corneal sagittal depth (CSD) measurements with OCT and to determine the impact of fit on fitting characteristics, visual acuity (VA) and comfort ratings. The specific aims of each chapter are as follows:

Chapter 2: To determine the repeatability and accuracy of the Oculus Pentacam HR$^{®}$ (Wetzlar, Germany) based on six polycarbonate aspheric surfaces of known radius of curvature and shape factors.

Chapter 3: The first purpose was to assess the repeatability of the Visante™ OCT and Oculus Pentacam HR$^{®}$ in measuring the topographic corneal thickness (TCT) in keratoconus (KC) and pellucid marginal degeneration (PMD). The second purpose was to compare the reproducibility of the two instruments for TCT measurements.

Chapter 4: The first purpose was to assess the repeatability of the Medmont E300™ and Oculus Pentacam HR$^{®}$ in measuring the topographic radius of curvature in KC and PMD. The second was to compare the reproducibility of the two instruments for topographic radius of curvature measurements.

Chapter 5: The main purpose of this study was to measure CSD using Visante™ OCT and its effect on the sSCL selection. The second purpose was to assess the effect of the fitting characteristics of sSCL on the cornea, and how VA is impacted by the choice of fit. The third purpose was to measure the topographic corneal clearance (TCC) using the ultra-long OCT (UL-OCT). The fourth purpose was to assess the effect of time on the TCC over 1 hour of sSCL. The last purpose was to assess the comfort ratings of the sSCL.

**Methods**

Chapter 2: Six polycarbonate aspheric surfaces (Bausch and Lomb, Rochester, NY, USA) of specific colour coding (red, white, blue, brown, green and yellow) and of known radius of curvature and shape factor were randomly selected and measured using the Oculus Pentacam HR®. Three repeated measurements of all the six surfaces were taken at approximately two minute intervals. These measurements were repeated at least 48hrs apart on three separate days.

Chapter 3: Twenty healthy participants who had been diagnosed with KC (n=18) and PMD (n=2) were recruited. This study involved two study visits where corneal thickness measurements were repeated after at least 48 hours. Measurements from one eye only were taken (right eye=12; left eye=8). On the first study visit, two repeated corneal thickness measurements were obtained, first with the Visante™ OCT and second with the Oculus Pentacam HR®. This measurement was repeated at least 48hrs later and the same order of measurements was maintained for all the participants. Topographic corneal thickness (TCT)

(microns) were recorded in the 90, 180 and oblique (45 and 135) meridians at 1mm intervals across 8mm of the central cornea.

Chapter 4: Twenty healthy participants who had been diagnosed with KC (n=18) and PMD (n=2) were recruited. This study involved two study visits where radius of curvature measurements was repeated after at least 48 hours. Measurements from one eye only were taken. Two repeated radius of curvature measurements were obtained, first with the Medmont E300™ and second with the Oculus Pentacam HR®. This measurement was repeated at least 48 hours and the same order of measurements were obtained for all the participants. Topographic radius of curvature (diopter) was recorded in the 90, 180 and oblique (45 and 135) meridians at 1mm intervals across 8mm of the central cornea.

Chapter 5: Three sSCL (Jupiter 15mm; Essilor) were fit to 20 subjects who had previous diagnoses of KC (n=18) or PMD (n=2). The fitting of the sSCL were based on the CSD measured with the Visante™ OCT at a 15mm chord on the horizontal meridian. To select the sSCL from the diagnostic trial lens set, values of 325 (lens 1), 375 (lens 2) and 425 (lens 3) µm were randomly added in sequence to the CSD. Subjects were allowed to wear each of the sSCL for 1hour. After this time, the central corneal clearance (CCC) was assessed using an UL-OCT, high contrast visual acuity (HCVA) and low contrast visual acuity (LCVA) were measured using a LogMAR VA chart and comfort ratings were obtained using a comfort rating scale (0-100).

**Results**

Chapter 2: To assess repeatability, the measurements were compared to the results obtained for the three separate days. There were no significant differences between the radius of curvature measurements obtained on the three separate days (p>0.05). Similar findings were also obtained for the shape factor (p>0.05) except for colour brown (r=7.81mm, p=0.70) (p=0.01). There was more variability relative to the mean in the distribution for the colour green (r=7.80mm, p=0.49) with coefficients of variation (COV) of 0.70%. Similar patterns were seen in colours blue and white with COV of 0.60% and 0.61% respectively. The highest COV for the shape factor was seen in the colour green with 33.19% and the yellow (r=7.3mm, p=0.75) surface recorded the lowest COV with 10.43%. There were significant linear correlations (r=0.99, p=0.001) between the mean radius of curvature, shape factors and the true values for all the three day sessions.

Chapter 3: The mean CCT for Visante™ OCT was 484.97±43.14μm and Oculus Pentacam HR® was 478.86±45.31μm. There was no significant difference in the TCT between the two visits (p=0.54) and measurements (p=0.63) for Visante™ OCT. There was also no significant difference in the combined visits, axes and locations (p=0.86). For Oculus Pentacam HR®, no significant difference was found in the visits (p=0.18) but difference exists in the measurements (p=0.001). There was also significant difference in the combined visits, axes and locations (p=0.001). Tukey post-hoc analysis shows the differences (p<0.05) were found in the +1 and +4 locations in the 135 meridian. For reproducibility, significant differences were found in the interactions between instruments, axes, measurements and locations (p<0.05).

Chapter 4: The mean central radius of curvature (CRC) for Oculus Pentacam HR® was 50.38±5.81D and that of Medmont E300™ was 49.41±4.93D. There was a significant difference in the visits (p<0.05) but no difference in the measurements (p=0.98) for the Medmont E300™. There was also no significant difference in the combined visits, axes and locations (p=0.12). Results from the Oculus Pentacam HR® show no significant differences in the visits (p=0.32) and measurements (p=0.66). There was also no significant difference in the combined visits, axes and locations (p=0.24). For reproducibility, significant differences were found between the instruments, axes and locations (p<0.05). Other interactions between the instruments did not show any difference.

Chapter 5: The mean CSD in the horizontal meridian was 3.78±0.53 (range: 3.33-4.17) mm at a 15mm chord. The mean CCC was 190±100, 360±120 and 450±170 μm for each lens respectively (p=0.001). The mean CCC loss was 30.00±40.00, 30±60.00 and 40.00±50 μm for each lens respectively (p>0.05). The mean HCVA for lenses 1, 2 and 3 were 0.05±0.12, 0.07±0.11 and 0.11±0.08 respectively, which were significantly different (p=0.02). Tukey post hoc analysis demonstrated that this difference was only significant between lenses 1 and 3 (p=0.01). Similar findings were found for LCVA. The overall comfort rating for all three sSCL was 77.7±10.6. The comfort ratings for lenses 1, 2 and 3 were 74.9±9.2, 79.7 ±11.6 and 78.6±10.8 respectively. These differences were not significantly different (p=0.24).

**Conclusions**

Chapter 2: Oculus Pentacam HR® was a repeatable and accurate instrument for this experiment for the majority of radii of curvature and shape factors. Based on the small number of test

surfaces in terms of number and curvature variations, it was unpredictable as to whether either the range of radii of curvature or shape factors were over or under-estimated by the instrument, as no clear trends were detected.

Chapter 3: The Visante™ OCT gave repeated measurements for the two visits as there were no significant differences in respective locations in all meridians. Oculus Pentacam HR® gave repeatable measurements for the majority of the locations. The two instruments were not reproducible and should not be used interchangeably; therefore, care must be taken interpreting the TCT from the two instruments. It is advisable to take at least two measurements and average in order to minimize variations between measures. Manufacturers of Oculus Pentacam HR® may consider including a calibration test surface so that practitioners would be able to calibrate the instrument each time it is being used.

Chapter 4: Each of the instruments per se gave repeatable measurements, as there were no significant differences in the two visits, axes and locations. However, although the two instruments were found to be produce similar results for the majority of the locations; there were significant differences between measurements of the two devices particularly for the oblique meridians in the periphery.

Chapter 5: Evaluation of CSD can be used effectively to select which sSCL to fit on the eye. The results of this study suggest that lens 2 (adding 375 μm to the CSD) gave the best combination of VA and comfort ratings. However, evaluation of the fluorescein pattern must be balanced with the VA and comfort ratings for successful fitting of sSCL in a clinical setting.

There was also a likelihood of topographic corneal loss after 1 hour of sSCL wear; however, this may vary depending on many factors such as scleral zone and its relationship with the scleral conjunctiva. Eyelid force, design of the contact lens and other unknown factors may play a part in the contact lens settling time and amount.

## Acknowledgements

I would like to express my sincere gratitude and appreciation to you Prof. Lyndon W. Jones and Prof. Luigina Sorbara for your immeasurable support, encouragement and guidance through this amazing journey. It has been a big opportunity to sit under your feet to learn of your rich experience in the field of contact lenses. Working with both of you has been a wonderful and enriching experience. My sincere thanks also go to you Prof. Emer. Desmond Fonn for trusting in me and the opportunity that was provided for me to join the Centre for Contact Lens Research (CCLR). Thank you ALL at the CCLR for all the assistance you provided to make my research at the center a success.

I would like to thank my committee members Prof. Natalie Hutchings, Prof. Sruthi Srinivasan and Dr. Marc Schulze for taking all their time to read the entire thesis and for their guidance and unlimited support. I am also grateful to Dr. Jalaiah Varikooty for his assistance and support with the software usage on special instruments at CCLR and STATISTICA for data analysis.

Sincere appreciation to Diane Bandura, Grace Dong, Alexandra Smith, Leona Voss, Marina Simpson, Jane Johnson, Nancy Keir, Lynn Ryan, Nadeera Careless, Lakshman Subbaraman, Doerte Luensmann, Jill Woods, Miriam Heynen, Doris Richter, Darcy Kroeker, Marilyn Thomp, Sarah Guthrie, Kathryn Dumbleton, for helping me to conduct my studies smoothly and the help with data entry and analysis work.

I am grateful to God for the gift of life, love, strength and grace throughout my studies in Waterloo, Canada.

Last but not the least I want to acknowledge the tremendous support from my mother (deceased), father and younger brothers as well as my extended family. I always feel the unconditional love, prayers and support in my education. Thank you all for standing by me in all the turbulent times and its impact especially when I had been away for some months.

## Dedication

To my mother (Grace Boateng-*deceased*), whose sad event occurred on 19<sup>th</sup> April, 2013. You never flipped many pages yet you showed me how to turn many and I am grateful to you for all your support, prayers and encouragement. I really appreciate you Mum.

*Mum, this is for you. I love you!*

# Table of Contents

# List of Figures

# List of Tables

# List of Symbols and Abbreviations

| | |
|---|---|
| μm | Micrometre |
| mm | Millimeter |
| ALDH3 | Aldehyde dehydrogenase 3 |
| ACC | Apical corneal clearance |
| AEL | Axial edge lift |
| ATR | Against-the-rule |
| BOZR | Back optic zone radius |
| CSD | Corneal sagittal depth |
| CRC | Central radius of curvature |
| CCC | Central corneal clearance |
| CCCl | Central corneal clearance loss |
| CCT | Central corneal thickness |
| COV | Coefficient of variation |
| CCLR | Center for Contact Lens Research |
| CXL | Corneal cross linking |
| DLK | Deep lamellar keratoplasty |
| D | Diopter |
| Dk/t | Oxygen transmissibility |
| DUSKS | Dundee University Scottish Keratoconus Studies |
| HCVA | High contrast visual acuity |
| HR | High resolution |
| INTACS | Intra corneal ring segments |

| | |
|---|---|
| IOL | Intra ocular lens |
| ISO | International Organization for Standardization |
| KC | Keratoconus |
| KCFF | Keratoconus forme fruste |
| LASIK | Laser assisted in situ keratomileusis |
| LoA | Limits of agreement |
| LED | Light emitting diode |
| LogMAR | Logarithm of the minimum angle of resolution |
| LCVA | Low contrast visual acuity |
| MDA | Malondialdehyde |
| mCCC | Mean central corneal clearance |
| mCSD | Mean corneal sagittal depth |
| mCCCl | Mean central corneal clearance loss |
| NaFl | Sodium fluorescein |
| OCT | Optical coherence tomography |
| PMD | Pellucid marginal degeneration |
| PBCL | Piggy-back contact lens |
| PCT | Peripheral corneal thickness |
| R | Radius of curvature |
| RGP | Rigid gas permeable lens |
| sSCL | Semi-scleral contact lens |
| SD-OCT | Spectral domain optical coherence tomography |
| SLD | Super luminescent diodes |

| | |
|---|---|
| TMS | Topographic modelling system |
| TCC | Topographic corneal clearance |
| TCT | Topographic corneal thickness |
| TD-OCT | Time-domain optical coherence tomography |
| US | Ultrasonic pachymeter |
| UV | Ultra violet |
| VRM | Vault reduction method |
| VA | Visual acuity |
| WTR | With-the-rule |

# Chapter 1

## Introduction and Literature Review

### 1.1  Keratoconus and Pellucid Marginal Degeneration

Keratoconus (KC) as it is known today has evolved from several prior names and descriptions, including hyperkeratosis, ochlodes, conical formed cornea, cornea conica, cornée conique, sugar loaf cornea, prolapses corneae, procidentia corneae, among many others. [1] Until 1854, the meaning, description and associations of the condition were somewhat obscured. [1] John Nottingham is credited to have given a treatise on KC [1,2] and current trends have been given by Krachmer et al. [3] Keratoconus is derived from the Greek word *kerato* (cornea) and *conus* (cone) and is the most common primary corneal ectasia. It is a bilateral, [4,5] asymmetric, [6,7] usually progressive corneal thinning [8] that results in corneal protrusion, irregular astigmatism and decreased vision. [9,10] Specifically, the cornea assumes a conical shape as a result of characteristic apical corneal epithelial thinning, [11] stromal degeneration and subsequent biomechanical alteration. [12] Research has shown that the corneal thinning is usually located in the infero-temporal region and the central region (as seen in so-called "nipple cones"), [13-15] though some authors have reported thinning in the superior regions of the cornea. [16-18] The protrusion of the cornea results in a significant increase in myopia and irregular astigmatism (typically with-the-rule astigmatism, WTR), which affects visual acuity (VA). The onset of the condition typically occurs around the onset of puberty, [6,19] although other reports show that it can occur as early as six years [20] and as late as 50 years. [21] The condition is known to progress until the fourth decade of life and then usually stabilizes. A recent report has shown that 50%

of individuals affected with KC in one eye will have the other unaffected eye develop the condition in 16 years. [22] Figure 1-1 shows both normal and keratoconic eyes.

A variety of risk factors have been shown to play a significant role in the development of the condition. These include constant eye rubbing, [6] the presence of systemic conditions such as sleep apnea and associated conditions like atopic dermatitis, [23-28] floppy eyelid syndrome, [29-35] chronic allergies and eczema, [24, 36-39] and genetics. [39, 40] KC is also associated with other syndromes. For examples, KC is found in 0.5-15% in patients with Down's syndrome. [3, 41-47] It has also been reported in individuals with Leber´s congenital amaurosis, [48, 49] Ehlers-Danlos syndrome [50-52] and osteogenesis imperfecta. [53, 54]



**Fig 1-1a: Normal cornea**          **Figure 1-1b: Keratoconic cornea.**

**Figure 1- 1 a&b: Comparison of normal and KC corneae.**

A condition that is often confused with KC is pellucid marginal degeneration (PMD). PMD is an idiopathic, bilateral, non-inflammatory, peripheral corneal ectasia usually affecting the inferior quadrant in a crescent fashion. [55-58] The word pellucid meaning *"clear"* was originally described by Schlaeppi in 1957 [55, 59] to denote the clarity of the cornea, irrespective of the ectasia that is observed under the slit lamp biomicroscope. Early studies had previously termed

the condition as pellucid corneal marginal degeneration [55] or pellucid marginal dystrophy. [60] The onset of PMD is not known, although some authors have reported the onset ranging from 20-40 years of age. [59, 61] There seems to be no sex, racial or ethnic preponderance, however, Sridhar et al. [62] reported higher prevalence in a male population and superior localization of the ectasia in some people. The corneal thinning is usually observed in the inferior portion of the cornea usually in the 4 to 8 o'clock position, accompanied by 1-2mm of normal cornea between the limbus and the thin area. [59] Though mainly inferior thinning is seen, there are cases of superior thinning. [63] This unusual characteristic of the corneal thinning results in marked irregular astigmatism (usually against-the-rule astigmatism, ATR) and subsequent reduction in VA. [62] Figure 1-2 shows early and advanced PMD.



**Figure 1-2a: Early PMD**                    **Figure 1-2b: Advanced PMD.**

**Figure 1- 2 a&b: Comparison of early and advanced PMD.**

## 1.2 Aetiology

### 1.2.1 The Role of Genetics

After many years of research into the probable cause of KC and PMD, many questions regarding the exact cause of these conditions still remain unanswered because no distinct factor has been identified to cause these ectatic conditions. However, clinical research suggests that

genetic factors (especially in KC) play a role, as a genetic link has been reported among family members by numerous authors. [2, 5, 43, 64-68] Previous family studies without the benefit of corneal topography reported 6-8% of individuals with KC had close family members affected by the disease. [67, 69] However, when studies use corneal topographers to assist with the diagnosis, it has been reported to be as high as 50% among family members. [70] Wang et al. [71] in a family study investigated genetic contributions to the development of KC using familial aggregation and by testing genetic models with segregation analysis, together with assisted Topographic Modeling System (TMS-1). They found the prevalence of KC in first degree relatives to be 3.34%. Again, they found KC to be 15 to 67 times higher in families with KC than that in the general population (0.23-0.05%) and show an autosomal dominant mode of inheritance with variable expression. [43, 65, 72] Twin studies by Tuft et al., [40] support the role of genetics in the development of KC. Irrespective of the genetic link associated with KC among twins, the Dundee University Scottish Keratoconus Study (DUSKS) [73] reported variability of the role of genetics in twins. This has also been reported by Bourne et al. [74] Ioti et al. [75] found KC or KC suspect patterns in 60.2% of family members of Japanese KC patients using the Orbscan (Bausch and Lomb, Rochester, NY, USA). Other researchers have also reported the influence of genetics in the development of this condition. [6, 17]

A strong genetic link for PMD has not been reported, though some authors have described some form of association in asymptomatic family members based on corneal topography and unilateral cases. [76, 77] Controversy still exists whether KC and PMD are distinct disease or phenotypic variations of the same disorders [3, 78] and that PMD is a peripheral form of KC. This hypothesis has been supported by various studies. [62, 79, 80] Kayazawa et al. [80] found 17 patients

out of 20 with PMD showed characteristics of PMD and central KC on the same cornea. Three patients with PMD without KC showed bilateral involvement of the condition. Among the 17 cases of PMD with KC, eight patients showed bilateral involvement and the others showed unilateral involvement. Their conclusion was that PMD with or without KC may be a variant of KC or a different manifestation of the same etiologic factor. Similar findings have been reported by Varley et al., [79] Karabatsas et al. [61] and Sridhar et al. [62]

### 1.2.2 Biochemical Factors

Biochemical factors (oxidative stress) may also be responsible for the ectasia in KC. [5, 6] Kenney et al. [10] proposed the *"oxidative stress"* hypothesis as the possible cause of KC. They presented one of the most comprehensive works on KC using immunochemistry and molecular techniques to explain the cause of the condition. Their study put forward four hypotheses, which according to them may explain the biochemical abnormalities found in KC corneae. The hypotheses are: (1) there is abnormal processing of the free radicals and superoxides within the KC corneas; (2) there is a build-up of destructive aldehydes or peroxynitrites; (3) the cells that are damaged irreversibly undergo the process of apoptosis; and (4) the cells that are damaged reversibly undergo wound healing or repair. As part of their conclusion, they stated that during the wound healing process (similar to corneal epithelial healing following extensive eye rubbing) various degradative enzymes and wound healing factors are upregulated, which leads to focal areas of corneal thinning and fibrosis.

According to their working hypothesis, factors which are capable of producing the free radicals and may contribute to the cascade of abnormal changes in the cornea include ultraviolet light,

atopy, mechanical eye rubbing, and poorly fitted contact lenses. They proposed that susceptible corneae exhibit an inability to process reactive oxygen species because they lack necessary protective enzymes such as aldehyde dehydrogenase class 3 (ALDH3) and superoxide dismutase. The reactive oxygen species result in an accumulation of toxic by-products such as malondialdehyde (MDA) and peroxynitrites that can damage corneal proteins and trigger a cascade of events that disrupt the cornea's cellular structure and function. According to them, this process can result in corneal thinning, scarring, and apoptosis. Figure 1-3 shows the oxidative stress pathway.

The cytotoxic effect of nitric oxide (NO) which serves as mediator in many chemical processes in the eye can also be affected by the free radicals. Their effects are mediated by peroxynitrite (a potent oxidant) and superoxides. The peroxynitrite reacts with certain proteins to form a stable compound nitrotyrosine (NT) which has destructive effect on the tissues of the cornea.
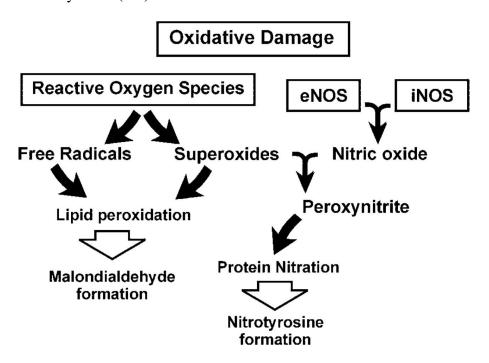


**Figure 1- 3:  The free radical hypothesis to explain KC.**

## 1.3 Epidemiology

Variations in the incidence and prevalence of KC have been reported by numerous authors. [81-83] The table below summarizes the incidence and prevalence rates of studies conducted by various authors.

**Table 1- 1: Incidence and prevalence rate of KC.**

| Author | Sample size | Incidence rate per 100,000 | Prevalence rate per 100,000 | Source |
|--------|-------------|----------------------------|-----------------------------|--------|
| Kennedy et al. [84] | 64 | 2.0 | 54.5 | Hospital |
| Pearson et al. [85] | 382 | 4.5 | 57 | Hospital |
| Nielson et l. [83] | 772 | 1.3 | 86 | Hospital |
| Tanabe et al. [86] | 2601 | - | 9 | Hospital |
| Jonas et al. [87] | 4667 | - | 2300 | Population |
| Ihalainen et al. [88] | 294 | 1.5 | 30 | Hospital |

In the case of PMD, no incidence or prevalence data exists. The general assertion is that it is rare, [3, 89] less common than KC but more common than keratoglobus or posterior KC. [3]

The effect of gender on KC remains unclear. Some authors have suggested that there is a male preponderance, [90-95] but others report higher percentages in females. [3, 5]

KC affects all ethnicities [39, 82, 96-99] but some authors have pointed out that individuals of Asian origin are more likely to be affected by the condition. [85, 100, 101]

## 1.4 Clinical Characteristics

KC and PMD present different clinical features, which largely depend on the severity of the condition. In the early stages, it may be difficult to make a definite diagnosis, without the aid of corneal topography. In KC, the subclinical type (also known as keratoconus forme fruste; KCFF), [102, 103] does not produce significant symptoms and may go unnoticed. Tobias et al. [104] defined it as an abortive form of KC, where the progression of the keratectasia has stopped at a certain point, possibly due to some form of undefined "biomechanical strength gain" of the cornea. However, with progression of corneal ectasia there is significant reduction in VA and this should raise suspicion when VA of 6/6 or better cannot be achieved, especially with increasing astigmatism. [2] Near VA seems much better than that linked with the distance acuity owing to the myopia. The characteristic *"scissor-reflex"* on retinoscopy confirms progression of the condition. The so-called "Charleux oil droplet" [105] that is observed by retro-illumination of the cornea is a warning sign of impending KC. At this stage the keratometric readings are typically found to be within the normal range and the thinnest location is also usually located outside the visual axis.

In moderate to advanced cases, the clinical signs by slit lamp biomicroscopy become obvious and make diagnosis much easier. Fleischer's ring, resulting from the deposition of iron deposits from the tear film, is usually seen at the base of the cone. [106, 107] According to Edrington et al., [108] 57% of individuals involved in their study had this characteristic feature. Another obvious sign is Vogt's striae, seen as fine vertical lines at the apex of the cone, resulting from the stretching of Descemet's membrane. These disappear when physical pressure is exerted on the cornea. [2, 3] Mocan et al. [109] reported 63.2% of their study population

exhibited Vogt's striae. With progression of the disease, the corneal nerves become more apparent, and superficial and deep corneal opacities may also be present at different stages of the condition. [3, 105] Mannion et al. [110] observed that although the total number of stromal nerve fiber bundles was reduced in patients with KC versus control subjects, the increased tortuosity and increased nerve fiber diameter may explain why the corneal nerves appear more visible in patients with KC (Figure 1-4). The characteristic V-pattern, Munson's sign, seen in the lower eyelid from downward gaze, and Rizzuti's sign are usually only observed in advanced cases. [84] Corneal hydrops due to ruptures in Descemet's membrane has also been reported. [111-117] This results in acute stromal oedema, significant pain and usually leaves a scar upon healing.
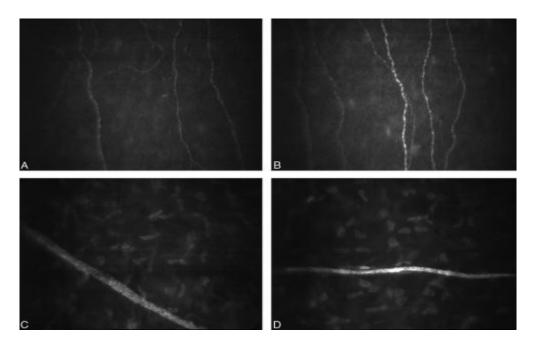


**Figure 1- 4: Comparison of corneal nerve fibres in normal and KC corneae.**

**Corneal nerve fibres in the subepithelial plexus of the cornea of a patient with KC (A) and a normal subject's cornea (B). Appearance of the stromal nerves in the KC patient (C) versus normal cornea (D).**

The clinical characteristics seen in PMD make it distinct from other corneal ectasias because of the thinning location and the absence of the inflammatory signs. The hallmark of PMD is the

characteristic 1-2mm of corneal thinning from the limbus, with a crescent fashion usually in the 4 to 8 o'clock position. [55, 58, 62, 118-121] The adjacent clear cornea protrudes markedly and usually results in ATR astigmatism seen on the topographic map and the consequent reduction in VA. Dundar et al. [122] and other authors [123, 124] report that the thinning can also occur in the superior portion of the cornea. This unique feature on the topographic map has been variously described as "lobster", "crab-claw" or "kissing dove" pattern. [58, 125] When viewed from the side, some authors classically describe the inferior-central cornea in PMD to show the side-profile contour of a *"beer-belly"*. [55, 107] Lee et al. [126] argue that the topographic "crab-claw" pattern should not be used as a diagnostic tool for PMD, as KC and other ectasias can also show such a characteristic pattern. [127] They suggested that the topographic pattern must be combined with slit lamp evaluations to make a firm diagnosis. Figure 1-5a&b show the characteristic patterns in KC and PMD. Interestingly, PMD does not appear to show Fleischer's ring, scarring or vascularisation, Munson's sign and Rizutti's sign, which are commonly seen in KC. [62]

Symptoms range from gradual to progressive reduction in VA and can be attributed to the increased ATR astigmatism. [3, 121] In rare conditions, patients also experience scleral injection with acute pain. Corneal hydrops (which is seen only in advanced KC) have also been reported in PMD. [128-132] Surprisingly, hydrops occur in the area above the ectatic zone. [62] A spontaneous bleed following corneal hydrops has also been reported. [133]
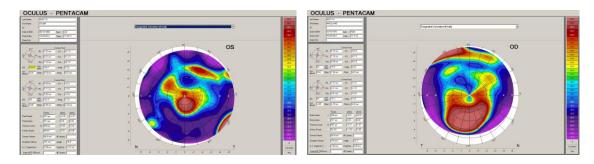
**Figure 1-5a: Asymmetric "bow-tie" in KC.**   **Figure 1-5b: Characteristic "crab-claw" in PMD.**

**Figure 1- 5 a&b: Comparison of corneal topography in KC and PMD.**

## 1.5 The Role of Corneal Topography in Differential Diagnosis

Corneal topographers have become an indispensable tool in the diagnosis of corneal ectasia and are now considered the gold standard. Lee et al. [126] proposed that topographic maps should be combined with the various clinical signs to make a definite diagnosis, as some of the corneal ectasias share certain topographic characteristics. Corneal topographers map the entire cornea and identify subtle changes over time (in addition to measuring corneal thickness) and play a significant role in diagnosing a particular corneal ectasia. [134] The TMS device (Computed Anatomy, NY, USA) [135] used Placido-based rings to topographically map the cornea. More recent topographers have advanced to slit-scanning devices and include the Orbscan II (Bausch and Lomb, Rochester, NY, USA) [136-140] and also utilise Scheimpflug technology such as that used in the Oculus Pentacam HR® (Wetzlar, Germany). [141-143] The Visante™ OCT (Carl Zeiss Meditec, Dublin, CA, USA) [144-148] uses optical coherence tomography techniques to derive corneal topography and thickness, in addition to anterior chamber analysis. These devices help in the early detection of subclinical ectasia, which is essential for pre-screening prior to various forms of corneal surgery. [149, 150]

Other peripheral conditions with clinical characteristics similar to KC (and particularly PMD) are Mooren's ulcer [151-157] and Terrien's marginal degeneration. [158-164] Mooren's ulcer is an idiopathic condition characterized by either unilateral or bilateral painful, inflammatory thinning or ectasia of the peripheral cornea. [157] Slit lamp assessment reveals perilimbal corneal infiltrates and epithelial defects within the ulcerated area. Vascularisation also occurs at the site of the ulceration during the healing process. [165] In comparison, Terrien's marginal degeneration is a non-inflammatory ectasia characterised by bilateral, slow progressive, marginal cornea thinning which usually originates from the superior part of the cornea and spread circumferentially. [55, 163] The hallmark of this condition is the characteristic thinning in the peripheral part of the cornea creating the *"gutter-like furrow"*. Corneal topography shows corneal flattening over the areas of peripheral thinning produced by the disorder. When the thinning is restricted to the superior and/or inferior areas of the peripheral cornea only, a relative steepening of the inter-palpebral peripheral cornea can be found, resulting in large magnitudes of ATR or oblique astigmatism. [166, 167]

## 1.6 The Role of Corneal Pachymetry in Differential Diagnosis

Pachymetry maps play an important role in the diagnosis of corneal ectasia. Assessment of both central and peripheral corneal thickness helps to locate the thinnest area of the cornea and subsequently help in the differential diagnosis of corneal ectasia. Reports show that there are significant differences in central and minimum corneal thickness in subclinical, moderate and advanced KC compared with the normal cornea. [9, 168-170] Table 1-2 compares the corneal thickness of normal and KC reported by various authors.

**Table 1- 2: Corneal thickness in normal and keratoconus population.**

| Author | Instrument | Normal | Subclinical | Keratoconus |
|---|---|---|---|---|
| Ahmadi et al. [168] | Pentacam | 543.51 ± 32.14 | 510.60 ± 21.78 | 499.68± 39.59 |
| Prakash et al. [171] | Orbscan IIz | 542.50 ± 39.60 | 539.90 ± 39.20 | 449.30 ± 73.70 |
| Schlegel et al. [172] | Orbscan IIz | 559.70± 36.10 | 513.52± 40.76 | - |
| Piñero et al. [173] | Pentacam | 549.90 ± 28.48 | 514.29 ± 43.59 | 457.61 ± 38.77 |
| Uçakhan et al. [174] | Pentacam | 539.52 ± 36.52 | 501.77 ± 38.38 | 488.02 ± 41.43 |

## 1.7 The Role of Sagittal Depth Evaluation in Differential Diagnosis

Numerous advancements in imaging techniques have occurred that provide information on the anterior part of the eye beyond the limbus. These imaging techniques include high resolution ultrasound (US) (Artemis-2, Arcscan Inc, Coloroda), [175, 176] high resolution OCT (Visante™ OCT, Carl Zeiss, Meditec, Dublin, California) [177] and a Scheimpflug camera system (Oculus Pentacam HR®, Wetzlar, Germany) [178-181] The Visante™ OCT and Oculus Pentacam HR® imaging techniques have made it possible to image and measure the corneal sagittal depth (CSD) at various chord diameters and this parameter continues to expand our understanding of how to effectively fit and assess semi-scleral contact lenses (sSCL).

Evaluation of CSD and its correlation with other anterior segment parameters through the use of OCT has been conducted by various researchers. [177, 182] Sorbara et al. [182] evaluated CSD in the horizontal meridian of 40 normal eyes at a 15mm chord and found the mean CSD of 3.74 ± 0.19 (ranges: 3.14-4.04) mm. In a related pilot study, [183] they found the CSD of normal eyes

and KC (n=14 in each group) to be 3.70 ± 0.16 (ranges: 3.39-3.94) mm and 3.93 ± 0.25 (ranges: 3.61-4.45) mm in the steepest meridian respectively.

## 1.8 Correction and Treatment Options for KC and PMD

### 1.8.1 Non-Surgical Options

### 1.8.1.1 Spectacle Prescription

The use of a standard spectacle prescription can be important in the management of both KC and PMD. [2, 5, 55, 119] In mild forms of both conditions, spectacles provide good visual performance. However, vision begins to deteriorate following the progression of the corneal ectasia, often due to the development of irregular astigmatism. Over time, the spectacle prescription changes owing to the progressive nature of the condition and will eventually not provide adequate VA, at which point an alternative form of vision correction (typically in the form of a contact lens) will be considered. Spectacles also help in cases of contact lens emergencies or as back-ups to provide a temporary vision correction.

### 1.8.1.2 Contact Lenses

### 1.8.1.2.1 Corneal Contact Lenses

Corneal contact lenses have been successfully used to manage corneal ectasias without surgical intervention for many years. [62, 184-191] Kompella et al. [184] and Tzelikis et al. [119] reported that almost 90% of their patients successfully used contact lenses for their visual correction. RGP lens designs include spherical, [192, 193] aspheric [194, 195] and bitoric designs. [196, 197] Fitting philosophies vary depending on the cone location and the design of the contact lens. [198-204] In KC, the fitting philosophies include those based on apical clearance, apical touch and three-

point touch. [5] The three-point touch method (Figure 1-6b), which allows the contact lens to touch slightly at the cone apex, has achieved wide-spread acceptance. [190, 205, 206] This technique provides good VA and comfort. [205, 207]

The use of an RGP lens for increasing visual performance in PMD has also been documented. [119, 184, 208, 209] However, fitting an eye with PMD with a standard diameter spherical RGP design usually leads to edge *"stand-off"* in the inferior portion of the cornea due to the marked astigmatism. This typically leads to lens awareness and discomfort [119, 121] which may be prevented by fitting a larger lens diameter. [119, 121, 209] These large diameter lenses often provide satisfactory VA, stability and lens tolerance. [5, 119]

Other designs such as reverse geometry for both KC and PMD [210, 211] have also been reported to achieve satisfactory visual performance. [212-214]
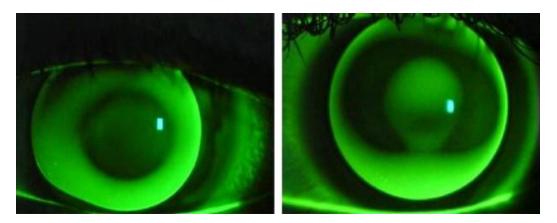


**Figure 1-6a: Central touch.**          **Figure 1-6b: Three point touch.**

**Figure 1- 6 a&b: Fluorescein patterns of two different RGP lens fittings in KC.**

### 1.8.1.2.2 Soft, Hybrid and Piggy-Back Contact Lenses

Soft contact lenses may provide adequate vision during the early stage of the condition. [5, 55] Mahadevan et al. [215] and Sridhar et al. [62] suggested that soft toric lenses can be used before the progression to irregular astigmatism. Katsoulos et al. [216] reported that customized soft contact lenses with correction of vertical coma improved both monocular and binocular visual performance for eyes affected with mild or moderate KC. Marsack et al. [217] found that wavefront-guided soft lenses provided equal to or better photopic high contrast and mesopic low contrast VA compared to RGP lenses.

Other specialised soft lenses such as Kerasoft® IC (Bausch and Lomb, Inc., USA), which employs a unique design (*"sector management control"*-for lens stabilization)*, have been reported as suitable alternatives for vision correction in both KC and PMD. [201, 218]

Hybrid contact lenses use an RGP lens at the centre and a peripheral soft contact lens "skirt" and can be used in the correction of mild forms of KC. [207, 219-225] The use of hybrid contact lenses as alternative to increase visual performance and comfort has been reported. [219, 226]

So called "Piggy-back" contact lens systems combine a soft contact lens on the cornea with a rigid lens on top, providing a combination of both comfort and good VA. These can be specifically ordered, in which a customized groove is made within the soft lens to place the RGP, but typically standard disposable soft lenses are used as the base lens. Sengor et al. [227] reported a significant increase in VA in all of his patients using such a combination, when compared with spectacles.

### 1.8.1.3 Semi-Scleral Contact Lenses

Over the past few years there has been resurgence in interest in the use of sSCL for the management of KC and PMD. [55, 94, 188, 207, 228-240] These lenses are also indicated for use in the management of post-corneal transplant [235] (when residual high refractive error and irregular astigmatism exist), severe dry eye, [235, 241] neurotrophic keratitis and multiple other conditions. [239, 241-245] Current research on sSCL indicates that more than 50% [188] of patients diagnosed with KC, PMD and keratoglobus are fitted with sSCL and constitute the majority of patients wearing such lenses. Corneal transplants constitute 15.8% while the remaining percentage of patients ranges from persistent corneal erosions, chronic graft-versus-host disease and other pathological conditions of the eye.
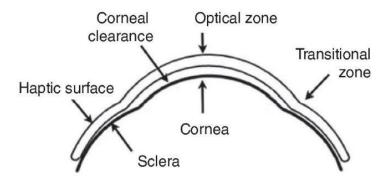


**Figure 1- 7: Schematic diagram showing the fitting relationship of the sSCL.**

The hallmark of these lenses is that they vault the cornea to rest on the sclera. [233] Thus, it is important to choose a lens such that the sSCL haptic (Figure 1-7) approximately contours over the sclera and that the sagittal depth of the lens is sufficient to completely vault the cornea. [240] This unique fitting characteristic of the sSCL require better understanding of CSD and the precise selection of an initial lens to completely vault the cornea while maximizing the effect on VA and comfort. [240]

One fitting philosophy for fitting sSCL is based on the *"Vault Reduction Method"* (VRM). [4, 55] This method requires that the sSCL be fitted one dioptre steeper than the steepest radius of curvature. This method of selecting the initial contact lens may result in an initial lens either too steep or too flat, in which case multiple further lenses are placed on the eye until an alignment pattern (without any areas of touch) is achieved. Estimation of the tear film width (or corneal clearance) may be very difficult since the initial lens selected may not necessarily correlate with the desired corneal clearance for an "ideal" fit. To overcome these issues, some authors have suggested that a better option for KC and PMD fitting may be to use the relationship between the corneal radii of curvature, back optic zone diameter for the overall cones in KC and PMD and the CSD for a lens of a given diameter. [246-248]

To verify this fitting philosophy, Schornack et al. [246] evaluated the relationship between the steepest corneal radius of curvature and the final sSCL base curve dispensed to patients. They retrospectively evaluated 33 eyes with dry eye syndrome and 21 eyes with KC. Initial sSCL selection was based on the reference sphere (from the topographic elevation map) and on gross assessment of the corneal contour from the lateral perspective. There was a good correlation between the steepest corneal curvature and the final sSCL base curve dispensed; however, they concluded that the steepest corneal radius of curvature cannot be used to accurately predict the final base curve of the sSCL that provided the most appropriate fit. The procedure often lead to random selection of lenses until one lens provides the appropriate fit, which obviously increases chair time. [177, 233, 240]

The estimation of the central corneal clearance (CCC) as observed using sodium fluorescein in the fitting of sSCL is currently problematic in fitting these lenses. The controversy surrounding the appropriate CCC stems from the fact that various authors have given different estimates of the "optimal fit", which makes it difficult to precisely fit and evaluate these lenses. [249] According to the 1997 ISO 11980 for Ophthalmic optics–Contact lenses and contact lens care products-guidance for clinical investigations, [250] it is recommended that for an "optimal fit", the CCC should range from 200µm *(0.2mm)* to 300µm *(0.3mm)* and a limbal clearance of approximately 100µm *(0.1mm)*.

Visser et al. [241] characterised an "ideal" fit with CCC of 250 µm and between 50-100 µm *(0.05 to 0.1mm)* of limbal clearance. Other authors have suggested between100-400 µm *(0.10 to 0.40mm)* [241, 242, 249] of CCC. Contact lens manufacturers (Essilor Contact Lens Division, Dallas, TX) also suggests that to achieve an "ideal fit", more attention should be focussed on "scleral alignment", with the edge of the lens neither impinging nor excessively clearing the scleral conjunctiva. Schornack et al. [246] reported on the management of KC with sSCL and considered an "ideal" fit with CCC between 150-400 µm *(0.15 to 0.40mm)*. They estimated the depth of the post-lens tear film by comparing it optically at the slit lamp to the thickness of the entire cornea. In this case, they suggested ¼ or ½ of the tear film thickness to the corneal thickness for an acceptable fit. Schornack et al. [246] hypothesized that the precise amount of clearance between the posterior surface of a sSCL and the anterior surface of the cornea is not critical to the success of the fit. They suggested that the ability to quickly and accurately align the scleral zone of the contact lens to the scleral contour would be of much greater value in fitting sSCL.

The use of sSCL results in a significant improvement in VA for patients with an irregular corneal surface. [188, 225, 241] Segal et al. [234] reported sSCL could improve VA in KC patients. They found a gain of two or more on Snellen lines in 94.5% of KC eyes fitted with these lenses. Similar results have been report by various authors. [225, 235, 237, 238, 241]

To date, no work has been conducted to effectively provide appropriate guidelines for the precise selection of an initial lens and to provide acceptable fitting characteristics for the final chosen lens. Current fitting procedures are still based on the steepest corneal curvature. [177, 233, 240, 246] This presents significant challenges to the practitioner, as there is little guidance available to aid in the selection of the initial fitting lens to provide an overall improvement in VA.

## 1.9 Surgical Options

Surgical intervention is one of the management options that are employed when the corneal ectasia has grown to the point where contact lens fitting cannot provide the optimum vision required. This procedure largely depends in part on the stage of the corneal ectasia, scar formation and contact lens intolerance level. [5, 55, 79, 239, 251-253]

## 1.9.1 Penetrating Keratoplasty

Penetrating keratoplasty (PKP) is one of the most frequently performed surgeries for KC and PMD and has a success rate of 80-90%. [239, 254, 255] This procedure typically removes a central 8mm full thickness "button" of the cornea from the host and an 8.25mm button from the donor. The new cornea is typically attached using a double running suturing technique, with the

addition of four to eight interrupted sutures and typically provides excellent results. [256-268] Irrespective of the significant improvement in vision, complications can include immune-mediated rejection of the graft (requiring long term use of immunosuppressive drugs), unpredictable degrees of astigmatism and a structurally weak eye susceptible to wound dehiscence following trauma. [256] PMD patients are usually poor candidates for surgery due to the peripheral thinning. As a result, a large eccentric corneal graft would be needed, which is positioned close to the limbus. This leads to increasing chances of graft rejections, corneal vascularization and other complications. [2, 62, 239]

## 1.9.2 Other Surgical Techniques

Other corneal surgical techniques for the treatment of moderate to advanced KC and PMD include deep lamellar keratoplasty (DLK), [107, 269-273] excimer laser-assisted anterior lamellar keratoplasty, [274-276] LASIK, [277-279] epikeratoplasty, [280-282] intra corneal ring segments, (INTACS®) [55, 107, 283-295] and corneal cross linking (CXL). [5, 55, 296-303]

## 1.10 Relationship between Contact Lens Fitting, Flexure and Vision

Flexure refers to the bending of a rigid contact lens which is fitted steeper than 'K' to conform to the corneal curvature. [304] Fitting the contact lens relative to the contour of the cornea is likely to induce ATR astigmatism which may cause unwanted visual distortions. [305]

According to Rosenthal et al., [305] increased flexibility of the contact lenses reduces their capacity to resist the compression forces from the eyelids during the closing phase in each blink. Apart from the thickness of the contact lens, other factors that may be responsible for

flexure include the amount of corneal astigmatism and fitting the lens steeper than K. The effect of RGP lens flexure and its impact on vision have been documented by various authors. [306, 307]

Sorbara et al. [306] found that the steepest RGP lenses produced significant lens flexure and astigmatism thus reduced VA on both HCVA and LCVA. The reduced VA was attributed to the uncorrected residual astigmatism and combination of other factors.

To date, no work has been done to effectively establish the relationship between sSCL fitting, flexure and vision.

## 1.11 Contact Lens Comfort with RGP and sSCL

Comfort plays a very important role in the successful wearing of contact lenses. [237, 241, 308-322] RGP lenses have achieved success owing to the better vision provided by the contact lens compared to soft contact lenses and comfortable wearing them after the period of adaption. [323-326] Fonn et al. [327] reported that in the initial adaptation period, subject acceptance of RGP lenses extended wear in terms of vision and comfort was superior compared to soft lenses. They suggested such lenses should offer high oxygen permeability to provide successful extended wear. Polse et al. [328] reported 69.6% of their subjects achieved comfort with RGP after 12 months of extended wear. Other studies [329-331] and clinical trials have shown RGP contact lenses to be comfortable and successful.

The effect of comfort level on sSCL has been reported. [232, 237] Visser et al. [237] reported that their subjects achieved comfort rate of 78.9 with sSCL and overall satisfaction of 87.7%. Other studies have also reported on the increased comfort with sSCL. [228, 232, 308, 332]

**1.12 Physiological Response to Contact Lens Wear**

Contact lens wear allows the material to interact mechanically with the pre-corneal tear film, the cornea and other tissues of the anterior segment of the eye. This interaction is likely to interfere or modify the normal physiological processes of corneal tissue and likely to induce contact lens related complications. [333-335] Clinical trials with RGP lenses have shown that corneal staining is possible after extended wear of contact lenses especially in the 3-to-9 o'clock direction. [327, 336] Graham et al. [337] reported the likelihood of developing keratopathy in overnight wearing of RGP lenses. Other complications such as redness, contact lens induced papillary conjunctivitis, corneal oedema and protein deposits have been reported. [338, 339]

Scleral contact lenses have been reported to impact on the physiological activities of the corneal thickness [340]. Smith et al. [341] reported that sSCL induced a variable amount of corneal swelling. They reported corneal swelling from 4.9% to 17.5%. Overnight corneal swelling also correlated strongly with endothelial cell density. Irrespective of these findings, they suggested that the degree of corneal swelling should not rule out overnight therapeutic use of sSCL in disease process but warn of complications for overnight wear refractive correction. The effect of corneal swelling and other physiological response such as limbal compression of sSCL have been reported by other authors. [340, 342, 343]

## 1.13 Instrumentation- Corneal Topographers

## 1.13.1 Medmont E300™

The Medmont E300™ (Medmont Pty Ltd, Australia) is a reflection based computerized videokeratoscope using Placido rings to map the surface of the cornea. The small cone Placido disc-based videokeratoscope utilizes an arc-step reconstruction algorithm. The instrument precisely determines the distance from the corneal apex to the instrument's camera and automatically captures images only when good focus and alignment are attained for easy measurement and evaluation. [344, 345] It uses integrated Medmont studio 4, software version 5.1.3 to analyze the scanned images. The Medmont E-300™ emits radiation in the visual range of wavelength 660nm for the red LED cone illumination, 565nm (green LED fixation target) and 430nm (blue LED profile illumination). It has 32 Placido rings and measures 9600 data points per scan. Each image captured is awarded a score out of 100 based on perfect centering, focus and minimal movement. The instrument also uses the measured data to construct a 3D model of the cornea. Scan scores higher than 75 are usually considered good according to the "Quality Specification" by the manufacturer. Figure 1-8a&b shows the Medmont E300™ and the corresponding interface.
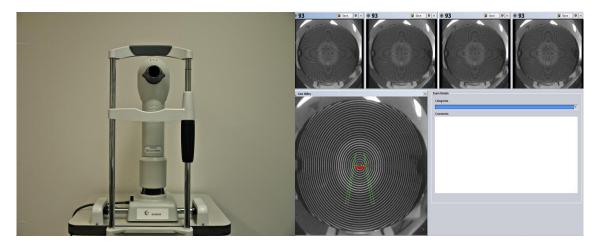
Figure 1-8a: Medmont E300™.      Figure 1-8b: Medmont E300™ interface.

Figure 1- 8 a&b: The Medmont E300™ and the interface showing the 4 real-time images.


### 1.13.2 Oculus Pentacam HR®

The Oculus Pentacam HR® (Wetzlar, Germany) uses a Scheimpflug camera that rotates through 360 degrees and captures 25-50 Scheimpflug slit images within approximately two seconds. [180, 346] The instrument uses the custom designed cobalt blue LED with a wavelength of 475nm, UV free, to capture images on the cornea. The images contain 25,000 data points and up to 138,000 data points are measured for various parameters of the cornea. The integrated software helps to construct a 3D model of the cornea. (Figure 1-9a&b)  The unique feature of Oculus Pentacam HR® is that it measures height or elevation data compared to an aspheric surface and uses the results to calculate the anterior and posterior corneal curvatures.  By subtracting the front and back elevation measurements of the cornea, it determines the corneal pachymetry. Other parameters that can be determined are corneal wavefront aberrations, [347, 348] densitometry and anterior chamber analysis [349-355] and intraocular (IOL) calculation. [356-359]
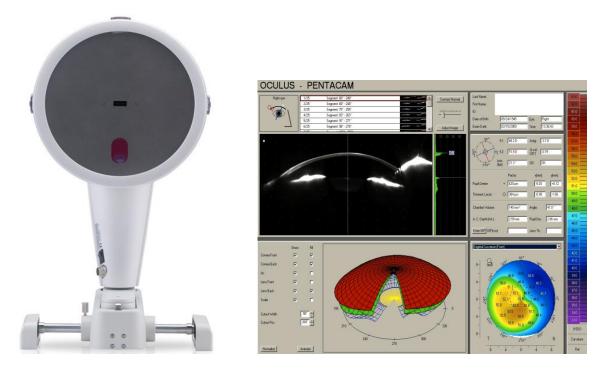
Figure 1-9a: Oculus Pentacam HR® unit.    Figure 1-9b: Scheimpflug image and 3D model.

Figure 1- 9 a&b: Oculus Pentacam HR® and the after image interface showing the Scheimpflug image and the 3D model.

## 1.13.3 Optical Coherence Tomography (OCT)

### 1.13.3.1 Visante OCT

The Visante™ OCT (Carl Zeiss Meditec, Dublin, CA, USA) was the first commercially available OCT system with sufficient speed to map the anterior segment of the eye (Figure 1.10). It is a time domain OCT (TD-OCT) that produces cross-sectional tomograms of the eye without contact. [182] The light source is a 1,310nm superluminescent diode (SLD) with axial resolution of 18μm and the transverse resolution of 60μm. The scan dimensions are 6mm by 16mm wide for the anterior segment scans and 3mm by 10mm for the pachymetry scans. [182, 360, 361]

The image acquisition system provides a real-time video image of the examined zone/area and stores the last seven images at a rate of eight frames per second and usually takes

approximately 0.5 seconds to scan the eye. The integrated software interprets the images and reconstructs the pachymetry map. The use of the Visante™ OCT to measure the thickness of the cornea has been previously been described by numerous researchers. [146, 182, 362, 363] The enhanced global pachymetry protocol was used for the corneal thickness measurements in this research. The Visante™ OCT generates a pachymetry map with concentric circles with diameters of 2, 5, 7, and 10 mm and each meridonial scan consists of 128 A-scans and can be visualized as a cross-sectional image. It also provides average, maximum, and minimum pachymetry at the respective areas. To achieve good centration, all scans were aligned on its visual axis and then adjusted to be on the geometrical axis according to the manufacturer's guidelines. The images obtained were further processed using custom-built software (Visante™ OCT, Data Compiler, CCLR, Waterloo) into four meridians (vertical, horizontal and obliques).



**Figure 1- 10: The Visante™ OCT.**

## 1.13.3.2 Custom-built Ultra-Long OCT

The custom-built ultra-long OCT (UL-OCT) is a spectral domain (SD) OCT with scan depth ~7.441mm and ~6μm optical resolution. It uses high speed of 24000 A-lines per second to scan any part of the anterior segment of the eye with a scan width of up to 18mm. The central wavelenght is 840nm and bandwidth of 50nm. Images can be captured in both 2D and 3D mode. It uses a computer controlled fixation blue target and auto-focussing colour camera viewing system with low illumination. It uses the real time image *x-y* alignment for scanning position and can scan in both the vertical and horizontal plane depending on the area of interest of the anterior segment of the eye. The manual adjustment focal plane allows the instrument to be set for specific regions of the anterior segment to be captured. Figure 1-11 show the custom-built SD UL-OCT.
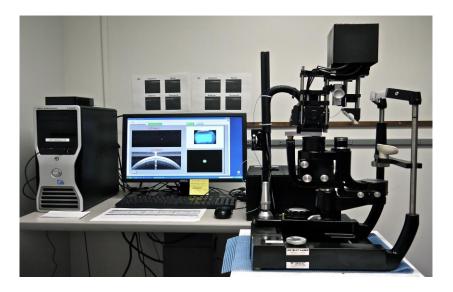


**Figure 1- 11: The custom-built SD UL-OCT.**

The SD UL-OCT has proven to be a versatile instrument for imaging various parameters of the anterior segment of the eye ranging from the evaluation of the pre-corneal tear film, [364-373] assessment and evaluation of the differential cells on the scleral conjunctiva, [374, 375] and the

assessment of the corneal epithelium and validating the thickness of the normal cornea and post refractive corneae [376-386] and anterior chamber biometry. [387-392] Other researchers have shown that the post-lens tear film thickness can easily be measured with the instrument. [373, 393]

Shen et al. [394] reported that SD UL-OCT was capable of imaging the entire soft contact lens both *in vivo* and *in vitro* with a lubricant drop to increase its contrast. In a related study, Wang et al. [395] evaluated the capability of using the instrument to visualize soft and RGP lenses on the eye using refresh liquigel. The post-lens tear film underneath the lens edge was clearly visualized and could easily be quantified.

Over the past years since its development and clinical research testing, measurements of the anterior segment parameters have been shown to be repeatable. [365-370, 396-398]

Chapter 2

**Repeatability and Accuracy of the Oculus Pentacam HR® Corneal Topographer in**

**Measuring Radius of Curvature and Shape Factor**

**2.1 Introduction**

Measurements of the central and peripheral corneal curvatures and asphericity are useful parameters for making clinical diagnoses in conditions such as KC and other degenerative conditions of the cornea, monitoring the shape of the cornea contour following LASIK or refractive procedures. It is also useful for the fitting and evaluation of contact lenses and the effectiveness of orthokeratology procedures. [1-3] To effectively assess and monitor the curvature measurements, the instrument used must be repeatable and accurate.

Measuring such parameters of the cornea has typically been with the use of reflection based technology such as the slit-scanning instrument used in the Orbscan II (Bausch and Lomb, Rochester, NY, USA). [2, 4, 5] However, the effects of the pre-corneal tear film volume and eyelid force affect the repeatability and accuracy of this technology. [6-9] This technology has recently been reported to underestimate corneal parameters such as corneal thickness measurement, and topographic maps of the posterior surface of the cornea show signs of corneal ectasia following LASIK procedures. [10-12] The effect of the slit-scanning technology led into culminated into the Scheimpflug technology. [5]

Since Scheimpflug principle was first introduced in 1904, there has been great interest among researchers and eye care practitioners. [13] This principle has been shown to be the most precise

and versatile method to document light scattering and biometry of the anterior eye segment using slit image photography. Scheimpflug cameras have advanced significantly and modern-day instruments provide comprehensive imaging and topographic analysis of the anterior segment. [13, 14] Oculus Pentacam HR® uses this technology and it is becoming popular among both eye care researchers and practitioners. [5]

The Oculus Pentacam HR® (Oculus, Wetzlar, Germany) uses a Scheimpflug camera that rotates through 360 degrees and captures 25-50 Scheimpflug slit images within approximately two seconds. The images contain 500 data points and up to 138,000 data points are measured to construct three-dimensional cornea. The Oculus Pentacam HR® measures height or elevation data compared to an aspheric surface to calculate the anterior and posterior corneal curvatures, [1, 15-22] corneal thickness, [15, 23 14, 17, 21, 24-26] anterior chamber depth and angle, [16, 27, 28] and corneal spherical aberration. [29-31] The Oculus Pentacam HR® also measures other parameters such as the corneal volume and IOL powers. [32-34] Topographic indices such as corneal asphericity and asymmetry continue to expand our understanding on making clinical diagnoses about the cornea, by comparing it with the cornea in a normal eye. Clinical measurements of the anterior segment of the eye can easily be done with this instrument. Calculation of keratometric index and IOL power as well as the assessment of IOL lens implant after surgery has improved tremendously with the use of Scheimpflug cameras. [35-39] The effectiveness of orthokeratology treatment can also be monitored accurately with this instrument. [40-42]

Although there are abundant papers on repeatability, reproducibility, and comparability of the Oculus Pentacam HR® undertaken by numerous researchers, there is no single data on repeatability and accuracy of this instrument done on any known test surface. [1, 15, 16, 23]

Repeatability is defined as the consistency between readings obtained on the same instrument by the same observer or different observer under conditions that are as constant as possible. Repeatability improves the clinician or researcher's ability to detect changes in curvature and other parameters over time for necessary intervention. Accuracy on the other hand is defined as the closeness of agreement between a measured quantity value and true quantity of a measurand. [1, 16]

## 2.2 Objective

To determine the repeatability and accuracy of the Oculus Pentacam HR® (Wetzlar, Germany) based on six polycarbonate aspheric surfaces of known radius of curvature and shape factors.

## 2.3 Material and Method

## 2.3.1 Research Design

This experiment involved three repeated measurements on three separate days. On each day, the polycarbonate aspheric surfaces were examined to make sure there were no defects or cracks on the surfaces. A lens cloth was used to clean the surfaces to make sure the surfaces were free of lint particles which may affect the radius of curvature measurements. The polycarbonate aspheric surfaces were randomized at each day of the measurements. The radius of curvature measurements were repeated thrice on each day.

## 2.3.2 The Polycarbonate Aspheric Surfaces

The six polycarbonate aspheric surfaces (Bausch and Lomb, Rochester, NY, USA) mounted on a transparent rectangular plastic block have predefined colour coding (red, white, blue, brown, green, and yellow) with corresponding radius of curvature (*r*) and shape factor (*p*). The rectangular block has a dimension of 263x50x18 mm (Figure 2-1). The aspheric surfaces are cylindrically shaped with a total diameter of approximately 13mm, which is similar to that of the human cornea. The shape factor is the measurement of the asphericity of the cornea. It is usually derived using the expression *p=1-e²,* where "e" is the eccentricity value.



**Figure 2- 1a: Polycarbonate block.**          **Figure 2- 1b: Dark cardboard on transparent edges.**
**Figure 2- 1: Polycarbonate block with the six aspheric surfaces.**

## 2.4 Instrumentation

### 2.4.1 Measurement of the Radius of Curvature and Shape Factor

The Oculus Pentacam HR® (Wetzlar, Germany) has been previously described in detail in Chapter 1.

The polycarbonate aspheric surfaces were randomly selected and their surfaces were gently cleaned with lens cloth before the measurements. The transparent rectangular plastic block was firmly attached to the Oculus Pentacam HR® unit to align with the optics and the internal

target of the Scheimpflug camera for easy measurement and evaluation. The room lights were all switched off and to reduce the reflection from the transparent rectangular surface, a piece of dark cardboard was used to cover the edges of the block leaving only the aspheric surfaces for the measurements to be taken (figure 2-1b). The investigator focussed and adjusted the joystick until the real-time image of the aspheric surface was shown on the computer monitor, with the instrument showing the centre of the surface. The mires displayed on the screen guided the investigator to perfectly align the horizontal and vertical (crosshairs) axes at the centre of the aspheric surface. To reduce the investigator dependence, the automatic release mode was used to take all the measurements.

The rotating camera was set to capture 25 Scheimpflug slit images in 360 degrees in approximately two seconds. This procedure was repeated in approximately two minute intervals for each scan. After every measurement, the Oculus Pentacam HR® was moved backwards and realigned for the next scan to minimize interdependence of the readings. Three scans were taken on each aspheric surface. Since the test objects involved in this research were plastic aspheric surfaces, any scan that registered as *"model!", "blinking!"* and *"ok"* were considered according to the "Examination Quality Specifications" within the standard of the instrument. This was to ensure that the scans were not affected by poor alignment/ misalignment with the optics of the instrument. Any misalignment observed was readjusted before the measurement. This procedure was repeated on all the six aspheric surfaces. The measurements were repeated on three separate days, with an interval of at least 48 hours between sessions.

The radii of curvature measurements were taken from the central 3mm while the shape factor measurements were taken within 20 degrees as this range was found to give consistent readings.

The true radii of curvature and shape factors were given by the manufacturer for each of the six aspheric surfaces.

## 2.5 Data Analysis

Data analysis was conducted using Statistica 11 (Statsoft. Inc., Tulsa, OK, US). The distributions of differences for the three days measurements were analysed to produce the mean, standard deviation and the 95% limits of agreement (LoA). The mean of the differences was compared to zero to indicate bias, i.e., to discover whether measurements in days differ significantly from each other. The 95% LoA is the range of values over which 95% of the differences lie and is calculated as the mean ± 1.96 times the SD of the differences. [43, 44]

## 2.6 Results

### 2.6.1 Radius of curvature (*r/mm)*

Table 2-1 shows the mean and the SD of the radii of curvature of the polycarbonate aspheric surfaces for all the 3 day sessions. The results show that almost all the mean radius of curvature values obtained for the colours were slightly higher than the true radius of curvature values except for the blue surface. The mean radii of curvature for blue were 7.78, 7.75 and 7.73mm for day 1, 2 and 3 respectively. The mean values for days 2 and 3 were lower compared to the true radius of curvature values. The differences observed were 0.03 and

0.05mm for days 2 and 3 respectively. The overall mean of the radius of curvature for blue was also slightly lower compared to the true radius of curvature. There was no statistically significant difference (p>0.05) in the measurements among the three day sessions.

**Table 2- 1: Mean radii of curvature, SD and COV of all the coloured surfaces for the three day sessions.**

| Colour | Day 1 (r/mm) | Day 2 (r/mm) | Day 3 (r/mm) | Mean of all the days (r/mm) | COV (%) | True radius of Curvature (r/mm) |
|--------|--------------|--------------|--------------|------------------------------|---------|----------------------------------|
| Blue   | 7.78±0.02    | 7.75±0.04    | 7.73±0.07    | 7.75±0.05                    | 0.62    | 7.80                             |
| Brown  | 7.87±0.01    | 7.86±0.02    | 7.87±0.03    | 7.87±0.02                    | 0.22    | 7.81                             |
| Green  | 7.83±0.07    | 7.90±0.06    | 7.86±0.04    | 7.86±0.06                    | 0.76    | 7.80                             |
| Red    | 8.36±0.01    | 8.40±0.00    | 8.38±0.04    | 8.38±0.02                    | 0.30    | 8.30                             |
| White  | 7.84±0.02    | 7.83±0.02    | 7.77±0.07    | 7.81±0.05                    | 0.61    | 7.80                             |
| Yellow | 7.38±0.01    | 7.35±0.02    | 7.37±0.01    | 7.36±0.02                    | 0.26    | 7.30                             |

There was more variability relative to the mean in the distribution for the colour green with COV of 0.76%. Similar patterns were seen in colours blue and white with COV of 0.62% and 0.61% respectively.

Pearson correlation was performed to determine the relationship between the radii of curvature values obtained for the three day sessions and the true radii of curvature. There were significant correlations (r=≈1.00, p=0.001) between the mean radii of curvature of the measured values and the true radii of curvature for all the three day sessions. Concordance correlation coefficients for the three days sessions were also found to be 0.98, 0.97, and 0.98

respectively. Figures 2-2a-c show the correlation graphs for the mean radii of curvature and the

true radius of curvature for the three days sessions.
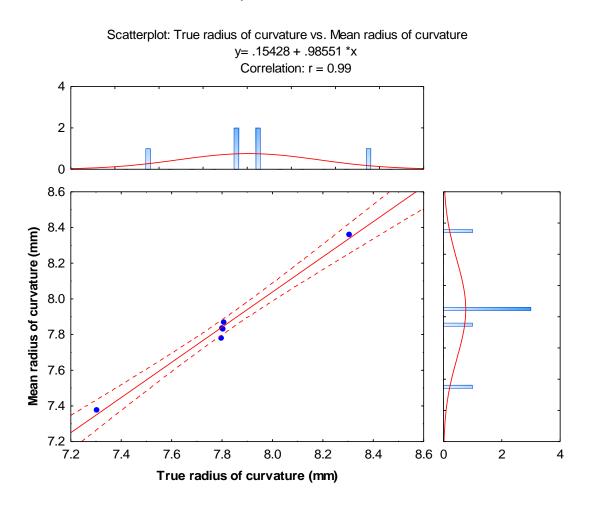


**Figure 2-2a: Correlation of mean radii of curvature and true radii of curvature for day 1.**
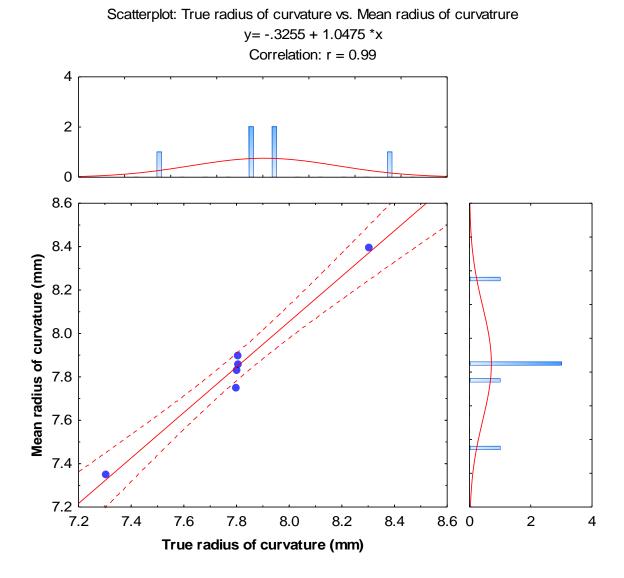
**Figure 2-2b: Correlation of mean radii of curvature and true radii of curvature for day 2.**
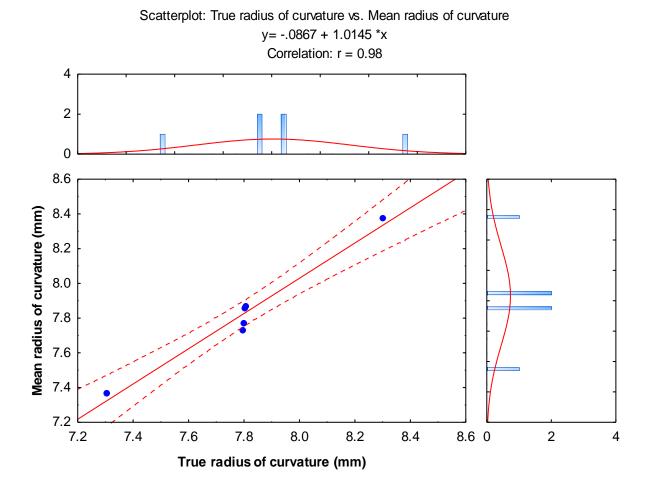
**Figure 2-2c: Correlation of mean radii of curvature and true radii of curvature for day 3.**

**Figure 2- 2 a-c: Correlation of mean radii of curvature versus true radii of curvature for days 1, 2 and 3. The equation for the best- fit for day 1, 2 and 3 were; y = .15428+.98551\*x; y = -.3255 + 1.0475\*x; and y = -.0867 + 1.0145\*x respectively.**

Bland-Altman plots were created to assess the difference in the days as a function of the mean and the true radii of curvature (Figure 2-3a-c). For all three day sessions, good agreement occurred; however, the Oculus Pentacam HR® slightly overestimated the radii of curvature measurements.
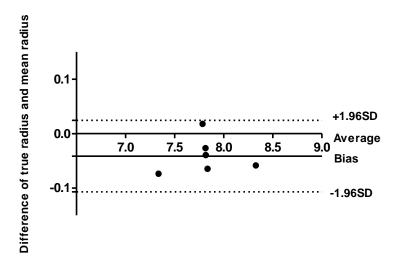
**Figure 2-3a: Bland-Altman plot for day 1.**
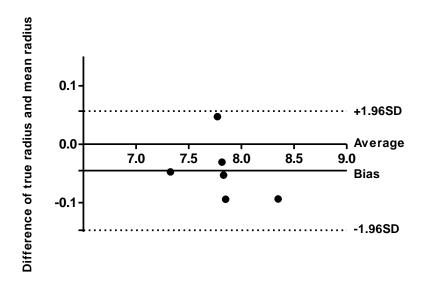


**Figure 2-3b: Bland-Altman plot for day 2**
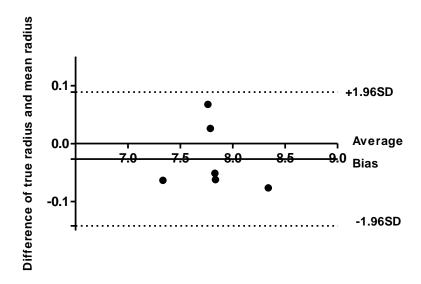
**Figure 2-3c: Bland-Altman plot for day 3**

**Figure 2- 3 a-c: Bland-Altman plot-Distribution of the means of radii of curvature and true radii of curvature for all the three day sessions.**

**The thick line represents the average and the dotted line represents the LoA.**

## 2.6.2: Shape Factor (p)

The table below shows the results obtained for the shape factor of the polycarbonate aspheric surfaces. There were no statistically significant differences among the three day sessions, with the exception of the brown surface (p=0.01). The mean shape factor obtained for red (0.52) on the third day was relatively low, however, there was no significant difference compared to the first and the second day sessions (p=0.15). Table 2-2 shows the mean of the shape factors for all the three day sessions.

**Table 2- 2: Mean shape factor, SD and COV of all the coloured surfaces for the three day sessions.**

| Colour | Day 1 | Day 2 | Day 3 | Mean of all the days | COV (%) | True shape factor |
|--------|-------|-------|-------|----------------------|---------|-------------------|
| Blue   | 1.33±0.08 | 1.32±0.41 | 1.50±0.43 | 1.37±0.31 | 22.44 | 1.29 |
| Brown  | 0.51±0.10 | 0.80±0.10 | 0.65±0.02 | 0.65±0.14 | 22.06 | 0.70 |
| Green  | 0.60±0.33 | 0.50±0.07 | 0.54±0.10 | 0.55±0.18 | 33.19 | 0.49 |
| Red    | 0.64±.0.03 | 0.74±0.08 | 0.52±0.10 | 0.63±0.11 | 18.01 | 0.70 |
| White  | 1.05±0.12 | 0.82±0.05 | 1.04±0.44 | 0.97±0.25 | 26.10 | 0.99 |
| Yellow | 0.75±0.09 | 0.80±0.11 | 0.72±0.01 | 0.76±0.08 | 10.43 | 0.70 |

There was more variability relative to the mean in the distribution for the colour green with COV of 33.19%. Similar pattern was seen in colour white with COV of 26.10%. Yellow colour recorded the least variability with COV of 10.43%.

There were significant linear correlations between the mean shape factors and true shape factors for all the three days sessions (p=0.001). Concordance correlation coefficients for the three days sessions were also found to be 0.93, 0.93 and 0.95 respectively. Figure 2-4a-c shows the correlation between the mean shape factors and true shape factor for all the day sessions.
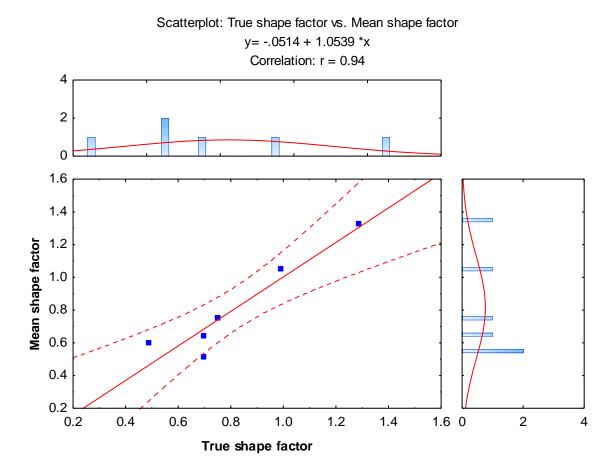
**Figure 2-4a: Correlation of mean shape factor and true shape factor for day 1.**

Scatterplot: True shape factor vs. Mean shape factor
y= .09073 + .90223 *x
Correlation: r =0.95
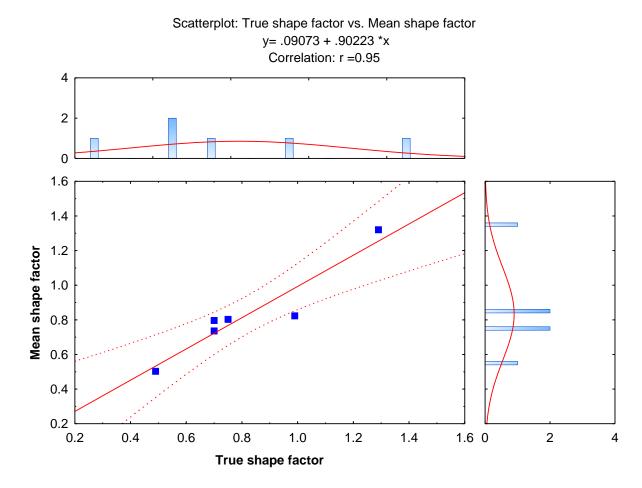
**Figure 2-4b: Correlation of mean shape factor and true shape factor for day 2.**

Scatterplot: True shape factor vs. Mean shape factor

y= -.2040 + 1.2515 *x

Correlation: r = 0.97
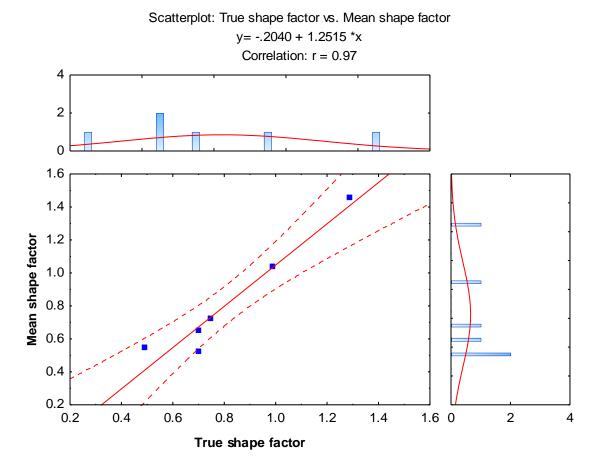
**Figure 2-4c: Correlation of mean shape factor and true shape factor for day 3.**

**Figure 2- 4 a-c: Correlation of mean shape factors versus true shape factor for days 1, 2 and 3.**
**The equation for the best- fit for days 1, 2 and 3 are; y = -.0514 + 1.0539*x; y = .9073 + .90223*x and y = -**
**.0.2040 + 1.2515*x respectively.**

The results in the Figures 2-5a-c also show the Bland-Altman plots for the shape factors for all the three day sessions. All the three days showed good agreement, however, the mean difference were slightly dispersed around the zero line.
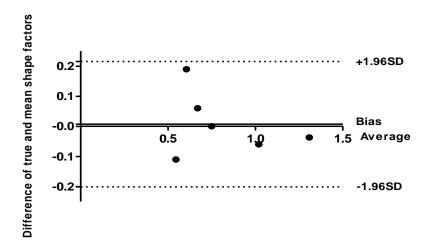
**Figure 2-5a: Bland-Altman plot for day 1.**
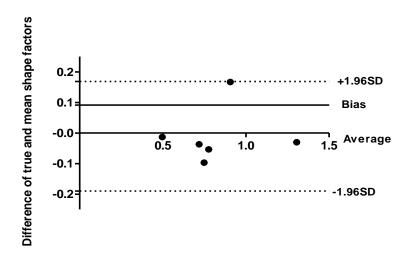


**Figure 2-5b: Bland-Altman plot for day 2.**
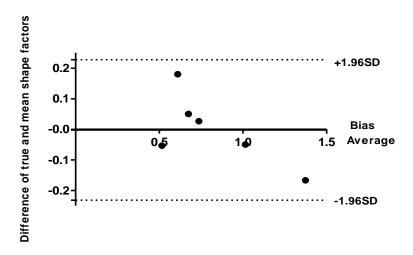
**Figure 2-5c: Bland-Altman plot for day 3.**

**Figure 2- 5 a-c: Bland-Atman plot-Distribution of the means of shape factors and true shape factors for all the three day sessions.**
**The thick line represents the mean difference and the dotted line represents the 95% LoA.**

## 2.7: Discussion

The Oculus Pentacam HR® is becoming the instrument of choice in most clinical and research settings. It uses a Scheimpflug rotating camera that captures Scheimpflug slit images for analysis of the cornea and the anterior chamber parameters. It calculates the radius of curvatures and other parameters that are very useful in making good clinical decisions. There are adequate data on precision such as comparisons, repeatability, reproducibility, [16, 23, 24, 45] however, there has been no report on repeatability and accuracy using a known surface.

The purpose of the study was to report on repeatability and accuracy of the Oculus Pentacam HR® using polycarbonate aspheric surfaces of known radius of curvature and shape factor. In this study, we found out that the Oculus Pentacam HR® was repeatable as the measurements obtained did not show any significant difference in terms of the mean variations on the three

47

day sessions. The measurements also show significant correlation (r=1.00, p=0.001) with both the true radii of curvature and shape factors.

The slight variations in the means of the three day sessions observed could be explained by the fact that mild reflection and the internal reflection of the polycarbonate aspheric surfaces may have affected the instrument's capacity to measure various parameters accurately. (Figure 2-6) Unlike the human cornea, the blue LED used in the Pentacam HR® has to pass through a precise radius of curvature and thick transparent polycarbonate. Reflection from the aspheric surface as well as the internal reflection may be accountable for such variations although polycarbonate has reflectance of <10% [46] similar to that of human eye. Potvin et al. [46] conducted a study on polycarbonate and steel ball surfaces and found that the reflection on a test surface is likely to affect the instrument's output though polycarbonate proved to give good results.
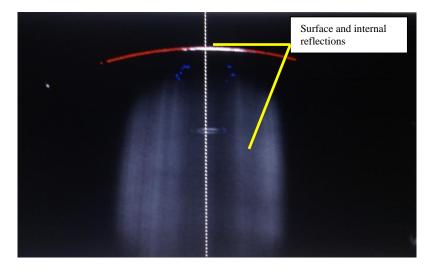


**Figure 2- 6: Scheimpflug image of the polycarbonate aspheric surface showing the surface and the internal reflections.**

According to McCarey et al., [47] object centration and a target off centre by more than 0.25mm can result in unreliable data and again, increasing the focal distance by greater than 1mm beyond the focal point results in a sharp decrease in accuracy. In the case of this study, centration was achieved by mounting the rectangular polycarbonate rectangular block to the headrest with a clamp making sure that the aspheric surfaces are perpendicularly aligned with the optics and the internal target of the instrument. Any variation in mean may results from the automatic mode used in taking the measurements of which the focusing power and algorithm could not be determined.

In conclusion, the Oculus Pentacam HR® was repeatable and accurate in this experiment for the majority of radii of curvature and the shape factors. Based on the small test surfaces in terms of number and curvature variations, it was unpredictable as to whether either the range of radii of curvature or shape factors were over or under-estimated by the instruments, as no clear trends were detected. The variations found with the radius of curvature were within the International Organization for Standardization (ISO) of ±0.10mm.

Repeatability of the Visante™ OCT and Oculus Pentacam HR® Topographers in

Measuring Topographic Corneal Thickness

## 3.1 Introduction

Over the years, attempts to measure and quantify the thickness of the cornea have been made

using several imaging systems. [1-13] Ultrasound pachymetry (US) has been considered the gold

standard for measuring the central corneal thickness (CCT). [14-21] The US pachymeter operates

at frequencies of 20 to 50 MHz, emits short acoustic pulses, and detects reflections from the

anterior and posterior surfaces of the cornea. Corneal thickness is then calculated from the

measured "time-of-flight" between these reflections. [18, 22-24] To measure the thickness of the

cornea, it is generally required that subjects are comfortably seated for the measurement. [16] The

probe of the instrument is then carefully aligned perpendicularly to lightly applanate the cornea

for the measurement. This imaging technique using the US pachymeter has proved to be an

outstanding method for measuring CCT, [22, 25-29] however, it has been criticized for the fact that

its measurement is limited to only single specific points on the cornea, and hence it is difficult

to monitor progression or change since the same point on the cornea may not be measured. [30-32]

It also requires applanation of the cornea and the use of appropriate aseptic precautions, along

with the use of anaesthesia. The possibility of injury to corneal epithelial cells and potential

infection thus exists. [33] This procedure presents a challenge to the already compromised

cornea, especially in KC and PMD.

The Artemis US pachymeter (ArcScan Inc, Morrison, Colorado, USA) does measure global

pachymetry but many authors have reported drawbacks with its use. [34-36] Current non-US

imaging systems are non-invasive, easy to use and also provide global pachymetry. They also help to monitor the progression of the cornea which makes them more efficient instruments for clinical and research purposes.

Currently, other imaging systems using slit-scanning technology such as the Orbscan IIz, (Bausch and Lomb, Rochester, NY, USA) [13], optical coherence tomographers (OCT) such as the Visante™ OCT (Carl Zeiss, Meditec, Dublin, CA, USA), [37] and Scheimpflug imaging technology (Oculus Pentacam HR®, Wetzlar, Germany) [38, 39] are now being used in many clinical and research settings. Repeatability and reproducibility of these imaging techniques are important for making clinical diagnoses, monitoring and evaluation of treatment regimens. Recent reports have shown that these anterior segment imaging techniques have been effective in imaging the anterior segment parameters needed to measure corneal pachymetry. [11, 20, 37, 40-42]

Visante™ OCT [43, 44] is a time domain OCT (TD-OCT), utilizing optical coherence tomography to image the anterior segment of the eye. The Visante™ OCT provides detailed in vivo examination of the anterior segment of the eye without contact. It provides high resolution cross-sectional images. The axial resolution of the Visante™ OCT image is 18μm and the transverse resolution is 60μm.

Repeatability of the Visante™ OCT has been reported. [45-48] Mencucci et al. [45] reported on the repeatability of the Visante OCT and compared it with the Scheimpflug imaging system with US techniques as the gold standard. They reported that Visante™ OCT had good repeatability

with the CCT and also showed good agreement compared to both the US and Scheimpflug technique. In another study, Mohamed et al. [49] assessed the repeatability and reproducibility of the central and peripheral cornea of normal and KC using the Visante™ OCT. Intra-observer and inter-observer repeatability was evaluated using intrasession and intersession measurements. They reported that the Visante™ OCT was repeatable and reproducible in both the central and peripheral corneal thickness measurements for each group.

The Oculus Pentacam HR® is an improvement over the earlier version of the Pentacam®. It has an improved optic design and a high resolution camera i.e. 1.45megapixels. The Oculus Pentacam HR® is a rotating Scheimpflug camera that generates images from the anterior surface of cornea to the posterior surface of crystalline lens. It acquires 25-50 Scheimpflug images in approximately two seconds using the monochromatic cobalt blue LED light source. [50] The "highly sophisticated and integrated" software system extracts 25,000 true elevation points from each of these images, obtaining approximately 138,000 true elevation points for each surface, including the centre of the cornea. [14, 51, 52] Repeatability and reproducibility with the Oculus Pentacam HR® have been done by numerous authors. [40, 41, 53-59]

Miranda et al. [60] reported on repeatability measurements of the corneal thickness at the apical and peripheral cornea of normal eyes. The measurements were obtained at one minute, one hour and one week intervals and they took three consecutive measurements of the cornea without re-alignment by the same observer. They reported that the Oculus Pentacam HR® was repeatable as their results showed no significant within-subject variance for the three sessions and that the variability of the instrument did not increase over time. Similar results have been

reported by Amano et al., [52] Sedaghat [61] and Lackner [56] using the same instrument for measuring the CCT in normal eyes.

Repeatability of CCT on KC eyes and comparing the results with other instruments has also been reported. [62] de Sanctis et al. [62] reported on the repeatability and reproducibility of the CCT using the Oculus Pentacam HR® and the gold standard US pachymeter, Allergan-Humphrey 850 (Allergan-Humphrey, Dublin, California, USA). They evaluated 30 eyes and took two measurements within a three to 10 minute interval by different examiners using these instruments. The Oculus Pentacam HR® showed higher inter-examiner correlation and lower inter-examiner variability compared to the US pachymeter. They concluded that the Oculus Pentacam HR® provided measurements of CCT that were more reproducible and repeatable than those obtained with the US pachymeter. They further suggested that it was imperative to consider such an instrument for monitoring the corneal thickness when repeated measurements may be done over time and by different examiners.

Although there is an abundance of papers on repeatability of the CCT of normal and KC corneae using the Visante™ OCT and the Oculus Pentacam HR®, there are few reports on cases of repeatability and reproducibility of these instruments in measuring the topographic corneal thickness (TCT) in KC and PMD corneae.

### 3.2 Objectives

The main objectives of this study were to:

1. Measure the repeatability of the Visante™ OCT and Oculus Pentacam HR® in KC and PMD in measuring TCT.

2. Compare the reproducibility of the two instruments for TCT measurements.

## 3.3 Materials and Methods

### 3.3.1 Research Design

This study involved two study visits where corneal thickness measurements were repeated after at least 48hours. Measurements from one eye only were taken (right eye=12; left eye=8). Participants were screened to make sure the selected eye was free from any active ocular pathology/infection such conjunctivitis. The cornea was stained with fluorescein and carefully examined with slit lamp biomicroscopy using a Wratten #12 yellow filter. This was to make sure that the cornea was free from any form of corneal staining resulting from contact lens wear. After this thorough examination, the eye was rinsed with non-preserved Unisol® 4 saline solution (Alcon Laboratories, Inc., TX, USA). Participants were allowed to sit for approximately 5 minutes to make sure the saline had completely dissipated from the eye. Corneal thickness measurements were taken twice, first using the Visante™ OCT and then Oculus Pentacam HR® at each measurement session.

### 3.3.2 Participants and Recruitment

Twenty participants who had been diagnosed with KC and PMD were enrolled in this study. These participants were recruited from the Centre for Contact Lens Research (CCLR) internal data/records as well as from the School of Optometry and Vision Science, University of Waterloo Contact Lens Clinic.

Approval from the university's human research ethics panel was obtained before the study commenced. All the participants were treated in accordance with the tenets of the Declaration of Helsinki, and were provided with a written informed consent to sign.

Eighteen of the participants had been diagnosed with KC and two with PMD. The majority of the participants had been wearing gas permeable contact lenses (RGP) (n=9), some were wearing spectacle prescriptions (n=7), a few wore piggy-back contact lenses (PBCL) (n=2), semi-scleral contact lens (sSCL) (n=1) and soft toric contact lens (n=1) for the correction of their condition. These participants had been using their contact lenses on a daily wear basis for at least 14 hours a day. On the day of the experimental visits, no contact lenses were worn. Measurements were repeated on two separate occasions. At each session, measurements were repeated twice.

### 3.3.3 Inclusion and Exclusion Criteria

A person was eligible for inclusion in the study if he/she:

1. Was at least 17 years of age and has full legal capacity to volunteer.

2. Had read and signed an information consent letter.

3. Was willing and able to follow instructions and maintain the appointment schedule.

4. Had been diagnosed with KC or PMD.

A person was excluded from the study if he/she:

1. Had any known active ocular disease and/or infection such as conjunctivitis.

2. Had a systemic condition that may affect a study outcome variable.

3. Was using any systemic or topical medications that may affect a study outcome variable.

4. Had known sensitivity to the diagnostic pharmaceuticals to be used in the study.

5. Was aphakic.

6. Had undergone refractive surgery.

7. Had had any form of surgery for the correction of KC or PMD.

### 3.3.4 Instrumentation

### 3.3.4.1 Corneal Thickness Measurement with Visante™ OCT

The Visante™ OCT has been previously described in detail in Chapter 1.

The Visante™ OCT was used to scan the anterior segment of the eye. No direct contact on the eye was made with the instrument. The participants were comfortably seated and properly adjusted on the chin rest making sure that their forehead made contact with the forehead rest. The participants were asked to look at the yellow fixation target and maintain gaze on this target. The instrument was set to enhanced global pachymetry mode for all the measurements. The examiner focused and adjusted the instrument until the real-time image of the cornea was shown on the computer monitor. The cornea was adjusted to align within the two green horizontal mires displayed on the screen. The image was considered to be optimally aligned when the specular reflex (vertical streak line), which is reflected from the center of the front surface of the cornea, was observed. The participants were also instructed to keep their eyes wide open during scanning. Once this was achieved, the capture release button was pressed once to scan the cornea. The integrated software (version 2.0) automatically processed the OCT images and simultaneously calculated a corneal pachymetry map along eight meridians.

Acceptable scans were judged to be of adequate quality based on the following criteria: good demarcation of the anterior and posterior boundaries of the cornea, horizontal alignment and absence of artefacts in the scanned area. This procedure was repeated after approximately two minute intervals for each scan to measure its repeatability and the images were immediately examined and assessed to make sure that they were of acceptable quality.

After every measurement, the participants were asked to pull away from the forehead rest and repositioned themselves for the next scan to minimize interdependence of the readings. Any scan that resulted from misalignment/poor alignment was immediately re-adjusted and the measurement was repeated. All the measurements took place in normal lighting conditions and these conditions were maintained for all the measurements. The measurements were repeated after two days.

The topographic maps generated by the Visante™ OCT were divided into zones by octants (superior, superotemporal, temporal, inferotemporal, inferior, inferonasal, nasal, superonasal) and annular rings (2, 5, 7 and 10mm chords). For analysis, the raw data unaltered binary image file "*.bin" were exported and processed with custom-built software.

### 3.3.4.1.1 Visante™ OCT Image Processing and Analysis

The Visante™ OCT software was used to export the raw unaltered binary image file "*.bin" for analysis. Custom-built software (Visante™ OCT Data Compiler, CCLR, Waterloo) was used to process the OCT images. The software locates the peak reflectance that corresponds to the front and back surfaces of the cornea. The custom-built software then generates all values

of total corneal thicknesses along multiple meridians. Once the image processing was completed, the software automatically generates an excel spreadsheet for recording. This procedure was used to process all the OCT images measured for both first and second visits.

Topographic corneal thickness (TCT) (microns) was recorded in the vertical (90 degrees), horizontal (180 degrees) and the oblique (45 or 135 degrees) meridians at 1mm intervals across 8mm of the central cornea (Figure 3-1a&b).

In order to represent the same locations for each eye, TCT for participants whose left eyes had been imaged were mirrored to represent the same locations on the right eye. Figure 3-1a&b shows the schematic diagram of the right eye and the mirrored left eye.
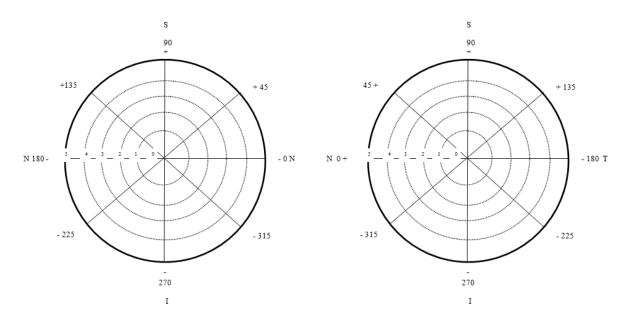


Figure 3- 1a: Right eye.    Figure 3- 1b: Mirrored left eye.

**Figure 3- 1a&b: Schematic diagram of the right eye and mirrored left eye.**
**N represents nasal, T represents temporal, S represents superior and I represents inferior.**

**3.3.4.1.2 Measurement of Corneal Thickness with Oculus Pentacam HR®**

The Oculus Pentacam HR® (Wetzlar, Germany) has been previously described in detail in chapter 1.

The Oculus Pentacam HR® was used to scan the anterior segment of the eye. No direct contact on the eye was made with the instrument. The participants were seated with their chin on the chin rest and their forehead against the forehead strap. The participants were asked to fixate on a red fixation target. The room lights were all switched off for all examinations to obtain a reflex-free image. The instrument was focused and adjusted using the joystick until the real-time image of the corneal surface was shown on the computer monitor, with the instrument marking the centre of the pupil and the corneal apex. The mires displayed on the screen guided the investigator to perfectly align the horizontal and vertical crosshairs (axes) at the centre of the pupil. To reduce investigator variability, the automatic release mode was used to take all the measurements. The rotating camera was set to capture 25 Scheimpflug slit images in 360 degrees in approximately two seconds. This procedure was repeated in approximately two minute intervals for each scan. After every measurement, the participants were asked to move away from the forehead strap and repositioned themselves for the next scan while the joystick was used to move the instrument backwards and realigned for the next scan to eliminate interdependence of the readings. Scans that registered as *"ok"* were considered acceptable according to the "Examination Quality Specifications" within the standard of the instrument. This was to ensure that the scans were not affected by poor alignment/misalignment with the optics of the instrument. Any misalignment observed was re-adjusted before the measurement

was taken. These measurements were performed on two separate sessions at least 48 hours intervals.

The TCT (microns) was recorded in the 90, 180 and oblique (45 or 135) meridians at 1mm interval across 8mm of the central cornea.

### 3.3.5 Conditions for Repeatability

Repeatability of the measurements taken was based on the standard definition adopted by the British Standards of Institution. [63] The conditions were standardized by ensuring that independent test results were obtained with the same order of measuring the corneal thickness, by the same examiner and on the same sets of corneal topographers used within the shortest possible time lapse and between the successive sets of measurements in the same environmental condition. For reproducibility, the examination was carried out with the same method on the same participants using the two corneal topographers. Two repeated measurements were taken on each of the two experimental visit days.

### 3.4 Data Management and Analysis

Data analysis was conducted using Statistica 11 (Statsoft. Inc., Tulsa, TX, USA). Mean and standard deviation (SD) are reported for both Visante™ OCT and the Oculus Pentacam HR[®] for the two visits. Coefficients of variation (COV) between visits were also performed for the two visits. Repeated measures analysis of variance (RM ANOVA) was performed to determine the statistical significance of the measurements of the two visits. P values of less than 0.05 were considered to be statistically different. For the purpose of reproducibility, several

interactions within and between the visits, measurements, locations and axes were compared to determine whether the two instruments can be used interchangeably.

## 3.5 Results

There were 16 males and four females enrolled in the study. Their mean age was 33.95±7.90 (range: 23-51) years. Two repeated measurements were taken on each of the two visits, first with Visante™ OCT and second with the Oculus Pentacam HR®. This order of measurement was maintained for all the participants.

The mean CCT for the Visante OCT™ was 484.97±43.14µm and that of Oculus Pentacam HR® was 478.86±45.31µm (P=0.67). There was no statistically significant difference in the TCT obtained between the two visits (p=0.54) and measurements (p=0.63) for Visante™ OCT. There was also no statistically significant difference in the combined visits, axes and locations (p= 0.86; Figure 3-2). In the case of Oculus Pentacam HR®, no significant difference was found in the visits (p=0.18) but difference exists in the measurements (p=0.001). There was also significant difference in the combined visits, axes and locations (p=0.001). Tukey post-hoc analysis shows that the differences (p<0.05) were found in the +1 and +4 locations in the 135 meridian. Figure 3-3 shows the plot of the visits, axes and locations of Oculus Pentacam HR®.

Visits*Axes*Location; Unweighted Means
Current effect: F(24, 456)=.69, p=.86
Vertical bars denote 0.95 confidence intervals
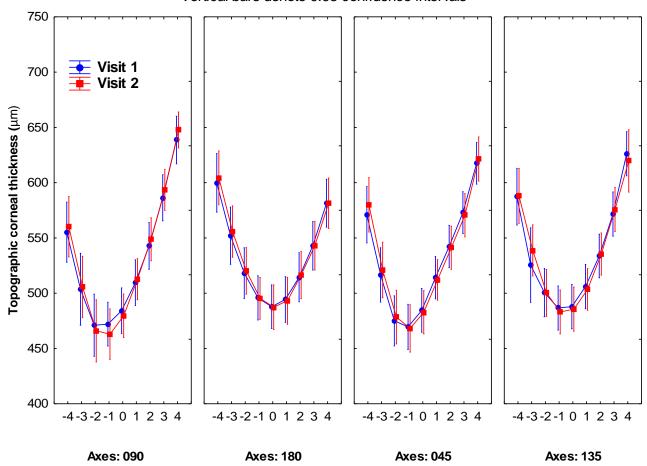
**Figure 3- 2: Plot of visits, axes and locations of TCT for Visante™ OCT.**
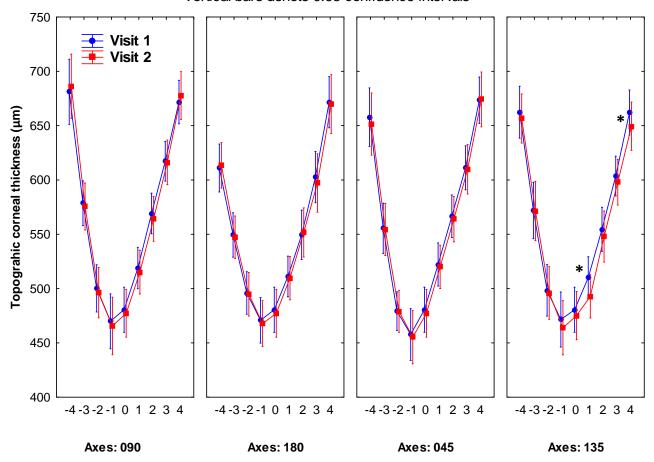
**Figure 3- 3: Plot of visits, axes and locations of TCT for Oculus Pentacam HR®.**
**Note: The asterisks (*) means locations of significant difference.**

For reproducibility, several interactions were compared. The first interaction of the results between the two instruments shows that there were significant differences between the instruments, axes and locations ($p<0.05$). Tukey post-hoc analysis shows that there was no significant difference in the central location; however, differences were at all other locations for both para-central locations and the periphery. For certain axes, differences were found as

close to 1mm out from the centre, as for example in the -1mm location in the 90 meridian (Figure 3-4).
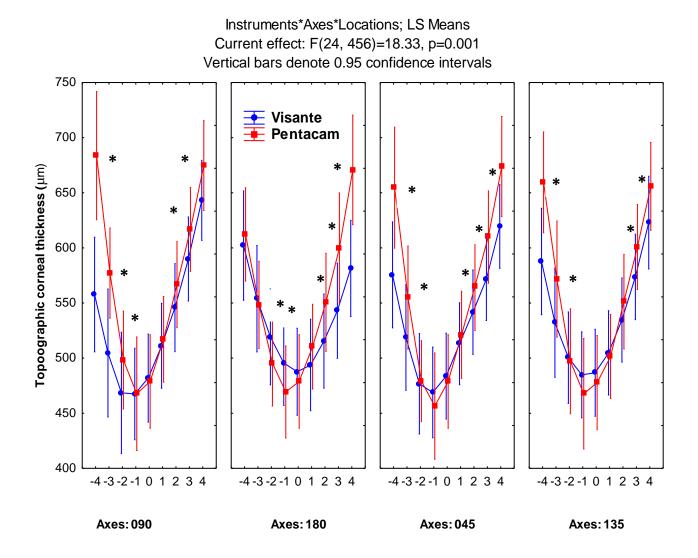


**Figure 3- 4: Plot of instruments, axes and locations of TCT for Visante™ and Pentacam HR®.**
**Note: The asterisks (*) means locations of significant difference.**

There were also significant differences for the interaction of instruments, visits, measurements and axes across all 9 locations (p=0.04). Tukey post-hoc analysis shows that there was no difference within Visante™ OCT; however, differences were found within the Oculus

Pentacam HR®. Table 3-1 shows significant differences between visits and measures within the

Oculus Pentacam HR®.

**Table 3- 1: Significant differences within Oculus Pentacam HR®, when comparing the repeated measurements and visits for each of the four visits; shown are the affected visits and measurements, and the corresponding p-value.**

|  | Interaction | | |
| --- | --- | --- | --- |
|  | Instruments*Visits*Measures*Axes | | |
| **090** | **180** | **045** | **135** |
| N/A | V1M1 vs V1M2 p=0.017200 | V1M1 vs V2M2 p=0.002215 | V1M1 vs V2M1 p=0.000151 |
| N/A | V1M1 vs V2M2 p=0.000415 | N/A | V1M1 vs V2M2 p=0.000258 |
| N/A | V2M1 vs V2M2 p=0.045520 | N/A | N/A |

Where: V1=visit 1, V2= visit 2, M1= measurement 1, M2= measurement 2, vs= versus

p= significant difference, N/A= not applicable.

There were also significant differences for the interaction of instruments, visits, measures, axes and locations across the four axes (p=0.001). Tukey post-hoc analysis shows that there was a difference within one pair of measurements within visit two for the Visante™ OCT (V2M1 vs V2M2 at 4mm; p=0.035600); however, such differences were not found for the Oculus Pentacam HR®.

Table 3-2 shows the COV expressed as a percentage of the total corneal thickness at the two visits for both Visante™ OCT and Oculus Pentacam HR®. There was slightly more variability relative to the mean of the corneal thickness in the -4mm location in the 90 meridian of the Visante™ OCT compared to the Oculus Pentacam HR®. The COV for CCT for Oculus Pentacam HR® was 9.46% and was found to be slightly more variable compared to the Visante™ OCT.

**Table 3- 2: Coefficient of variation (%) of the mean corneal thickness (µm) at the centre and selected locations.**

| | | Visits Locations (%) | | |
|---|---|---|---|---|
| | | | Centre | |
| **Instrument** | **Axis** | **-4** | **0** | **4** |
| **Visante** | **090** | 10.88 | 8.90 | 6.62 |
| | **180** | 9.24 | 8.90 | 8.50 |
| | **045** | 9.71 | 8.90 | 6.88 |
| | **135** | 9.33 | 8.90 | 10.26 |
| **Pentacam** | **090** | 9.38 | 9.46 | 6.72 |
| | **180** | 7.74 | 9.46 | 8.15 |
| | **045** | 9.43 | 9.46 | 7.53 |
| | **135** | 7.67 | 9.46 | 7.29 |

## 3. 6 Discussion

Repeatability measurements for corneal thickness are important for monitoring changes in various corneal conditions overtime, and as such corneal topographers must offer repeatable measurements. Reproducibility of the instruments is also important to determine whether they can be used interchangeably in clinical and research settings. Ultrasound pachymetry has been the gold standard for measuring corneal thickness partly because of its reliability and

effectiveness in detecting the anterior and posterior corneal surfaces and therefore measuring corneal thickness [18, 64, 65]; however, current non-invasive imaging techniques provide another alternative for imaging corneal thickness. Bechmann et al. [31] also reported that US overestimates the corneal thickness by approximately 49µm.

Commercially available imaging techniques such as Visante™ OCT and the Oculus Pentacam HR® are commonly used in both clinical and research settings to measure the central and peripheral corneal thickness for diagnosis, [16, 44, 50] pre and post corneal surgical evaluation, [3] screening for refractive surgery and IOL calculation. [51]

In this study, we compared the repeatability of each of the instruments for the two day visits. For reproducibility measurements, several interactions within and between the visits, measurements, locations and axes were compared to determine whether the two instruments can be used interchangeably. We found the mean CCT with the Visante™ OCT to be 484.97±43.14µm. Brautaset et al. [6] reported 470.63±58.6µm with Visante™ OCT for KC corneae. Other authors have also reported similar CCT in KC patients. [6, 45, 66-68] The CCT for Oculus Pentacam HR® was 478.86±45.31µm. Numerous authors have reported similar CCT in patients with KC. [51, 62, 69, 70] Uçakhan et al. [71] reported 488.00±41.43µm in KC patients using Oculus Pentacam HR® while Ahmadi Hosseini et al. [72] reported CCT of 499.68±39.59µm with the same instrument.

The Visante™ OCT did not show any significant difference for the interaction of visits, axes and locations for the repeated measures (p>0.05). Similar results were found for Pentacam

HR[®] except in the +1 and +4mm locations in the 135 meridian where significant differences were determined.

The difference in the mean CCT between the Visante™ OCT and Oculus Pentacam HR[®] was 6.11μm, where the Oculus Pentacam HR[®] measures were thinner.

On the other hand, the total corneal thickness in the para-central and periphery for all meridians were slightly higher with the Pentacam HR[®] compared with the Visante™ OCT. For example the mean difference of the corneal thickness in the -4mm along the 090 meridian was found to be 126.04±3.45μm (p=0.001) greater with Oculus Pentacam HR[®] compared to the Visante™ OCT. Such a characteristic pattern, with increased peripheral corneal thickness (PCT) measurements variation has been observed by Prospero Ponce et al. [70] and Mencucci et al. [45] Prospero Ponce et al. [70] evaluated the CCT and PCT using the Oculus Pentacam HR[®] (Wetzlar, Germany), Visante™ OCT (Carl Zeiss Meditec, Dublin, CA, USA), and US pachymeter (Sonogage Corneo-Gage Plus, Cleveland, Ohio, USA) in normal, KC-suspect, and post LASIK eyes. They reported CCT with the US were consistently higher than Oculus Pentacam HR[®] and Visante™ OCT. They observed mean CCT difference of 0.9±1.4 μm with Visante™ OCT higher than the Oculus Pentacam HR[®]. No significant difference was found between the two instruments. They further observed that the PCT with the Oculus Pentacam HR[®] were slightly higher than Visante™ OCT measurements; however, they showed more agreement with each other.

Based on the interactions, we found that the two instruments were not reproducible and care must be taken when interpreting the measurements from each of the instruments. Oculus Pentacam HR® was found to give varied measurements within and across visits and this suggests that to achieve more reliable measurements, it is commendable to take repeated measurements of the same patient during a visit and average these multiple readings in order to minimize the observed variability between measurements for the same eye. (Figure 3-4).

The observed characteristic pattern for the CCT and PCT of our results may be based on the fact that Visante™ OCT obtains corneal thickness profiles in less time and corneal thickness measurements are not affected by stromal reflections or haze especially centrally. [67, 73, 74] It measures corneal thickness as a direct measure of reflection peaks occurring at the anterior cornea to the posterior surfaces, which is the distance between the two peaks. The Visante™ OCT has also been reported to have good intra-operator reliability when compared with US and Oculus Pentacam HR®. This makes it versatile and a promising imaging technique for clinical and research purposes. [45, 75] Mohamed et al. [49] reported that the COV of the Visante™ OCT in KC was <3% for evaluating the corneal thickness. Prospero Ponce et al. [70] reported that the OCT device gathers information about peripheral thickness within a specific area by averaging a number of points, while the Scheimpflug system presents the mean value along the line segment of a specific diameter. The differences in the softwares for evaluating corneal thickness are likely to result in the variation of the measurements. In this study, custom-built software (Visante™ OCT Data Compiler, CCLR, Waterloo) was used to process all the total corneal thickness at different meridians. Variations in the CCT and PCT measurements may be attributed to the algorithm used by the instruments in generating the topographic corneal

thicknesses as well as the custom-built software used in processing all the data. Moreover, in the periphery, there is more light scattering with the OCT and loss of lateral resolution contributing to the more peripheral error.

The Oculus Pentacam HR[®] has gained popularity for its repeatable and reproducible results in measuring corneal thickness. [3, 14, 42, 51, 52, 70] Its effectiveness and reliability has also been compared with US, Orbscan II (Bausch and Lomb, Rochester, NY, USA) and Galilei (Ziemer Group, Port, Switzerland). [2, 20, 41, 49, 58, 59, 69, 70, 76] One of the advantages of the Oculus Pentacam HR[®] is that it automatically captures the image on the eye when perfect alignment is achieved. [70, 77] It does not depend on the reflectivity of the tear film to capture the image on the eye; therefore, a poor tear film does not distort the corneal imaging characteristics and measurements. [77] It measures corneal thickness by subtracting the elevation values found for the anterior corneal surface from the posterior elevation measurements. Irrespective of the advantages, repeatable and reproducible results, recent publications have criticized the Oculus Pentacam HR[®]. [42] They report that it slightly underestimates the CCT in comparison with slit a scanning imaging system, and in more advanced cases of KC, the difference in CCT was found to be statistically significant. [56, 62] Lam et al. [78] reported greater variability with the Scheimpflug system at the corneal periphery and therefore suggested that repeated measures are necessary to assess the pachymetric readings at the periphery to ensure accuracy.

In this study, looking at the data for the Oculus Pentacam HR[®] only (Figure 3-3), it was found to provide repeatable measurements for most of the locations except for the +1 and +4mm in the 135 meridian. However, it needs to be kept in mind that this finding was based on the data

for the Oculus Pentacam HR® only, while the significant differences that were found the interactions of the instruments, visits, measures and axes across locations (Table 3-1) indicate the need for multiple, averaged measurements with this device. This variability may be attributed to focussing error or other unexplained factors accounting for the variations in those locations.

The fact that the Oculus Pentacam HR® is pre-calibrated by the manufacturer but does not provide a precise test/calibration tool raises concerns over the measurements taken in a clinical setting; the Visante™ OCT on the other hand has to be calibrated prior to each use by the operator. The effect of the light scattering and reflections from the scleral conjunctiva at the limbus and reflection from the iris reduces the image quality with the Oculus Pentacam HR® (Figure 3-5). These reflections may affect the pachymetry values especially at the para-central and peripheral cornea regions. [79] The effect of light scattering could explain the slightly high corneal thickness values observed in the corneal periphery compared to the Visante™ OCT. This effect may be important especially in cases of KC and PMD where significant amounts of corneal scarring may be found, hence, affecting the ability to measure corneal thickness accurately.
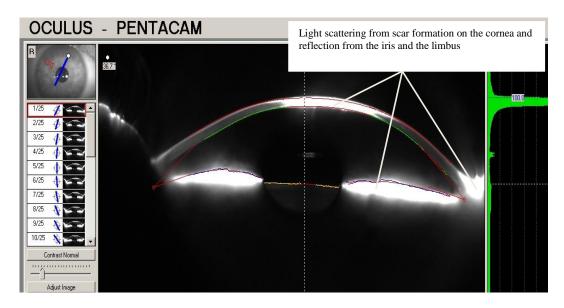
**Figure 3- 5: Effect of light scattering and reflection from the iris and limbus.**

In conclusion, the Visante™ OCT gave repeated measurements for the two visits as there were no significant differences in all the respective locations in all meridians. Oculus Pentacam also gave repeatable measurements for the majority of the locations. The two instruments were found not to be reproducible and should not be used interchangeably; therefore, care must be taken interpreting the TCT from the two instruments. It is advisable to take at least two measurements and average these in order to minimize variations between measures. In addition, the manufacturers of Oculus Pentacam HR® may consider including a calibration test surface so that practitioners would be able to calibrate the instrument each time it is being used. Again, more research may be needed to ascertain the effect of the light scattering on the measurement parameters, especially corneal pachymetry in the para-central and the peripheral areas of the cornea.

**Chapter 4**

**Repeatability of the Medmont E300™ and Oculus Pentacam HR® Topographers in Measuring Topographic Corneal Curvature**

## 4.1 Introduction

The ability to determine corneal curvature measurements with a high degree of precision is important in both clinical and research purposes. The instruments are also expected to be repeatable and reproducible to provide a consistent reading under the same or similar conditions. Measurements of the central and peripheral corneal curvatures are highly important for clinical scientists and ophthalmic practitioners. [1-3] The reliability of these measurements is critical for providing the necessary information for calculating IOL power, [3-6] detecting and evaluating the progression of ectatic cornea conditions, [7-9] screening and managing corneal refractive surgeries, [10-13] and designing, fitting and monitoring of contact lens wear. [14] The recent introduction of overnight orthokeratology procedures to reshape the corneal curvature has also made corneal topographers an indispensable tool to effectively map the cornea and detect any significant changes following such treatment resulting from poorly fitting contact lenses. [15-20] Indices derived from the corneal topographic measurements are also useful in the diagnosis and classification of corneal conditions such as KC and PMD. [1, 21] Repeatability of corneal topographers is important in every clinical measurement for the effective monitoring of specific treatment as well as for research purposes. [21]

Due to the increased usage of corneal curvature measurements, including measurement of surface aberrations and tear-induced aberrations during blinking, [22, 23] the standards of

precision for modern videokeratoscopes have increased as the success of corneal topography-based strategies to improve vision relies entirely on the accuracy and precision of such calculations.

Instruments based on Placido-based technology have most commonly been used to measure corneal curvature. This technology is currently used in modern day instruments such as the Medmont E300™ (Medmont Pty Ltd, Australia), small cone-head type topographer. Research has shown that this technology is limited by tear film instability, shadows from the eyelashes, and the eyelids partly because of the use of reflection from the pre-corneal tear film. This effect has been shown to adversely interfere with the accuracy of the measurements. [14, 24] The performance of this technology is further limited by several factors including alignment and focusing techniques, low camera resolution, and the computer algorithms used in analyzing the data on the anterior corneal surface. [21, 25, 26] Two different mire design categories exist for Placido-disc topographers: large and small. [27] The Medmont E-300™ uses small ring topographer and therefore offers greater coverage and better spatial resolution from having a greater number of rings, but is more sensitive to focus errors. [28]

Studies on test surfaces show that the Placido-disc videokeratoscopes are generally accurate in the central area, as reflected mires are illuminated perpendicular to the central area, but it is worse toward the periphery and is less reliable on surfaces where there is a sudden change of curvature. [21, 26, 29-31] Peripheral rays of illuminated rings reflected on the cornea suffer from an error known as *"skew ray error"* when measuring rotationally symmetrical surfaces, but this error is believed to be small on normal corneas. [29-32] According to Mattioli et al., [32] the

peripheral effect is often not apparent on the topographic maps shown on videokeratoscope software because interpolated data are used to bridge/fill in some of the resultant gaps in the map. This effect has also been reported by Wilson et al. [30] and Tomidokoro et al. [33]

Irrespective of these limitations, available studies suggest that Placido-disc technology continues to provide accurate measurement of the anterior corneal curvature. [14, 33, 34] Tang et al. [21] in their study on test surfaces showed that the Medmont E300™ was the most precise instrument among four videokeratoscopes for detecting spherical and aspheric test surfaces. Other researchers have also investigated on predefined test surfaces and have proven the accuracy and performance with this technology. [31, 35-37]

Repeatability measurements on normal corneae have also been reported. [14] Cho et al. [10] evaluated the performance of the Medmont E300™, Humphrey Atlas 991 (Carl Zeiss Meditec, Dublin, CA, USA), Orbscan II (Orbtek, Bausch and Lomb, Rochester, NY, USA) and Dicon CT200 (Dicon, Vismed Inc., USA) on 22 normal corneae. They reported no significant within-examiner and between-examiner differences with Medmont E-300™. The Medmont E-300™ was also repeatable compared with the Humphrey Atlas 991. They reported that the number of repeated readings taken for a precision of 2 μm (elevation map) was 12 for the Humphrey Atlas 991 and 2 for the Medmont E-300™.

Since its inception of Oculus Pentacam HR® into the mainstream of ophthalmic corneal topographers, measurements on both test surfaces and normal corneae measurements have been reported. [14, 24, 38-41, 42, 47]

We [46] have previously reported on the repeatability and accuracy of the Oculus Pentacam HR® on polycarbonate aspheric surfaces. The instrument proved to be repeatable and accurate for the majority of the radii of curvature and shape factors measured.

Repeatability and reproducibility measurements on the anterior corneal surface have been undertaken by numerous researchers. [39, 41, 48-52] Kawamorita et al. [48] reported that the Oculus Pentacam HR® proved to be repeatable and reproducible for central corneal curvature measurements when compared with Keratron® topography systems (Optikon 2000 SpA, Italy). In a related study, Kawamorita et al. [48, 53] compared the Scheimpflug photography and slit-scanning topography, Orbscan II (Bausch and Lomb, Rochester, NY, USA) to evaluate the repeatability, reproducibility and agreement with these two instruments. They reported that the between-instrument agreement was moderate. They concluded that the repeatability and reproducibility were higher in the Oculus Pentacam HR® than it was in the Orbscan II.

Although there is an abundance of literature on repeatability of normal cornea curvature measurements using the Medmont E300 and Oculus Pentacam HR®, [1, 4, 9, 15, 24, 48-51, 53] there are no reports on the cases of repeatability and reproducibility of these instrument in measuring the topographic corneal radius of curvature in KC and PMD corneae.

## 4.2 Objective

The main objectives of this study were to:

1. Assess the repeatability of the Medmont E300™ and Oculus Pentacam HR® in KC and PMD corneae.

2. Compare the reproducibility of the two instruments for topographic radius of curvature measurements.

## 4.3 Materials and Methods

### 4.3.1 Research Design

The research design, participants and recruitment for the study as well as the inclusion and exclusion criteria have been described in detail in chapter 3.

### 4.3.2 Instrumentation

#### 4.3.2.1 Corneal Curvature Measurements (Corneal Topography)

#### 4.3.2.1.1 Corneal Curvature Measurement with Medmont E300™

The Medmont E300™ (Medmont Pty Ltd, Australia) has been previously described in detail in chapter 1.

Medmont E300™ was used to measure the corneal curvature. No direct contact on the eye was made with the instrument, though the instrument went very close to the eye. The participants were seated and properly adjusted on the chin rest, making sure that the forehead made contact with the forehead strap. The participants were asked to look at the green fixation target and maintain gaze on this target. The examiner focused and adjusted the joystick until the real-time image of the cornea was shown on the computer monitor. The green crosshair and the red horizontal bar guided the researcher to properly centre and focus on the cornea. Once this was achieved, the software automatically captured the image on the eye. Four sets of images were displayed in the view pane on the computer monitor. Only one image of the four sets of images

was chosen. The criteria used was the image with highest percentage of image quality (>95%) according to the "Quality Specification" within the instrument. The selected image was saved. This procedure was repeated after approximately two minute intervals for each scan and the best image was saved. After every measurement, the participants were asked to pull away from the forehead strap and repositioned themselves for the next scan while the joystick was used to move the instrument backwards and realigned for the next scan to eliminate interdependence of the readings. Any misalignment observed was re-adjusted before the measurement. The measurement was taken in the normal lightening condition and this was maintained for the participants during the visits. These measurements were repeated on two separate sessions. The topographic tangential corneal curvatures (diopters) were recorded in the vertical (90 degrees), horizontal (180 degrees), and oblique (45 or 135 degrees) meridians at 1mm interval across 8mm of the central cornea.

### 4.3.2.1.2 Corneal Curvature Measurement with Oculus Pentacam HR[®]

The Oculus Pentacam HR[®] (Wetzlar, Germany) and the procedure used to measure the corneal curvature have been previously described in detail in chapters 1 and 3.

### 4.3.3 Data Recording

The corneal topography measurements were manually recorded first with the Medmont E300™ and then Oculus Pentacam HR®. The examiner carefully placed the cursor of the mouse at the respective position of 1mm on the topographic tangential map. The value displayed was recorded in diopters (D). The topographic corneal curvature was recorded in the 90, 180, and the oblique (45 or 135) meridians at 1mm interval across 8mm of the central

cornea. This procedure was used to record all the data for the corneal topography measurements.

### 4.3.4 Conditions for Repeatability

The conditions of repeatability and reproducibility have been described in Chapter 3.

### 4.3.5 Data Management and Analysis

Data analysis used in this study has been described in details in Chapter 3.

### 4.4 Results

The mean age, SD and range have been described in Chapter 3.

Two repeated measurements were taken on each of the two visits, first with Medmont E300™ and second with the Oculus Pentacam HR®. This order of measurement was maintained for all the participants.

The mean CRC for Oculus Pentacam HR® was 50.38±5.81D and Medmont E300™ was 49.41±4.93D (p=0.26). The mean difference of the CRC between the two instruments was 0.97±0.88 D. There was a significant difference in the visits and locations (p<0.05) but no significant difference in the measures (p=0.98) for the Medmont E300™. There was also no significant difference in the combined visits, axes and locations (p=0.12). Figure 4-1 shows the plot of visits, axes and locations for the Medmont E300™. Results from the Oculus Pentacam

HR® show that there were no significant differences in the visits (p=0.32), measures (p=0.66), however, significant difference was found in the axes. There was also no significant difference in the combined visits, axes and locations (p=0.24). Figure 4-2 shows the plot of visits, axes and locations for the Oculus Pentacam HR®.



Visits*Axes*Locations; Unweighted Means
Current effect: F(24, 456)=1.36, p=.12
Vertical bars denote 0.95 confidence intervals
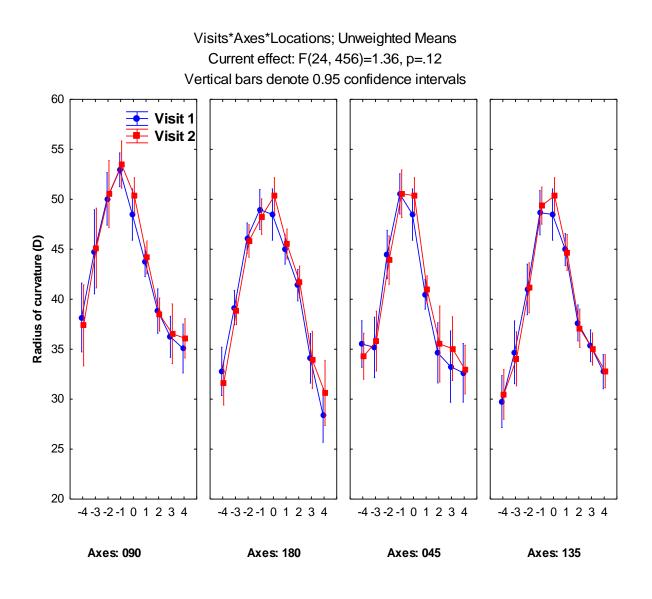
**Figure 4- 1: Plot of visit, axes and locations for Medmont E300™.**
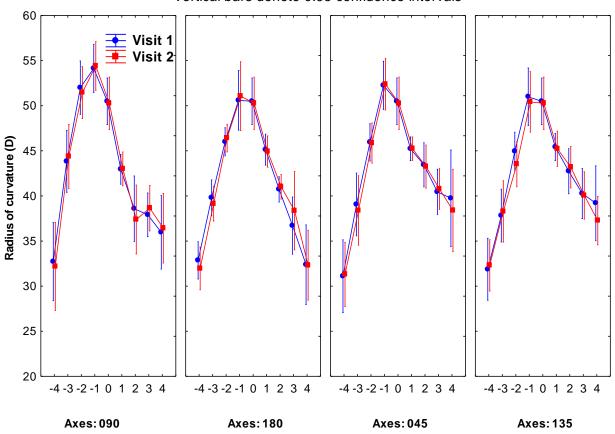
**Figure 4- 2: Plot of visits, axes and locations Oculus Pentacam HR®.**

For reproducibility, interactions of instruments, visits, measures, locations and axes were evaluated to determine whether the two instruments can be used interchangeably. The results show that there were significant differences for the interaction of instruments, axes and locations (p=0.001). Tukey post-hoc analysis showed that there were no significant differences in the centre and out to ±2mm, however, differences were found further out in the periphery especially for the oblique meridians. Figure 4-3 shows the locations of significant differences

in the respective meridians for the two instruments. No other significant interactions were found.



Instruments*Axes*Locations; Unweighted Means
Current effect: F(24, 456)=3.81, p=.001
Vertical bars denote 0.95 confidence intervals
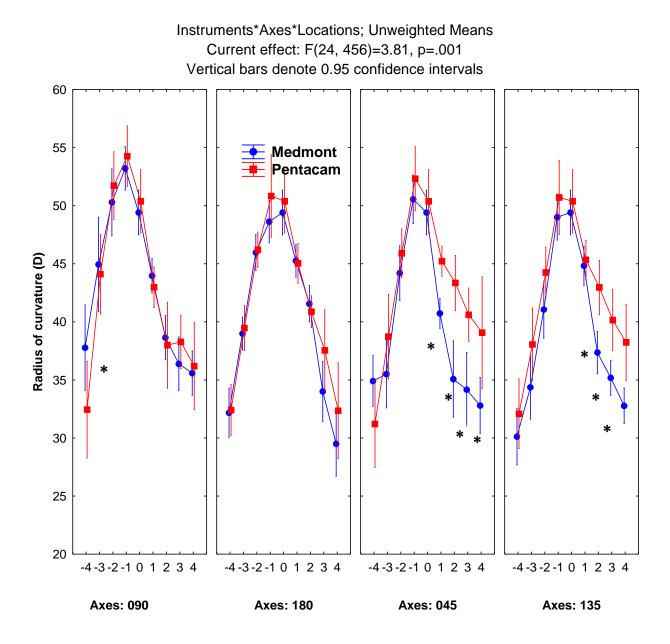
**Figure 4- 3: Plot of instruments, axes and locations of radius of curvature for Medmont E300™ and Pentacam HR®.**

**Note: The asterisks (*) means locations of significant difference.**

Table 4-1 shows the COV expressed in percentage of the mean radius of curvature of the two day visits for both the Medmont E300™ and the Oculus Pentacam HR®. There was more variability relative to the mean in the distribution of the radius of curvature for Oculus Pentacam HR® compared to the Medmont E300™. The central COV for the Oculus Pentacam HR® was 12% and it was slightly higher than the Medmont E300™. The highest variability of the Oculus Pentacam HR® was seen in the -4mm locations in the 090 meridian with COV of 31%.

**Table 4-1: Coefficient of variation (%) of the mean radius of curvature (D) at the centre and selected locations.**

| Visits Locations (%) | | | | |
|---|---|---|---|---|
| | | | Centre | |
| **Instrument** | **Axis** | **-4** | **0** | **4** |
| **Medmont** | **90** | 15.00 | 10.00 | 21.00 |
| | **180** | 15.00 | 10.00 | 23.00 |
| | **45** | 14.00 | 10.00 | 18.00 |
| | **135** | 20.00 | 10.00 | 12.00 |
| **Pentacam** | **90** | 31.00 | 12.00 | 25.00 |
| | **180** | 15.00 | 12.00 | 27.00 |
| | **45** | 26.00 | 12.00 | 28.00 |
| | **135** | 25.00 | 12.00 | 21.00 |

## 4.5 Discussion

Interest in corneal topography in clinical and research purposes has increased in the past decade with the possibility of computerized corneal topography assessment. Radius of

curvature information derived from corneal topography have a number of applications in contact lens fitting and assessment, [8, 54-59] eye modeling and ocular surface aberration analysis, [22, 26, 31, 54] corneal refractive surgery, [38, 60-64] detection and follow-up of corneal pathological condition. [65-68] The relatively recent introduction of orthokeratology have made corneal topographers an indispensable tool, as this procedure relies heavily on the anterior radius of curvature measurements and continual monitoring of the corneal changes following such treatment. [69-79] Current clinical corneal topographers continue to use Placido-based technology, while other devices such as Oculus Pentacam HR® employ Scheimpflug based technology to determine corneal curvature by means of elevation derived data. [45, 48, 49]

In this study, we assessed the repeatability and reproducibility of two devices for measurement of corneal topography; Medmont E300™ and Oculus Pentacam HR® when used to measure CRC. We also looked at the COV at the centre and ±4mm locations in all the meridians.

The mean CRC with the Oculus Pentacam HR® was 50.38±5.81D. This was slightly higher than the Medmont E300™ of 49.41±4.93D. Miháltz et al. [80] measured the radius of curvature of 41 eyes of KC patients using the Oculus Pentacam HR® in the central region. They reported a mean CRC of 50.20±5.70D. De Stefano et al. [81] also reported 50.44±1.69D in KC patients with the same instrument.

We found no significant difference in the combined visits, axes and locations (p=0.12) in the mean topographic radius of curvature with the Medmont E300™. Similar results were found

with the Oculus Pentacam HR® (p=0.24). The Oculus Pentacam HR® generally produced higher CRC measurements although there was no significant difference between the two instruments.

It is interesting to note that the graphs shown in figures 4-1 and 4-2 look like a *"smeared cone"*, especially in the oblique meridians. The steepest cone area (cone apex) is located at the -1mm location for most of the axes and generally starts from the central portion of the cornea. There is flattening in the 2 to 3mm locations and further flattening towards the periphery. This may be explained by the fact that in KC PMD, the cone location is mostly always located in the temporal portion of the cornea and may also give a clue to the location of the cone apex and the extent of the cone diameter. [80] It also points to the fact that in KC and PMD, the most specific changes in the corneal curvature are steepening and protrusion of the cornea and usually temporal to the visual axis. [82-89]

The two instruments were found to be reproducible for most of the locations; however, significant differences were found in the periphery especially in the oblique meridians. Care must be taken interpreting the measurements from the two instruments in the clinical and research settings.

The Medmont E300™ used in this study is a small cone head type topographer based on Placido-based technology. The principle used in calculating the radius of curvature (D) is based on the angle of reflection from the tear film, which is then converted to the slope of the

surface measured. [31] According to Applegate et al., [31] the power (D) of the corneal surface is obtained by differentiation of the slope.

The possible explanation for the slightly lower radius of curvature values in the central and the steepest location may be the instrument's inability to correctly detect the sharp contour of the cornea surface, especially where there is more steeping. According to Mattioli et al., [32] in certain circumstances where there are sharp contours on a given surface, the mire reflections from an irregular surface may be seen to be either overlapping, doubling, or missing. In such situations, they reported that the Placido-ring technology may not measure accurately. In the case of KC, the apex of the cone is slightly displaced in the infero-temporal direction relative to the visual axis. [89-97] The shape of the cone is likely to affect the reflected mires, hence causing them to overlap, which may impact on the accuracy of the radius of curvature measurement. Another optical reason is that, light does not hit the corneal periphery at a normal angle of incidence hence inability to map the cornea. Figure 4-4a shows the loss of information in the corneal periphery.
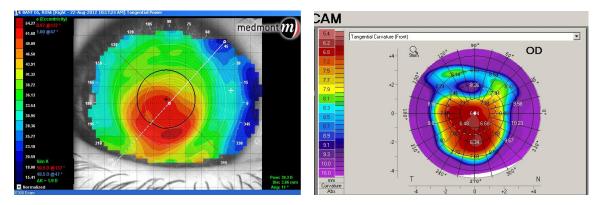
**Figure 4- 4a: KC shown on Medmont E300™ HR®**

**Figure 4- 4b: KC shown on Oculus Pentacam**

**Figure 4- 4 a&b: Tangential corneal topography of KC of the same patient on both Medmont E300™ and Oculus Pentacam HR®.**

González-Méijome et al. [98] found that there were inherent errors when measuring corneal topography with the Medmont E300™. They examined axial curvature in 60 eyes and a second observer registered incidences with the potential to affect data acquisition. They reported 70% of the eyes were very easy to measure, with 27% considered to be difficult and the remaining 3% very difficult. External factors such as fixation instability, head repositioning were the major causes of the difficulty in measuring the corneal topography. Other related factors were tear instability, the patient's upper orbital or nose interference with the keratoscope for centering and focusing processes. Irrespective of the challenges inherent in the use of Placido-based technology in measuring the radius of curvature, there was no significant difference in the repeated visits, axes and locations for the two day visits with the Medmont E300™ and such difficulties were not observed in this study.

The images which are produced by the Oculus Pentacam HR® during the rotation process are

the basis for calculating height data which is used to extrapolate all other results of the anterior segment of the eye. To convert height data to the diopters, the formula (1.3375-1)*(1000)/R mm, where R is the radius of curvature (mm) is used.

In this study, we found that the Oculus Pentacam HR® over-estimated the radius of curvature compared to the Medmont E300™. Our results also show higher variability in the COV in both the central and the periphery of the cornea. According to Shankar et al., [99] the slightly higher variation usually seen in the peripheral cornea on the tangential map with the Oculus Pentacam HR® probably reflects the greater rate of change in peripheral corneal curvature that occurs with the tangential method as a function of calculating curvature locally rather than with reference to the topographer axis. They argue that the greater rate of change in the periphery leaves the peripheral cornea vulnerable to variability. This scenario becomes even worse in the case of KC and PMD, as the degree of flattening becomes apparent from the corneal apex where the cone is usually located. This effect has also been explained by Salmon et al. [100] The effect of Scheimpflug camera's orientation/configuration on the quality of the image is not fully known, however, Chen et al.[24] reported that there is geometrical distortions of the images produced by the instrument. This may impact on some of the corneal parameters.

In conclusion, our results show that each of the instruments per se can give repeatable measurements, as there were no significant differences in the two visits, axes and locations. However, although the two instruments were found to be produce similar results for the majority of locations, there were significant differences between measurements of the two devices particularly for the oblique meridians in the periphery. Therefore, it is crucial to always

identify the specific measurement device when reporting corneal curvature data.

# Chapter 5

## Fitting Semi-scleral Contact Lenses

### 5.1 Introduction

The use of sSCL has become an indispensable option in modern contact lens practice. [1-5] sSCL are indicated for several primary corneal ectasia including KC, [1, 3, 5-8] PMD, [4, 9] post-corneal transplant  (when residual high refractive error and irregular astigmatism cause significant reduction in vision), [2] severe dry eye, [2, 10] neurotrophic keratitis, and multiple other conditions. [7, 10-14]

Recent reports claim that patients who use these lenses exhibit significantly improved VA in the presence of an irregular corneal surface. [10, 15, 16] These lenses also provide mechanical protection and restore function in conditions such as scarred eyelids, entropion, and ptosis. [10] They can also be used to relieve symptoms in dry eye and corneal dystrophies, and to facilitate the healing of corneal epithelial cells following recurrent corneal erosions. [17]

The fitting of sSCL requires that they make no contact with the fragile or sutured cornea and completely vault over the entire cornea to rest on the scleral conjunctiva. [3] Thus, it is important to choose a lens such that the scleral haptic parallels the conjunctival sclera and that the sagittal height of the sSCL is sufficient to completely vault the cornea. [4] This unique fitting characteristic of the sSCL require better understanding of CSD and the precise selection of an initial lens to completely vault the cornea while maximizing the effect on VA and comfort. [4]

To date no study has been undertaken to evaluate the CSD for fitting sSCL.

## 5.2 Objectives

The main aims of this study were:

1. To measure the CSD using Visante™ OCT and to determine its impact on the sSCL selection.

2. To assess the effect of the fitting characteristics of sSCL on the cornea, and how VA is impacted by the choice of fit.

3. To measure the topographic corneal clearance (TCC) of the sSCL using UL-OCT.

4. To assess the effect of time on the TCC over 1 hour of sSCL wear.

5. To assess the comfort ratings of the sSCL.

## 5.3 Materials and Methods

### 5.3.1 Study Design

This was a prospective, non-dispensing fitting study involving two visits. The first visit involved establishing baseline measurements while the second visit facilitated fitting three (3) sSCL on the eye. The CSD was measured with the Visante™ OCT at 15mm chord in the horizontal meridian. This measurement was conducted on the first visit and was used primarily to ensure that participants were eligible based on the availability of the sSCL. Hypothetical values of 325 (Lens 1), 375 (Lens 2) and 425 (Lens 3) µm were randomly added in sequence to the measured CSD. Figure 5-1 summarises the study design. Only the 15mm chord CSD in the horizontal meridian with the Visante™ OCT was used to select the sSCL as this has been evaluated in previous work.[18, 19]

High contrast visual acuity (HCVA) and low contrast visual acuity (LCVA) were measured with the participant's contact lenses or the spectacle prescription presented at Visit 1. The anterior segment was assessed with and without NaFl with the use of slit lamp biomicroscope.
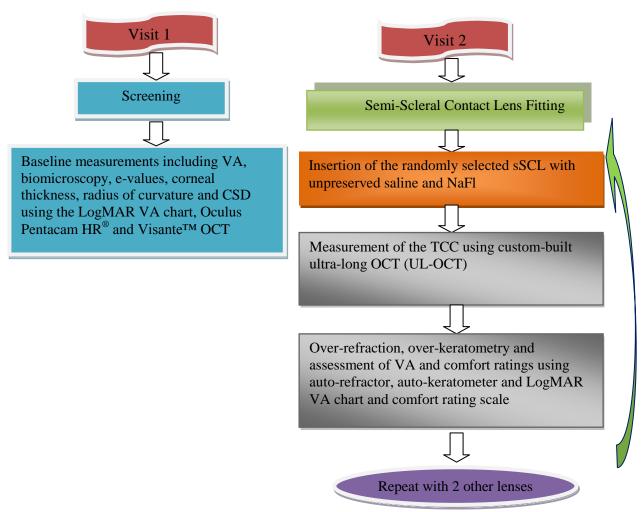


**Figure 5- 1: Study design flow chart**

## 5.3.2 Participants and Recruitment

The participants and recruitment details for the study, inclusion and exclusion criteria have been described in detail in chapter 3 and 4.

### 5.3.3 Study Lenses

### 5.3.3.1 Semi-scleral Contact Lens Design (Jupiter 15mm)

The sSCL used in this study are designed such that they bear on the scleral conjunctiva and completely vault the cornea. The scleral portion is designed to allow adequate tear exchange but hold a relatively large volume of tears. It addresses the most irregular and asymmetric corneas as well as providing a tear reservoir for severe dry eye cases. They are also designed in such a way that the capillary force be maintained to prevent the tear layer from unwarranted bubbles and corneal desiccation.

The Jupiter 15mm has 5 curves (Figure 5-2) that are organized into 3 main zones:

1. The corneal zone, which comprises the central corneal curve and the second curve.

2. The limbal zone area over the limbus.

3. The scleral zone which comprises the landing curve and the edge lift curve.

Depending upon the variations of radius of curvature and the stage of the ectatic or diseased condition being fit, the Jupiter 15 mm sSCL design are grouped into three fit configurations. Changes are made to the fit by varying the posterior design. The Jupiter "standard design" is designed in such a way that the second curve is 2mm (approx. 1.00D) flatter than the central corneal curve and is indicated for KC and post-surgical cornea. The Jupiter "advanced KC design" is designed in such a way that the second curve is 4.00D or 8.00D flatter than the central corneal curve, while the Jupiter "reverse geometry design" has the second curve 4.00D steeper than the central corneal curve.

All the contact lenses of any diameter share the same fundamental design characteristics and the radius of curvature of the lens may range from 4.00 to 9.00 mm.
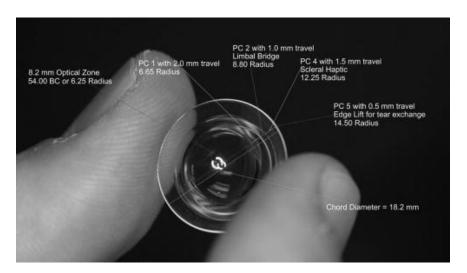


**Figure 5- 2: Jupiter sSCL.**
**PC=peripheral curve.**
**(Photo courtesy Dennis Neifert, Essilor contact lens)**

### 5.3.3.2 Diagnostic Trial Lenses

A fourteen predesigned diagnostic trial lens set (Jupiter 15mm; Essilor) was used in this study. These sSCL have labelled parameters including the back optic zone radius (BOZR) or base curve, power and a standard diameter of 15mm. These sSCL are grouped into 3 main categories represented by B, K and S where B represents a lens edge with a standard periphery, K represents a KC contact lens design with secondary curve of 4D flatter than the base curve and S represents a KC contact lens design with the secondary curve 8D flatter than the base curve. The details of the lens parameters are listed in Table 5-1. These contact lenses are manufactured in Boston XO material with oxygen permeability (DK) value of 100. The material is a fluorosilicone acrylate with an added UV absorber. Figure 5-3a shows the Jupiter 15mm sSCL in a case and figure 5-3b shows the lens fitted on the eye.

Figure 5.3a: sSCL in a case.                     Figure 5.3b: sSCL on the eye.

**Figure 5- 3 a&b: SCL in a case and the lens fitted on the eye.**

**Table 5-1: Parameters of the diagnostic trial set.**

| BOZR (D/mm) | Power (D) | Diameter (mm) |
|---|---|---|
| 40.00/8.44B | 0.00 | 15.00 |
| 42.00/8.04B | -1.75 | 15.00 |
| 44.00/7.67B | -3.50 | 15.00 |
| 46.00/7.34B | -5.50 | 15.00 |
| 48.00/7.03B | -7.75 | 15.00 |
| 50.00/6.75B | -9.50 | 15.00 |
| 52.00/6.49B | -11.75 | 15.00 |
| 54.00/6.25B | -13.50 | 15.00 |
| 57.00/5.92K | -15.50 | 15.00 |
| 59.00/5.72K | -17.75 | 15.00 |
| 61.00/5.53K | -19.25 | 15.00 |
| 63.00/5.53K | -21.25 | 15.00 |
| 66.00/5.36S | -12.50 | 15.00 |
| 68.00/4.96S | -13.75 | 15.00 |

B=standard periphery.

K= KC design (secondary curve is 4D flatter than the base curve).

S= KC design (secondary curve is 8D flatter than the base curve).

### 5.3.3.3 Verification of the Parameters of the Diagnostic Trial Lenses

The diagnostic trial lenses were clinically examined and carefully verified before using them in the study. This was done to ensure the sSCL were devoid of defects and the predefined parameters were within the tolerable range. The radii of curvature were measured with the radiuscope (Bausch and Lomb, Rochester, NY, USA) and the power was measured with a

digital auto lensmeter SLM 5000 (Ryusyo Industrial Co. Ltd., Gun, Japan). The central thickness of the lenses were measured using a thickness gauge (Rehder thickness gauge), while the diameter of the lenses were measured using a profile projector (Mitutoyo Corp., Tokyo, Japan). Slight variations were observed compared to the manufacturer's given values. (Table 5-4)  These variations were found to be within the tolerable range deemed acceptable for the study. The variations were seen in the power of the sSCL while the other parameters were found to be accurate.

### 5.3.3.4 Measurement of Sagittal Depth/Height of Lenses

The sagittal heights (sag) of the sSCL were measured with a radiuscope (Bausch and Lomb, NY, USA) using a technique described by Dr. Stephen Byrnes (Optometrist, Londonderry, NH, USA). [20] A front surface silvered mirror was placed on the stage of the radiuscope directly under the microscope (Figure 5-4a). With the aperture wide open, the mire image was reflected off this surface and brought into focus. (Figure 5-4b). The measuring gauge was set to zero. Next, the sSCL to be measured was placed on the mirror concave side down under the microscope objective lens (Figure 5-4c). The examiner, looking in the eyepiece of the microscope adjusted the lens position on the mirror until the faint, blurred image of the light bulb filament that reflected off the apex of the contact lens was clearly seen. The objective lens of the microscope was moved away from the stage holding the lens and front surface mirror until the filament image came into focus (Figure 5-4d). The objective lens was gradually moved away until the faint reflection of the mire image was seen. This third image was identified as the mire reflecting off the inner surface of the contact lens (Figure 5-4e). Very close to this third image was the fourth image, which reflected off the outer surface of the

sSCL (Figure 5-4f). The smaller aperture was rotated into place and this most distinct image was centred and focused. The measurement was read and recorded as the sagittal height of the front surface of the sSCL (measured perpendicular from the surface of the silvered mirror to the front surface of the sSCL). The centre thickness of the sSCL was measured with a centre thickness gauge (Rehder thickness gauge) and subtracted from the sagittal height of the sSCL to obtain the actual sagittal height of the inside of the sSCL.
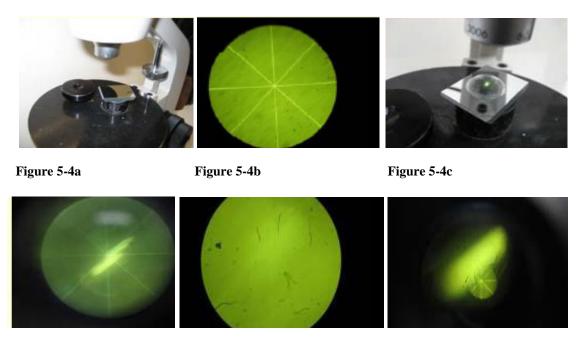


|          Figure 5-4a          |          Figure 5-4b          |          Figure 5-4c          |

|          Figure 5-4d          |          Figure 5-4e          |          Figure 5-4f          |

**Figure 5- 4 a-f: Stages of measurement of the sagittal height of the sSCL.**

**(All photos reproduced with permission from Dr. Stephen Byrnes-Optometrist, Londonderry, NH, USA)**

## 5.4 Study Visits

There were two visits in the study. The first visit involved screening and establishing baseline measurements, while the second visit was for fitting three (3) sSCL on the eye (Table 5-2). The examiner was masked to the sSCL type used in the fitting on the second visit.

The visits consisted of the following.

1. **Screening visit (2 hours per visit)**

   Subject eligibility for the study was determined as well as establishing baseline measurements.

2. **Fitting visit (6 hours per visit)**

   Fitting visit involved fitting three (3) sSCL on the eye and their assessment. Randomization of lenses was assigned. Topographic corneal clearance (TCC), over-refraction, over-keratometry, VA and comfort ratings measurements were obtained.

**5.5 Study Procedure**

**5.5.1 Slit Lamp Biomicroscopy Screening**

A slit lamp biomicroscope was used to examine the anterior segment of the eye. The participants were comfortably seated and properly adjusted on the chin rest making sure that the forehead made contact with the forehead strap. The ocular adnexa, upper and lower eyelids were examined first to rule out any conditions affecting the eye lashes and also any abnormal skin growth. This was followed by examining and quantifying the redness of the bulbar conjunctiva. Participants with redness graded as 75% and above were disqualified and not enrolled. The corneal epithelium, the endothelium as well as the anterior chamber were examined in great detail to rule out any corneal erosion, infiltrates and any abnormal anterior chamber reaction. Classical corneal signs in KC and PMD (such as corneal scar, Vogt's striae, Fleischer's ring, corneal thinning) were recorded and not used to discontinue participants from the study. Participants with extremely thin corneas ($< 200\mu m$) were not enrolled. The cornea

was stained with NaFl and examined with cobalt blue light and a Wratten #12 yellow filter. This was to rule out any excessive corneal staining or marked complications from prior contact lens wear. A cotton swab was used to evert the upper eyelids and the palpebral conjunctiva was examined. Participants with redness graded as 75% and above as well as cobblestone papillae were not enrolled. The eye was finally rinsed with non-preserved Unisol® 4 saline solution and participants were allowed to sit for approximately 5 minutes to ensure the saline had completely dissipated from the eye.

**Table 5-2: Summary of the procedures conducted at the study visits.**

| Visit | Procedure | Instrument | Form (Appendix #) |
|---|---|---|---|
| **Screening & Baseline Measurement** | Sign information and consent letter | Information consent letter | Appendix 3 Information consent letter |
| | Screening | Screening form | Appendix 4 Screening form |
| | Measure VA with present CL or spectacle prescription | LogMAR (HCVA & LCVA) chart | Appendix 5 sSCL examination forms |
| | Assessment of anterior segment with and without NaFl | Slit lamp biomicroscope | Appendix 4 Biomicroscopy form  Appendix 5 sSCL examination forms |
| | Topography measurements | Oculus Pentacam HR® | |
| | Recording of *e-values* | | |
| | Corneal thickness measurement | Oculus Pentacam HR® and Visante™ OCT | |
| | CSD measurement at 15mm chord | Visante™ OCT | |
| **Semi-scleral Fitting and assessment** | sSCL selection and fitting | Diagnostic lens, Unisol® 4 solution and NaFl strip | Appendix 5 sSCL examination forms |
| | Photography of the sSCL lens on the eye | Video slit-lamp biomicroscopy camera, wratten #12 yellow filter | |
| | TCC assessment and measurement. | UL-OCT | |
| | Over-refraction and over-keratometry | Auto-refractor and auto-keratometer | |
| | Assessment of VA | LogMAR (HCVA & LCVA) chart | |
| | Comfort ratings | Comfort rating scale | |

### 5.5.2 Baseline Measurements

Immediately after the screening, the Oculus Pentacam HR® was used to take baseline measurements, including corneal pachymetry, corneal topography (radius of curvature) and eccentricity. The procedure has previously been described in detail in chapters 3 and 4.

The Visante OCT was used to measure the CSD at a 15mm chord. The CSD was primarily used to select the three sSCL for the participants. Eligibility of the participants was determined after the screening and the baseline measurements.

### 5.5.3 Measurement of Corneal Sagittal Depth using the Visante™ OCT

A Visante™ OCT was used to measure the CSD (described in detail in chapter 3). The integrated software (version 2.0) automatically processed the OCT images and displayed the images in the view pane. Acceptable scans were judged to be of adequate quality based on the following criteria: good demarcation of the anterior and posterior boundaries of the cornea, and absence of artefacts.

The built-in callipers were used to measure the CSD of the cornea at a 15mm chord. Two scans were taken at approximately 2 minute intervals and the average CSD of the two measurements was used to select the three sSCL for the participants. Figure 5-5 represents the CSD using the enhanced anterior segment mode.

**Figure 5- 5: CSD measurement with Visante™ OCT.**

## 5.5.4 Semi-scleral Contact Lens Insertion/Fitting

### 5.5.4.1 Semi-scleral Contact Lens Preparation and Disinfection

The lens care system used in this study consisted of: Boston Advance Cleaner, Boston Advance Comfort Formula Conditioning Solution, (Bausch and Lomb Inc., Rochester, NY, USA), Clear Care Cleaning and Disinfectant Solution (CIBA VISION® Inc., Mississauga, ON, CA), and Unisol® 4 Saline Solution (Alcon Laboratories, Inc., TX, USA). To clean the sSCL, Boston Advance Cleaner was used and rubbed gently on the front and back surfaces of the sSCL as recommended by the manufacturer. This was followed by thorough rinsing with the Unisol® 4 saline solution. After this process, the sSCL were disinfected in Clear Care cleaning and disinfectant solution for at least 6 hours. The sSCL were dried with KimWipes® (Sigma-Aldrich, St. Louis, MO, USA) to make sure the sSCL were free from lint and other micro particles. They were stored dry in their respective cases. To fit the sSCL, a drop of Boston Advance comfort formula conditioning solution was used on the front surface of the contact

lenses to provide initial comfort on insertion. Unisol® 4 saline solution was used to fill the sSCL before insertion on the eye.

## 5.5.4.2 Semi-scleral Lens Contact Fitting and Assessment

## 5.5.4.2.1 Selecting the Semi-scleral Contact Lenses from the Diagnostic Trial Lens Set

Based on the CSD measured at a 15mm chord, *hypothetical values* of 325 (Lens 1), 375 (Lens 2), 425 (Lens 3) µm were added to the measured CSD. These values were matched with the sagittal heights of the diagnostic contact lenses. Three sSCL that closely matched these values were chosen for this experiment. A typical example is shown in the tables 5-3 and 5-4 on how the three lenses were selected from the diagnostic trial lens set. Note that the highlighted values (bold) were the available lenses from the diagnostic lenses. The sSCL were randomized by an optometric assistant before they were inserted on the eye.

**Table 5- 3: Selecting sSCL from the diagnostic trial lens.**

| Corneal Sag | Lens 1 (325µm) | Lens 2 (375µm)) | Lens 3 (425µm) |
|:---:|:---:|:---:|:---:|
| **4.17** | 4.49 (**4.39**) | 4.54 (**4.55**) | 4.59 (**4.69**) |
| **3.33** | 3.66 (**3.52**) | 3.71 (**3.72**) | 3.76 (**3.80**) |

**Table 5- 4: Diagnostic trial lenses with sagittal height and thickness.**

| Lens ID | Sagittal Height (mm) | Thickness (mm) |
|---------|----------------------|----------------|
| 1 | 3.45 | 0.45 |
| 2 | **3.52** | 0.50 |
| 3 | **3.72** | 0.50 |
| 4 | **3.80** | 0.50 |
| 5 | 3.97 | 0.51 |
| 6 | 4.06 | 0.55 |
| 7 | 4.23 | 0.48 |
| 8 | **4.39** | 0.50 |
| 9 | **4.55** | 0.54 |
| 10 | **4.69** | 0.40 |
| 11 | 4.88 | 0.40 |
| 12 | 5.07 | 0.43 |
| 13 | 5.20 | 0.50 |
| 14 | 5.40 | 0.50 |

## 5.5.4.2.2 Semi-scleral Contact Lens Fitting and Assessment with Slit Lamp Biomicroscopy and NaFl

The first sSCL was mounted on a suction cup and was well adjusted in place (Figure 5-6a). The lens was then filled with Unisol® 4 saline solution and a strip of NaFl dye was dipped into the saline before insertion, in order to evaluate the fitting characteristics.

Immediately after the lens was inserted onto the eye, (Figure 5.6c) a video-slit lamp camera (Canon Inc., China) was used to examine the sSCL on the eye using cobalt blue and enhancing Wratten #12 yellow filter. This was to ensure there were no bubbles trapped under the sSCL.

Bubbles that were bigger than 3-5mm and caused any discomfort were eliminated by removing the sSCL from the eye and the lens was then re-inserted. Micro bubbles that did not interfere with the visual axis and did not cause any discomfort were left in place on the eye. After 1 hour of wearing the sSCL, the video slit lamp was used to capture the sSCL on the eye. The video-slit lamp camera was set at a magnification of 8x and this setting was used to capture all the images in the experiment. The characteristic fluorescein pattern of the central zone, mid-periphery (over the limbus) and the periphery were assessed and recorded at the end of 1hour of lens wear.




**Figure 5.6a: sSCL mounted on the suction cup.**     **Figure 5.6b: Insertion of the sSCL on the eye.**



**Figure 5-6c: sSCL with NaFl on the right eye.**

**Figure 5- 6 a-c: Stages of fitting the sSCL on the eye.**

### 5.5.4.2.3 Fluorescein Fitting Characteristics Grading Scale

An internally generated grading scale was used as a guide to assess the fit of the sSCL on the eye. The graded areas of the sSCL on the eye were the central, mid periphery; edge width or

axial edge lift (AEL). Numerical values ranging from -2 to +2 where +2 represented the steepest sSCL and 0 represented the "ideal" fit where the sSCL completely parallels/contour the corneal to land on the conjunctival sclera. Any touch on the cornea was graded as negative and depending on the amount of touch on the cornea it was graded as -1 or -2, where most of the sSCL touched the cornea. (See appendix 5) The NaFl fitting characteristics were purely subjective after many trials to effectively assess the fit of the sSCL. The assessment was done at the end of 1 hour of sSCL wear. This grading scale and assessment was used for all the participants.

**5.5.4.2.4 Slit Lamp Photography (Photo-documentation of NaFl patterns)**

The video-slit lamp camera was used to capture the images of the sSCL on the eye. The participants were comfortably seated and properly adjusted on the chin rest making sure that the forehead made contact with the forehead rest. The participants were instructed to fixate on a yellow target on the camera which caused them to look straight ahead and maintain gaze on this target. The slit lamp was gently moved forward to focus on the sSCL. The real-time image was seen on the flat screen monitor connected to the video slit lamp camera. The real-time image guided the examiner to carefully focus on the sSCL to make sure the entire lens could be captured. Once the sSCL was in focus, the participants were asked to blink once and the video slit lamp shutter was pressed once to capture the sSCL on the eye. The image was automatically displayed on the computer screen. The software displays two images at a time for each image. Acceptable images were judged to be of adequate quality based on the following criteria: sharp full image showing the centre, mid periphery and the periphery, no interruption with the eye lashes.

Three images were taken for each sSCL and this procedure was repeated for all the other lenses used in the study (Figure 5-7).
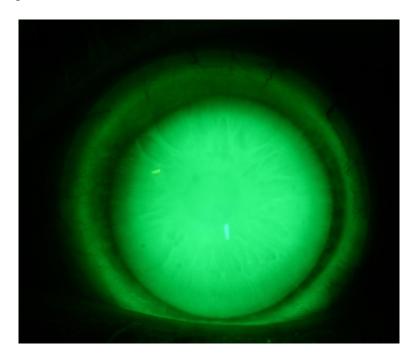


**Figure 5- 7: sSCL on the eye.**

## 5.5.4.2.4 Measurement of Tear Film Width/Topographic Corneal Clearance with UL-OCT

A custom-built UL-OCT was used to take corneal topographic images of the sSCL on the eye. These measurements were carried out at approximately 10 minute intervals over a period of 1 hour to determine the effect of time on the tear film clearance. The amount of TCC was measured using the instrument's custom-built software.

## 5.5.4.2.5 Imaging the Semi-scleral Contact Lens on the Eye

The UL-OCT used to capture the images of the sSCL on the eye has been described in detail in chapter 1.

No direct contact on the eye was made with the instrument. The participants were comfortably seated and properly adjusted on the chin rest making sure that the forehead made contact with the forehead strap. A scan depth of ~7.441mm, a scan width of up to 14mm and an optical resolution of up to ~6μm was used to image all the sSCL on the eye. The focal plane was set to 2.8mm to capture all the images. The scan measurements were done in the vertical meridian using the appropriate settings. The participants were instructed to fixate on a blue target in the instrument in order to correctly align the eye with the optics of the instrument for easy measurement and evaluation. No fluorescein was used after the insertion of the lens to avoid unnecessary *"fluorescein flooding"* of the eye, which may have affected the TCC.

The examiner focussed and adjusted the joystick until the real-time image of the surface of the sSCL was shown on the computer monitor, with the instrument showing at least 13mm diameter of the sSCL in both the *x*-and *y*-meridians. The real-time images displayed on the screen guided the investigator to perfectly align both the *x* and *y*-meridians of the sSCL. The image was considered to be optimally aligned when the specular reflex (vertical streak line), which has a high intensity, was reflected from the center of the front surface of the sSCL. The participants were also instructed to keep their eyes wide open during scanning. Once this was achieved, a manual footswitch was hit once to scan the sSCL eye. The integrated software automatically processed the OCT image and displayed it in the view pane. Acceptable scans were judged to be of adequate quality based on the following criteria: good demarcation of the anterior and posterior boundaries of the sSCL, good demarcation of the front and back surface of the cornea, vertical and horizontal alignments and absence of artefacts in the scanned area.

The UL-OCT processes three scan images at a time in approximately two seconds. The scan images were immediately assessed and evaluated to make sure they were within the established standards of imaging a contact lens on the cornea. Again, this was to ensure that the scans were not affected by poor alignment/misalignment with the optics of the instrument. If any misalignment was observed, the instrument was readjusted and the scan was repeated. After every scan, the UL-OCT was moved backwards and realigned for the next scan to ensure interdependence of the readings. This procedure was repeated at approximately 10 minute intervals for a period of 1 hour for each of the three sSCL fitted on the eye. The scans took place in normal lighting and the same environmental conditions were maintained for all measurements

### 5.5.4.2.6 UL-OCT Image Processing and Analysis

Using the recommended custom-built software for image analysis, the images were first processed into a readable (*FFT) format. Image J software (National Institutes of Health, Bethesda, MD, USA) [21] was used to resize all the images into an appropriate size (2048 x 1088pixels) required for a 14mm image scan. The investigator manually outlined at least 25 reference points (**a, b** and **c**) (figure 5-8) on the front and back surfaces of the sSCL and the front surface of the cornea image was displayed on a 22-inch flat screen monitor (LG Flatron W2242TQ) using the custom-built image analysis software (TD Analyzer). The software simultaneously calculates the thickness of the three surfaces (**a** and **b**, **a** and **c**). To obtain the TCC (**d**), the total thickness of the front surface of the sSCL and the front surface of the cornea were subtracted from the front and back surfaces of the sSCL. The values were recorded in 1mm intervals at the central 8mm of the entire diameter of the sSCL, as this dimension was

found to give consistent values (Figure 5-8). To account for the fact that light was passing through the thick sSCL and through the tear film layer, a correction factor of **1.336** was used, which accounts for the refractive index of the tear film layer. The upper half (upper eyelid area) was recorded with a positive sign, while the lower half (lower eyelid) was recorded with a negative sign. This procedure was used to analyze all the scan images, with seven scan images for each of the three sSCL.
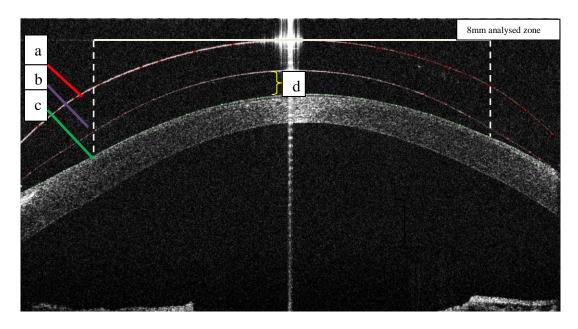


**Figure 5- 8: Scan of the sSCL on the eye.**

**The reference points outlined on the surfaces of interest are indicated by the colours red, purple and green. The letters "a"=front surface of the sSCL, "b"= back surface of the sSCL, "c"= front surface of the cornea and "d"= tear film layer/topographic corneal clearance. The horizontal thick line represents the 8mm analysed zone area while the vertical thick dotted lines represent the range (8mm) within which the measurements were recorded at 1mm intervals.**

### 5.5.4.2.7 Over-refraction and Visual Acuity Assessment

At the end of 1 hour of sSCL wear, over-keratometry and over-refraction were performed to measure the residual astigmatism and the corresponding refractive power. The sphere and the cylinder powers were recorded.

Spherical subjective refraction was performed over the sSCL using the phoropter. To measure the VA, a standard LogMAR visual acuity chart was projected on the computer screen. HCVA and LCVA were measured and recorded in decimal values as it is consistent with the use of LogMAR VA chart. This procedure was used for all participants.

### 5.5.4.2.8 Comfort Rating

Before removing the sSCL at the end of the 1 hour, the participants were asked to give a comfort rating score for the sSCL. This subjective rating was assessed using a comfort grading scale ranging from zero (representing very poor comfort) to 100 (representing excellent comfort). Figure 5-9 shows the comfort rating scale. This procedure was repeated for all three sSCL in this experiment.

0                                                                    100
|——————————————————————————————————————————————|
Very poor comfort                                    Excellent comfort
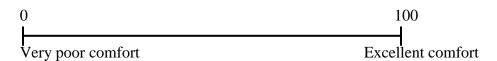
**Figure 5- 9: Comfort rating scale.**

### 5.6 Data Management and Analysis

Data analysis was conducted using Statistica 11 (StatSoft. Inc., Tulsa, OK, USA). The means and SD were used to analyse the CSD as well as the VA. Analysis of variance (ANOVA) was

performed to determine the statistical significance of the HCVA and LCVA as well as comfort ratings with the three sSCL. *P* values of less than 0.05 were considered statistically significant. Pearson correlation was also performed to determine the relationship between the HCVA and LCVA and comfort rating for all the three sSCL. To determine the effect of time on the TCC, the differences between the corneal TCC at time 0, 20, 40 and 60 minute intervals were taken. The mean and SD were also determined. Two point locations (±3mm) in the upper and lower portions of the cornea were taken for the TCC analysis for all the sSCL.

**5.7 Results**

The mean age, sex, and the visual correction presented by the participants at the time of study has been described earlier in chapters 3.

The mean K-reading was 48.72±4.11D while the steepest K-reading was 56.57±7.39D. The mean CCT was 493.89±39.55µ while the overall cone diameter was 4.19±1.13mm. The mean CSD in the horizontal meridian was 3.78±0.53 (ranges: 3.33-4.17) mm at 15mm chord. The measurement of the CSD in horizontal meridian was used to select the three sSCL from the diagnostic trial lenses as this meridian has been evaluated by some researchers. [18, 19]

The table below shows the baseline measurements obtained on the first visit of the study.

**Table 5- 5: Mean baseline measurements.**

| | K-readings (D) | | | | Pachymetry (µm) | | CSD (mm) | Cone diameter (mm) | | Eccentricity |
|---|---|---|---|---|---|---|---|---|---|---|
| | Sim Flat | Sim Steep | Average | Steepest | Centre | Thinness | @ 180 | Apex | Overall | e |
| **Mean** | 46.90 | 50.75 | 48.72 | 56.57 | 493.89 | 447.85 | 3.78 | 2.00 | 4.19 | 0.83 |
| **SD** | 4.45 | 4.02 | 4.11 | 7.39 | 39.55 | 48.76 | 0.53 | 1.14 | 1.13 | 0.26 |

The details of the topographic pachymetry as well as radius of curvature have been described in chapters 3 and 4.

The mean sagittal height of the sSCL was 4.38±0.63 (range: 3.46-5.53) mm. The mean central thickness of the sSCL was 0.50±0.05 (range: 0.48-0.56) mm. The residual astigmatism (flexure) for all the three lenses was insignificant (-0.23±0.14) likely due to the thickness of the lenses.

Slight differences (±0.25D) in the power measurement were found with the 46.00/7.34B and 61.00/5.53K sSCL as well as the total diameter of the sSCL. However, they were all within the tolerable range for the study. The table below shows the measured parameters of the diagnostic trial lenses.

**Table 5- 6: Measured parameters of the diagnostic trial lenses.**

| Lens | Total Sag(mm) | Power (D) | Diameter (mm) | Central Thickness(mm) |
|---|---|---|---|---|
| 40.00/8.44B | 3.46 | 0.00 | 15.00 | 0.48 |
| 42.00/8.04B | 3.71 | -1.75 | 15.05 | 0.53 |
| 44.00/7.67B | 3.86 | -3.50 | 15.04 | 0.55 |
| 46.00/7.34B | 3.82 | -5.75 | 15.05 | 0.52 |
| 48.00/7.03B | 3.93 | -7.75 | 15.05 | 0.55 |
| 50.00/6.75B | 4.23 | -9.50 | 15. 05 | 0.56 |
| 52.00/6.49B | 4.23 | -11.75 | 15.05 | 0.51 |
| 54.00/6.25B | 4.45 | -13.50 | 15.07 | 0.51 |
| 57.00/5.92K | 4.42 | -15.50 | 15.00 | 0.51 |
| 59.00/5.72K | 4.47 | -17.75 | 15. 03 | 0.41 |
| 61.00/5.53K | 4.75 | -19.00 | 15.00 | 0.41 |
| 63.00/5.53K | 5.10 | -21.50 | 15.00 | 0.45 |
| 66.00/5.36S | 5.37 | -12.50 | 15.02 | 0.50 |
| 68.00/4.96S | 5.53 | -13.75 | 15.02 | 0.53 |

It was evident that most Lens 1 options touched the cornea or were slightly decentered after 1 hour of sSCL wear. The areas of touch were seen in the mid-periphery, the nasal or the temporal portions of the eye (Figure 5-10b).

Figures 5-10a-b show sSCL Lens 1 fitted on different eyes with different characteristic pattern after 1 hour of sSCL wear. The NaFl characteristic grading concentrated on the central (C), mid periphery (MP) and the axial edge lift (AEL).

sSCL parallels on the cornea with visible iris. The AEL was optimal.

**Figure 5-10a: sSCL Lens 1**



Visible touch on the nasal portion with slight central pooling.
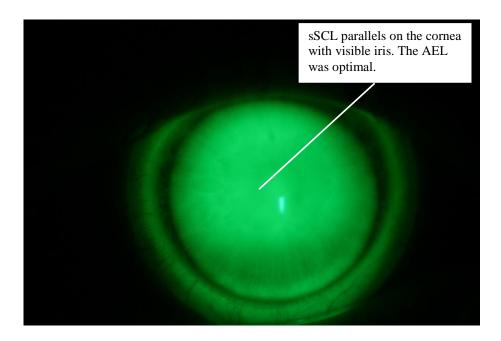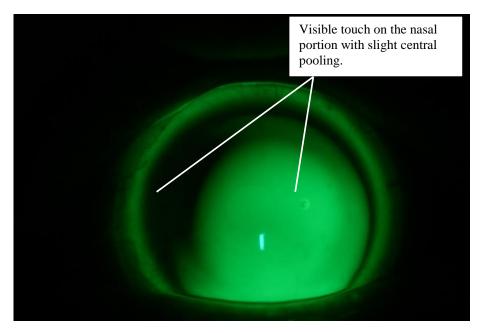
**Figure 5-10b: sSCL Lens 1**

**Figure 5- 10 a&b: sSCL Lens 1 fitted on two eyes with different NaFl patterns.**

**Lens 1 in figure 5-10a was graded with C=0, MP=optimal, AEL=optimal. Lens 1 in figure 5-10b was graded with C=0, MP=-1, AEL=optimal.**

Most Lens 2 options exhibited adequate vault over the entire cornea to the limbal region. This resulted in improvement in vision (similar to Lens 1). Figures 5-10 a&b show sSCL (Lens 2) fitted on two eyes with characteristic patterns after 1 hour of wear.



Adequate vault over the entire cornea with optimal AEL.

**Figure 5-11a: sSCL Lens 2**

Adequate vault over the entire cornea with "feathery" touch in the upper area and visible AEL
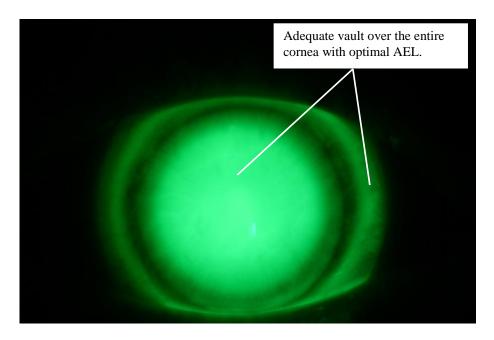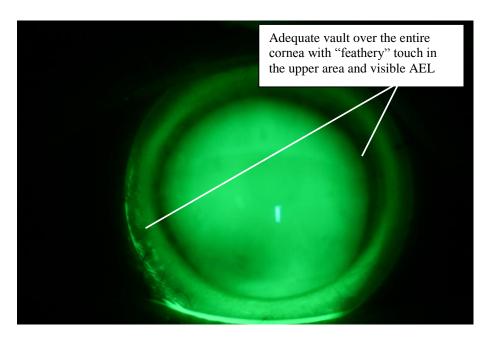
**Figure 5-11b: sSCL Lens 2**

**Figure 5- 11 a&b: sSCL Lens 2 fitted on two eyes with different NaFl patterns.**
**Lens 2 in figure 5-11a was graded with C=1, MP=1, AEL=0. Lens 2 in figure 5-11b was graded with C=1, MP=1, AEL=1.**

Lens 3 yielded excessive TCC especially in the central portion. The central pooling over the cornea extended partly to the mid-periphery. Generally, there was slight reduction in VA compared to Lens 1 and 2. Comfort level with Lens 3 was quite high similar to Lens 1 and Lens 2. Figures 5-12a-b show Lens 3 fitted on different eyes with characteristic patterns after 1 hour of wear.

Excessive CCC (pooling) with slightly tight AEL (dark band)

**Figure 5-12a: sSCL Lens 3**



Excessive CCC (pooling) with slightly tight AEL (dark band)
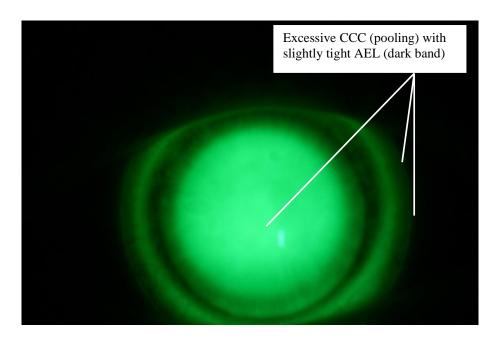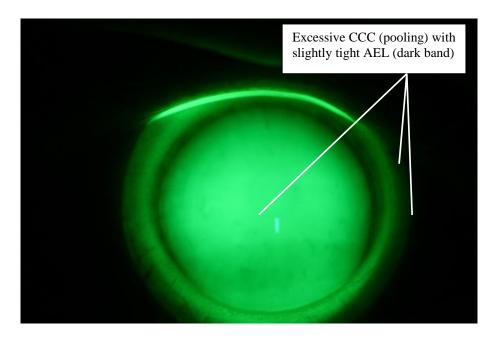
**Figure 5-12b: sSCL Lens 3**

**Figure 5- 12 a&b: sSCL Lens 3 fitted on two eyes with slightly different NaFl patterns.**

**Lens 3 in figure 5-12a was graded with C=+2, MP=+1, AEL=+1. Lens 3 in figure 5-12b was graded with C= +2, MP=+2, AEL=+2.**

Analysis of variance for all the three sSCL show there were statistically significant differences in the time, lens and locations (p=0.001) after 1 hour of sSCL wear. Figure 5-13 shows mean TCC and the effect of time on all the three sSCL at the different locations on the cornea. It is evident from the graph that Lens 1 did not have enough clearance and has evidence of corneal touch. The corneal touch was evident with the NaFl mostly in the nasal and superior portions on the cornea (Figures 5-10a&b). Lens 2 exhibited a TCC within a documented acceptable range, [3, 10, 22, 23] while Lens 3 had unacceptable TCC (too high) even after 1 hour. The difference between Lens 1 and 2 on the graph could be considered as a critical amount, below which the sSCL chosen will likely vault less and increase the possibility of touching any part of the cornea. This could impact on the NaFl fitting characteristics as well as comfort, although VA may be increased.
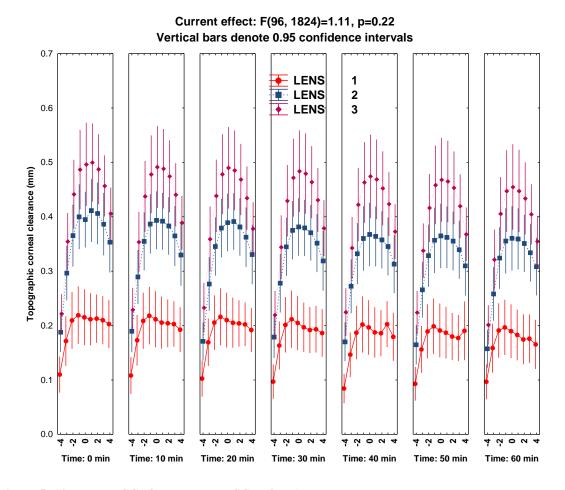
**Figure 5- 13: Mean TCC of all the three sSCL after 1 hour.**

**Note: Lens 3 has excessive TCC even after 1 hour of sSCL wear. Lens 1 has the least TCC. The negative sign on the *x-axis* represent inferior location and the positive sign represent superior location in the 8mm diameter at 1mm interval.**

The overall mean and SD of the CCC loss (CCCl) after 1 hour for all the three sSCL was $0.03\pm0.08$mm ($30\pm80\mu$m). Table 5-5 shows the mean and SD of $\pm3$mm locations in the superior and inferior portions of the cornea. The greatest CCCl was found with Lens 3. The CCCl for Lens 3 was $0.04\pm0.05$mm ($40\pm50\mu$m) at the end of 1 hour of the SCL wear. There was no significant change over time from insertion to 60 minutes ($p>0.05$) at the central and $\pm3$mm locations for each of the three lenses.

**Table 5- 7: Mean TCC loss (μm) and SD at the end of the 1 hour and the selected points.**

| | Lens 1 | | | Lens 2 | | | Lens 3 | | |
|---|---|---|---|---|---|---|---|---|---|
| | **Superior** | **Location** | **Inferior** | **Superior** | **Location** | **Inferior** | **Superior** | **Location** | **Inferior** |
| **Time** | **+3** | **Centre** | **-3** | **+3** | **Centre** | **-3** | **+3** | **centre** | **-3** |
| **20 min** | 0.00±10.00 | 10.00±10.00 | 10.00±20.00 | 20.00±40.00 | 10.00±20.00 | 20.00±60.00 | 0.00±30.00 | 10.00±20.00 | 20.00±30.00 |
| **40 min** | 30.00±20.00 | 20.00±30.00 | 10.00±90.00 | 20.00±60.00 | 30.00±60.00 | 40.00±70.00 | 10.00±20.00 | 20.00±20.00 | 30.00±30.00 |
| **60 min** | 10.00±10.00 | 30.00±30.00 | 30.00±40.00 | 40.00±60.00 | 30.00±60.00 | 50.00±70.00 | 30.00±30.00 | 40.00±50.00 | 50.00±50.00 |

Irrespective of the small amount of TCC loss, there were variations among these values after 1 hour of lens wear. A typical example is shown for Lens 1 (Figures 5-14a&b), where there was CCCl of 104µm after 1 hour of sSCL wear. This was found to be significantly higher compared to Lens 2, where there was 50µm CCCl, while Lens 3 recorded only 6µm. The changes in the CCCl were evident under the slit lamp biomicroscope and UL-OCT. Figures 5-14a-h show the three sSCL fitted on the same eye with varied CCCl after 1 hour. The details of the TCC loss of selected time intervals and locations for all the three SCL are shown in the appendices.
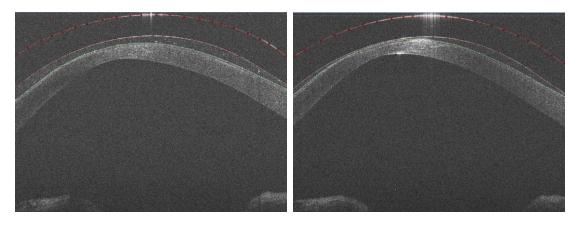


**Figure 5-14a: Time @ 0 minute for Lens 1.**     **Figure 5-14b: Time @ 60 minutes for Lens 1.**



"Slight" touch

Visible touch
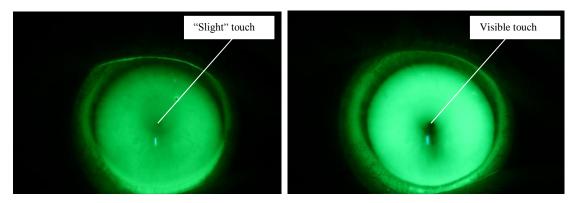
**Figure 5-14c: NaFl @ 0 minute for Lens 1.**     **Figure 5-14d: NaFl @ 60 minutes for Lens 1.**
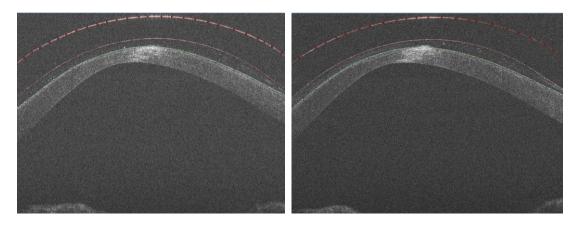
**Figure 5-14e: Time @ 0 minute for Lens 2.**    **Figure 5-14f: Time @ 60 minutes for Lens 2.**
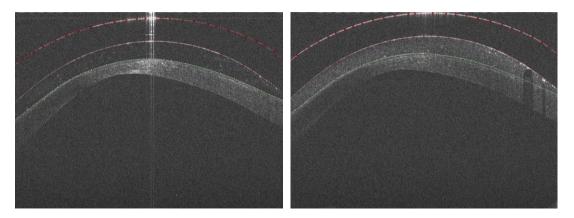


**Figure 5-14g: Time @ 0 minute for Lens 3.**    **Figure 5-14h: Time @ 60minutes for Lens 3.**

**Figure 5- 14 a-h: UL-OCT images and NaFl patterns of the three sSCL fitted on the same eye for 1 hour. Note: Visible touch in Lens 1 after 1 hour. This was evident both in the UL-OCT scan and the NaFl pattern. The CCC loss for Lens 1 was 104 μm (Figure 5-14 a&d), Lens 2 was 50 μm (Figure 5-14e-f), Lens 3 was 6 μm (Figure 5-14g-h).**

At the end of the 1 hour of sSCL wear, mean CCC was 190±100μm, 360±120μm and 450±170μm for each lens respectively (p=0.001). Lens 1 had the least CCC while Lens 3 had the highest corneal clearance value. Further analyses of Lens 1, 2 and 3 show that there were statistically significant differences in time and location (p=0.001), except for Lens 1 (p=0.06).

It is evident from Figure 5-15 and 16 that there was no change in TCC after 30 minutes; however, in Lens 3 (figure 5-17) there was a change even at the end of the 1 hour.

Current effect: $F_{(48, 912)}=1.35$, $p=0.06$

Vertical bars denote 0.95 confidence intervals
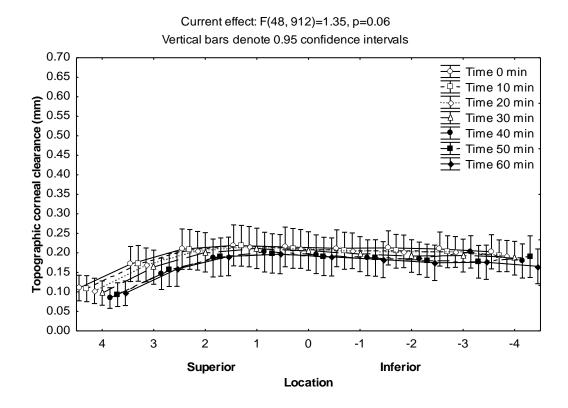


**Figure 5- 15: Mean CCC and effect of time on sSCL Lens 1.**

Current effect: F(48, 912)=1.68, p=0.00
Vertical bars denote 0.95 confidence intervals
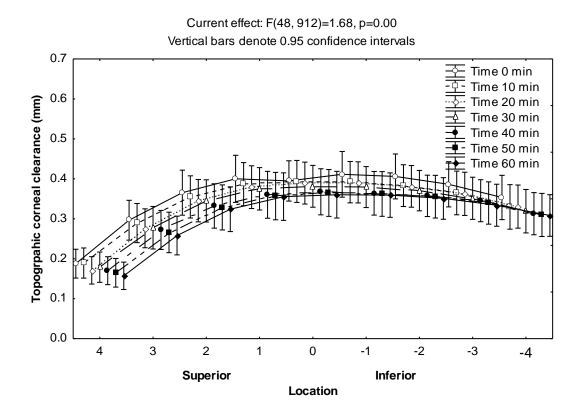
**Figure 5- 16: Mean CCC and effect of time on sSCL Lens 2.**

**Current effect: F(48, 912)=1.59, p=0.01**
**Vertical bars denote 0.95 confidence intervals**
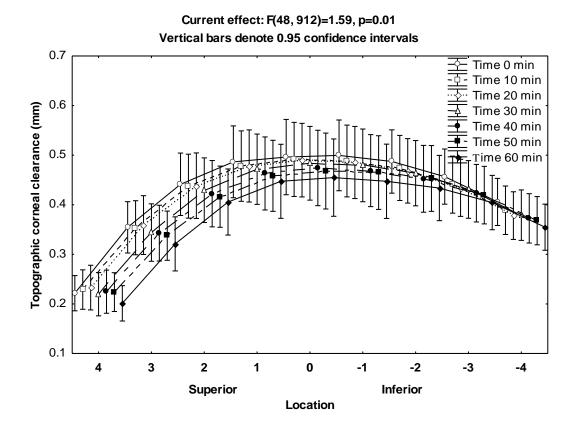
**Figure 5- 17: Mean CCC and effect of time on sSCL Lens 3.**

The mean HCVA was highest for Lens 1 (LogMAR=0.05±0.12). Lens 3 recorded the lowest HCVA (LogMAR=0.11±0.08). There was a significant difference between the three lenses (p=0.02). Tukey post hoc analysis shows that there was no significant difference between Lens 1 and Lens 2 (p=0.32) or Lens 2 and Lens 3 (p=0.27), however, there was a significant difference between Lens 1 and Lens 3 (p=0.01). Similar findings were found for LCVA, with p=0.02. Tukey post hoc analysis shows that only Lens 1 was significantly different from Lens 3 (p=0.02). Table 5-6 shows the mean and SD of the HCVA and LCVA for the three sSCL.

**Table 5- 8: Mean HCVA and LCVA.**

|  | HCVA | | | LCVA | | |
|---|---|---|---|---|---|---|
|  | **Lens 1** | **Lens 2** | **Lens 3** | **Lens 1** | **Lens 2** | **Lens 3** |
| **Mean** | 0.05 | 0.07 | 0.11 | 0.41 | 0.45 | 0.50 |
| **SD** | 0.12 | 0.11 | 0.08 | 0.16 | 0.19 | 0.17 |

The overall comfort rating for all three sSCL was 77.7±10.6 (range: 40-100). From Table 5-7, Lens 2 recorded the highest comfort rating with 79.7 ±11.6 after 1 hour of wear, while Lens 1 recorded the lowest comfort rating of 74.9±9.2. There was no statistically significant difference between the three lenses (p=0.24).

**Table 5- 9: Mean comfort ratings for all three sSCL.**

| COMFORT RATINGS | | | |
|---|---|---|---|
|  | **Lens 1** | **Lens 2** | **Lens 3** |
| **Mean** | 74.9 | 79.7 | 78.6 |
| **SD** | 9.2 | 11.6 | 10.8 |

Pearson correlation was performed to assess the relationship between comfort and VA for Lenses 1, 2 and 3 for both HCVA and LCVA. There was no correlation between comfort and VA for all the sSCL, with the exception of HCVA for Lens 2, where there was a negative correlation. (Figure 5-20).

The figures below show the correlation between HCVA and LCVA and comfort for all the sSCL.
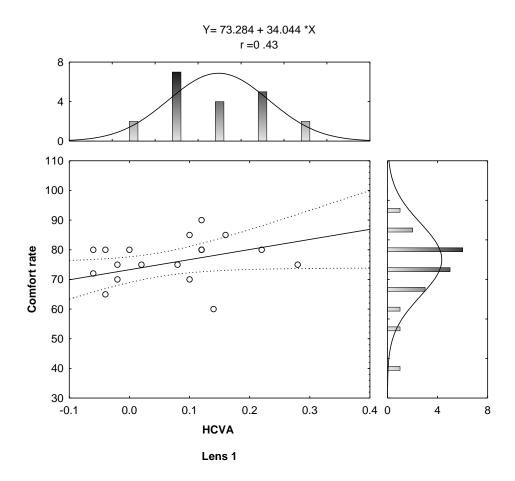


Figure 5- 18: Correlation between HCVA and comfort for Lens 1.
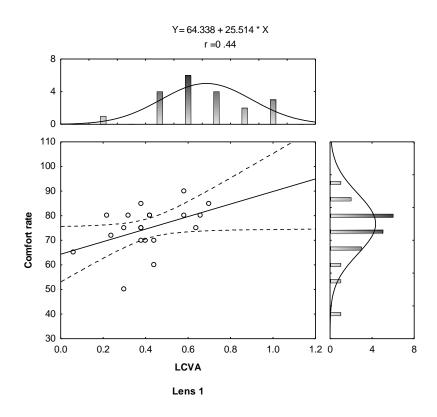
**Figure 5- 19: Correlation between LCVA and comfort for Lens 1.**
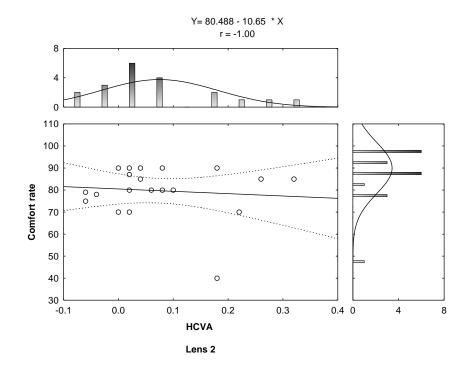


**Figure 5- 20: Correlation between HCVA and comfort for Lens 2.**

129

Y= 76.457 + 7.1913 * X
r =0.12

Lens 2
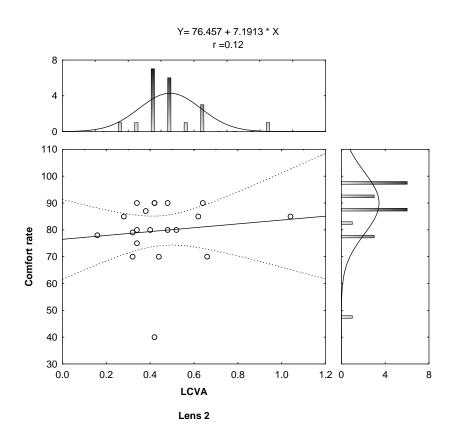
**Figure 5- 21: Correlation between LCVA and comfort for Lens 2.**



Y= 79.040 - 3.899  * X
r =0 -.03

Lens 3
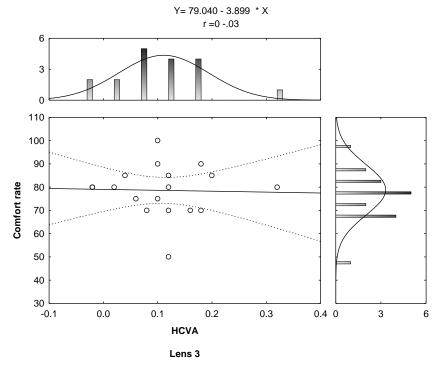
**Figure 5- 22: Correlation between HCVA and comfort for Lens 3.**
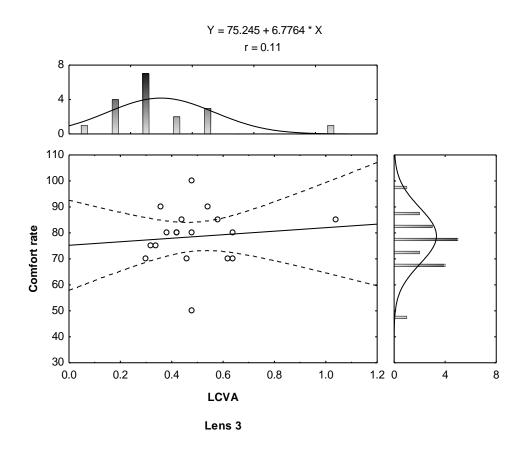
**Figure 5- 23: Correlation between LCVA and comfort for Lens 3.**

.

## 5.8 Discussion

Recently, there has been a marked resurgence in interest in the use of sSCL for managing various conditions. The major advantage is that they offer greater comfort compared to regular RGP lenses and can provide some therapeutic effects in some conditions affecting the cornea. [24] These lenses are primarily indicated for use in KC, PMD and other corneal ectasia, [1, 10, 24-27] post graft management, [21] dry eye [28, 29] and limbal cell disease. [30] They are also indicated for complicated cases such as Sjogren's syndrome, ocular cicatricial pemphigoid and other related conditions. [29, 31-33]

131

In this study, we experimentally assessed whether sSCL can be appropriately fitted using CSD measurements on patients diagnosed with KC (n=18) and PMD (n=2). We evaluated the CSD and how to effectively use this measurement to select sSCL from the diagnostic trial lenses. Fitting characteristics of the sSCL based on the NaFl pattern under the slit lamp biomicroscope in the central, mid periphery and the peripheral regions were assessed. The HCVA and LCVA as well as comfort ratings were also assessed at the end of 1 hour of lens wear.

The mean CSD in the horizontal meridian was 3.78±0.53 (range: 3.33-4.17) mm at 15mm chord. Similar results have been previously reported by Sorbara et al. [18]

The majority of the sSCL vaulted completely over the cornea to rest on the conjunctival sclera. An interesting observation was the fact that most of the sSCL were seen to be tight, with a "yellowish ring/band" in the mid-periphery, followed by a slightly dark band, indicating a tight or inadequate AEL. A possible explanation of this pattern could be attributed to the design of the sSCL (from the transitional zone to the landing zone) perhaps to make the lens more stable in the mid periphery on the corneal with slight flattening towards the periphery to allow for adequate tear film exchange.

The estimation of the appropriate TCC (especially CCC) remains a challenge to effectively fit and assess these lenses. The controversy lingers on the amount of clearance expected between the corneal epithelium and the back surface of the sSCL. Some authors have suggested 250µm, [10] or 100-400µm. [25] According to 1997 ISO for Ophthalmic Optics-contact lenses and contact lens products, [34] CCC was recommended to grange between 200 to 300µm for optimal fit. To

subjectively quantify the amount of clearance, Schornack et al. [25] suggested ¼ or ½ of the tear film thickness to the corneal thickness through the optic section of the slit lamp biomicroscope. In this study, we added 325 (Lens 1), 375 (Lens 2) and 425 (Lens 3) µm respectively to the CSD to select three sSCL to fit on the eye.

At the end of the 1 hour of sSCL wear, mean CCC was 190±100, 360±120 and 450±170 µm for each lens respectively (p=0.001). The mean CCC loss after 1 hour for all the three sSCL (Table 5-5) was 0.03±0.08mm (30±80µm). Caroline et al. [35] reported an average of 96 (range: 70-180) µm of apical corneal clearance (ACC) loss after 8 hours of sSCL on normal eyes. Mountford [36] reported 146 (range: 106-186) µm of ACC loss after one month of sSCL. One question that remains unanswered is the thickness profile of the sSCL used in their study and the clinical effects of the ACC loss on the VA and comfort rate. Irrespective of the small CCCl found in this study, there were variations at the end of the 1 hour period.

The cause of the variations are unknown; however, we propose that eyelid force, dissipation of the saline or the tear film reservoir, design of the sSCL scleral zone radius, thickness profile, flexure and other unknown factors may be responsible for such variations.

To assess the success of sSCL, VA plays a very important role. Schornack et al. [25] hypothesized that the amount of TCC between the posterior surface of the sSCL and the anterior surface of the cornea is not critical to the successful fitting of these lenses. In this study, we found a significant difference in the TCC (p=0.001) of the three lenses. There was also significant difference between Lenses 1 and 3 in both HCVA and LCVA. Tukey post hoc

analysis for both HCVA and LCVA for comparing Lenses 1and 3 were p=0.01 and p=0.02 respectively. We found poor correlation in both HCVA and LCVA for the lenses. Based on our results, we suggest that their hypothesis is not necessarily correct. Fitting sSCL with increased or excessive amount of CCC may not give the best VA though comfort rate may be high.

Comfort and successful wearing of sSCL have been documented by various authors. [4, 27] In this study, the overall comfort rating was 77.7±10.6. There was no significant difference (p=0.24) in the comfort ratings for the three lenses. Visser et al. [27] reported comfort rate 78.9 in their study with sSCL.

From our results, it is evident that Lens 2 (CCC=360µm) gave the best combination of VA and comfort ratings. In clinical practice, it may be important to consider the mean CCCl (30µm) to select the initial sSCL. Therefore, the suggested mathematical expression to select the initial sSCL is given by:

**Initial sSCL= mCSD+mCCC+mCCCl**

Where;

mCSD represents mean CSD, found to be 3.78mm,

mCCC represents mean CCC, found to be 0.36mm and

mCCCl represents mean CCC loss, found to be 0.03mm.

In order to choose the initial lens from the diagnostic trial lens set, add the CSD and the amount of CCC and the anticipated CCCl (i.e Initial sSCL=3.78+0.36+0.03=4.17mm). Thus, according to our study, the initial sSCL sag value to start is **4.17mm (4170µm).** Fluorescein

pattern must be assessed, especially the AEL, and this must be balanced with the resultant VA and comfort rating of the lens.

In conclusion, our results show that a mCCC of "360"μm could be the "starting point" clinical value to add to the measured CSD and the expected CCCl to choose the initial sSCL for fitting and assessment on the eye. It is also evident from our study that adding more than 400μm to the measured CSD may affect the HCVA and LCVA (Figure 5-12a&b). Adding the range of less than 200μm may also cause the sSCL to touch the cornea, especially the superior part of the cornea or the corneal apex. This will likely reduce the comfort ratings, though there may be an improvement in VA.

Based on our findings in this study, we propose the following:

1. Evaluation of CSD can be used to effectively select sSCL to fit on the eye.

2. The results suggest that lens 2 (adding 375μm with mCCC=360μm to the CSD) gave the best combination of VA and comfort ratings. However, evaluation of the fluorescein pattern must be balanced with the VA and comfort ratings for successful fitting in a clinical setting.

3. There is a likelihood of TCC loss after 1 hour of sSCL wear. However, this will vary and depends on many factors, including eyelid force, design of the sSCL, and dissipation of the saline or the tear film reservoir, scleral zone radius, thickness profile, flexure and other unknown factors.

4. LCVA could be used as a predictor for successful fit for sSCL when improvement in VA is the primary reason for fitting the lenses.

5. Allowing the patient to sit for approximately 1 hour is clinically important to determine the actual fit of the lens especially the AEL.

6. Further research is needed to confirm the validity of the mCCC of "360" µm.

# Chapter 6

## General Discussion

This thesis has mainly focussed on using OCT and Oculus Pentacam HR® as aids to fitting sSCL. It also focussed on how to effectively use the CSD using Visante™ OCT to select the appropriate sagittal depth of sSCL to fit on the eye. In addition, the evaluation of the sSCL fitting characteristics with NaFl was subjectively assessed. The UL-OCT was used to quantify the TCC and its change over time. Questions pertaining to initial sSCL selection, amount of CCC and CCCl were assessed and evaluated. Measurement of HCVA and LCVA as well as comfort ratings were also evaluated. Repeatability of the instruments in measuring the radius of curvature on test surfaces, radius of curvature on the corneal surfaces as well as evaluating the corneal thickness in KC and PMD corneae were also reported.

Chapter 2 focussed on the repeatability of the Oculus Pentacam HR® on predefined test surfaces (polycarbonate aspheric surfaces). There was no statistically significant difference in the measurements among the three day sessions for the radii of curvature, however, slight variations were found with the instrument. There was no statistically significant difference between the three day sessions for the shape factors, with the exception of one test target (brown). Significant correlations were also found with both the radii of curvature and shape factors for the three day sessions. Because of the small number of the test surfaces and variation in the radii of curvature and shape factors, the results could not predict whether the Oculus Pentacam HR® had a specific bias, that is, to either over or under-estimate the predefined surfaces.

To the best of my knowledge, there is no available report [1] with the  Oculus Pentacam HR® on predefined surfaces. The absence of a predefined test surface for the calibration before using the instrument leaves many clinicians and researchers with questions regarding the accuracy of the instrument, despite many reports of the instrument showing good repeatability. [2-6] This study calls for manufacturers of the instrument to include a test surface for calibration each time it is being used for both clinical and research purposes.

Chapter 3 looked at the repeatability and reproducibility of the Visante™ OCT and Oculus Pentacam HR®. The Visante™ OCT gave repeated measurements for the two visits as there were no significant differences in all the respective locations in all meridians. Oculus Pentacam HR® also gave repeatable measurements for the majority of the locations. The two instruments were found not to be reproducible and should not be used interchangeably; therefore, care must be taken interpreting the TCT from the two instruments. It was evident in our study that the Oculus Pentacam HR® underestimated the CCT and overestimated the PCT measurement relative to the Visante™ OCT. The mean difference between the two instruments was 6.11µm. Ho et al. [7] reported that the Oculus Pentacam HR® underestimated the CCT in post LASIK myopic patients by 4.10±10.65µm compared to the Visante™ OCT. They also reported a significant correlation with Visante™ OCT. Several other authors have reported that the Oculus Pentacam HR® underestimated the CCT [3, 8, 9] while other authors have also reported that the Oculus Pentacam HR® overestimated CCT. [10, 11] This controversy calls for more research with the instrument to find out whether or not the Oculus Pentacam HR® under or over-estimates corneal thickness and the factors associated with this.

The literature search indicated that there are no reports on the effect of light reflection from the limbus and the iris on the quality of the image and its effect on pachymetric values and other corneal parameters. The light reflection was seen as a consistent problem with images captured by the Oculus Pentacam HR®, even though the examination took place in a completely dark room. Interestingly, such an effect was not evident in images captured with the Visante™ OCT. This may in part explain the variability in the CCT and PCT measurements using KC and PMD corneae. Modification may be needed to reduce the amount of corneal reflection from the limbus and the iris to improve the image quality.

The results in chapter 4 show each of the instrument per se can give repeatable measurements, as there were no significant differences in the two visits, axes and locations. The two instruments were found to produce similar results for the majority of locations except for the oblique meridians in the periphery. Therefore, it is crucial to always identify the specific measurement device when reporting the corneal curvature measurement data.

The major problem associated with Placido-based technology is the use of the reflection from the pre-corneal tear film. [12-14] This means that data output is likely to be affected when there is poor quality of the pre-corneal tear film. [15-17] Dogru et al.[18] report significant changes in tear film quality in KC patients compared to normal corneae. This effect is likely to manifest itself in corneal topography measurements. [17] One of the underlying factors which may have accounted for the observed radius of curvature measurements in this study may be attributed to the quality of the pre-corneal tear film in KC and PMD corneae in the study. It was also observed that the steeper the cornea, the more peripheral data loss with Medmont E300™

(Figure 4-3a). The possible reason is unknown, though the instrument offers greater coverage and better spatial resolution for mapping the entire cornea. [19]

We found slightly increased variability in the central and peripheral cornea with the Oculus Pentacam HR® compared to the Medmont E300™. Shankar et al. [20] and Salmon et al. [21] reported that there is greater change in the peripheral cornea and this is likely to result in errors with the measurements on a tangential maps. This result from the fact that there is no topographic reference axis for tangential topographic mapping hence the use of local reference axis in mapping the cornea results in peripheral changes in measurements. More research may be needed on the radius of curvature derived from height data from the corneal surface which in turn is used to extrapolate all the other parameters of the cornea.

In chapter 5, we looked at how to effectively use the CSD to fit sSCL on the eye. We used the horizontal CSD (the simplest meridian to measure) measured at 15mm chord to select the lenses. The mean CSD was 3.78±0.53mm. Sorbara et al. [22] reported 3.93±0.25mm CSD in the steepest meridian in KC patients and this was significantly different compared to normal cornea. The difference in the CSD is attributed to different meridians chosen for each study and may partly depend on the stage of the KC.

To the best of my knowledge, there is no single report on how to use the CSD to fit sSCL on the eye. A current fitting philosophy is still based on the radius of curvature measurement (VRM). [23-25] This philosophy has been questioned recently because sSCL vaults completely over the cornea and bears no relationship to the radius of curvature of the corneal surface. [26, 27]

Schornack et al. [26] have also established that there is no relationship between the steepest radius of curvature and the sSCL that provided the "optimal" fit for their patients. The use of the VRM allows the CCC to be evaluated based on subjective estimation which might lead to many clinical errors and will present a lot of challenges to the clinician and researchers. We propose that the best way to use the radius of curvature from topography or keratometry is to use the expression below to derive the sagittal depth of the cornea in order to choose the initial lens. Sagittal depth expression is given by:

$$sag = \frac{r - \sqrt{r^2 - p(\frac{chord}{2})^2}}{p}$$

Where:

r = radius of curvature (mm) in the flat meridian.

p = shape factor derived from the eccentricity ($p = 1 - e^2$).

chord = any diameter.


It was determined from this study that "lens settling" in sSCL fitting has more clinical significance than physiological adaptation to the lens. We found mCCCl of 30±80μm after 1 hour of lens wear. Caroline et al. [28] reported mCCCl of 96μm after 8 hours of sSCL wear. It may be very difficult to compare the two studies due to participants used (normal eyes) and the sSCL (different lens designs) used in the study. Irrespective of the difference in mCCCl found in each study, it is evident that there is the likelihood of corneal clearance loss after some period of wearing time. Variation in corneal clearance loss also exists and will depend on many factors. We propose that several factors such as eyelid force, dissipation of the saline or the

tear film reservoir, design of the sSCL scleral zone radius, thickness profile of the lens, and other unknown factors may be responsible for such variations.

Based on the findings in this study, I suggest that neglecting the amount of the post-lens tear film and focusing on the "scleral alignment" as proposed by Schornack et al. [26] may not be clinically acceptable in determining the best fit of the lens. We found significant differences (p=0.001) in the TCC in the three sSCL used in the study. Therefore, I suggest the TCC should be taken into consideration when fitting these lenses. It was also evident in this study that the higher the TCC, the poorer the HCVA and LCVA. We found the mean CCC of 360μm to give the best combination of VA and comfort ratings.

The results show an overall comfort rating of 77.7±10.6 after the 1 hour of sSCL wear. Similar findings have previously been reported by Visser et al. [29]

The mathematical expression given in chapter 5 can be used for the initial selection of the sSCL in a clinical setting; however, care must be taken regarding the CCCl, which may also depend on the thickness profile of sSCL. It was not investigated in this study as to whether thinner sSCL may cause more "lens settling" than the lens thickness used in this study. In any case, the corneal clearance loss should be compensated for to account for lens settling before prescribing the final lens in a clinical setting.

Based on our study and the results obtained, we propose this fitting guide to help practitioners and researchers to be able to select and fit SCL in using the CSD.

1.  Measure the CSD along the horizontal meridian at 15mm chord with Visante™ OCT.

2. Add the estimated amount of corneal clearance to the CSD (360µm).

3. Add the anticipated corneal clearance loss (30µm).

4. Select the initial lens.

5. Insert the lens and allow it to settle for approximately 1 hour.

6. Assess and evaluate lens to make sure that there is compression or blanching on the scleral conjunctiva and the lens vault over the limbus.

In summary, the evaluation of the CSD could offer another alternative where clinicians and researchers can effectively select the initial lens and assess the fit on the eye. Appropriate estimation of corneal clearance can be measured using OCT rather than the current subjective assessment, which compares the thickness of the post-lens tear film to the thickness of the cornea with the use of the slit lamp biomicroscope. [26]

In my opinion, future research should focus on validating the mCCC and understanding of the tear flow dynamics in sSCL wear to improve oxygen exchange beneath the lens. Research should also focus on accumulation of protein or other tear film components beneath the sSCL which is seen as one of the complications of wearing sSCL on long term basis. This will hopefully improve the successful wearing of these lenses.

# APPENDICES

**Appendix 1:** **Results from Chapter 3**

**Mean and SD of TCT in all the meridians for the two visits for Visante™ OCT and Oculus Pentacam HR®.**

| Instrument | Visits | Axis | | | | | Location | | | | |
|---|---|---|---|---|---|---|---|---|---|---|---|
| | | | **-4** | **-3** | **-2** | **-1** | **0** | **1** | **2** | **3** | **4** |
| **Visante** | **V1,2M1,2** | **90** | 557.70±60.70 | 504.61±65.83 | 468.52±60.07 | 467.49±46.35 | 484.97±43.14 | 511.13±42.85 | 545.78±43.37 | 589.9±42.96 | 643.13±42.58 |
| | | **180** | 602.12±55.64 | 553.89±52.79 | 519.22±47.64 | 495.61±42.25 | 484.97±43.14 | 493.77±45.67 | 515.44±47.24 | 543.00±47.70 | 581.37±49.42 |
| | | **45** | 575.49±55.93 | 518.79±54.41 | 476.70±50.51 | 468.87±44.77 | 484.97±43.14 | 513.05±40.76 | 541.71±41.41 | 571.71±42.91 | 619.43±42.64 |
| | | **135** | 587.66±54.80 | 532.11±73.40 | 500.45±46.50 | 484.85±43.60 | 484.97±43.14 | 504.74±42.60 | 534.58±42.00 | 573.66±42.80 | 622.91±63.89 |
| **Pentacam** | **V1,2M1,2** | **90** | 683.74±64.15 | 577.10±44.89 | 498.24±47.67 | 467.73±54.77 | 478.86±45.31 | 517.05±41.64 | 566.69±42.16 | 616.71±42.58 | 674.71±45.33 |
| | | **180** | 612.23±47.38 | 548.29±43.48 | 495.38±42.53 | 469.28±44.75 | 478.86±45.31 | 510.40±41.40 | 550.60±48.89 | 599.93±54.71 | 670.73±54.67 |
| | | **45** | 654.63±61.75 | 554.94±50.29 | 479.11±39.60 | 456.53±51.27 | 478.86±45.31 | 521.10±42.32 | 565.28±42.97 | 610.54±45.88 | 673.81±50.72 |
| | | **135** | 659.48±50.50 | 571.68±56.92 | 497.14±50.78 | 467.71±53.78 | 477.81±45.72 | 501.49±45.53 | 551.23±47.72 | 600.79±41.97 | 655.78±47.83 |

**V1, 2: Visits 1 and 2.**
**M1, 2: Measurement 1 and 2 on each separate visit.**

Mean and SD of topographic radius of curvature (D) for all the meridians for the two visits for Medmont E300™ and Oculus Pentacam HR®.

**V1, 2: Visits 1 and 2.**
**M1, 2: Measurement 1 and 2 on each separate visit.**

| Instrument | Visits | Angle | | | | | Location | | | | |
|---|---|---|---|---|---|---|---|---|---|---|---|
| | | | -4 | -3 | -2 | -1 | 0 | 1 | 2 | 3 | 4 |
| Medmont | V1,2M1,2 | 90 | 37.78±8.07 | 44.94±8.74 | 50.29±6.7 | 53.22±4.34 | 49.41±4.93 | 43.96±3.32 | 38.64±4.14 | 36.39±5.46 | 35.58±5.21 |
| | | 180 | 32.18±4.94 | 38.99±3.37 | 45.97±3.35 | 48.62±4.20 | 49.41±4.93 | 45.25±3.23 | 41.56±3.36 | 34.01±5.67 | 29.50±6.47 |
| | | 45 | 34.91±5.10 | 35.49±6.57 | 44.20±5.16 | 50.55±4.76 | 49.41±4.93 | 40.73±3.09 | 35.08±7.22 | 34.16±7.31 | 32.79±6.05 |
| | | 135 | 30.12±5.88 | 34.36±7.39 | 41.06±5.40 | 49.01±4.76 | 49.41±4.93 | 44.83±3.64 | 37.36±4.24 | 35.18±4.22 | 32.77±3.84 |
| Pentacam | V1,2M1,2 | 90 | 32.45±9.99 | 44.11±7.53 | 51.73±6.17 | 54.27±5.94 | 50.38±5.81 | 42.98±3.92 | 37.99±8.01 | 38.28±5.71 | 36.19±9.07 |
| | | 180 | 32.41±4.77 | 39.47±4.17 | 46.21±3.39 | 50.83±7.51 | 50.38±5.81 | 45.03±3.64 | 40.88±3.00 | 37.54±9.48 | 32.35±8.79 |
| | | 45 | 31.21±8.21 | 38.72±7.82 | 45.90±4.59 | 52.32±5.82 | 50.38±5.81 | 45.23±2.78 | 43.35±5.12 | 40.61±5.59 | 39.07±10.81 |
| | | 135 | 32.09±7.24 | 38.05±6.88 | 44.24±5.27 | 50.71±7.28 | 50.38±5.81 | 45.33±3.92 | 42.97±5.26 | 40.16±6.41 | 38.23±7.88 |

## Appendix 3: Declaration of Informed Consent

I have read the above description prior to deciding to participate in this study.  I have had an opportunity to ask questions and have received acceptable answers. I agree to adhere to the fitting of the semi-scleral lenses during the experimental period. If I am unable to comply due to difficulty wearing or tolerating with the lenses that will be fitted, I shall report this to the investigator as soon as possible.

I am aware that my participation in this study does not replace the need for regular eye examinations, and that attending regular eye examinations (at least every two years) is essential to ensure that my eyes are healthy. I am aware that eye conditions such as glaucoma, diabetes, cataracts and macular disease can only be detected during a full eye examination, and that only the front portion of the eye – and, more specifically, only conditions associated with contact lens wear – are assessed during the initial screening visit and all subsequent visits needed for participation in a CCLR study.

I am aware that I may withdraw from the study at any time without affecting my relationship with the CCLR or the School of Optometry.  I am aware that the investigator reserves the right to discontinue my participation from the study at any time, either in regards to the research or the health of my eyes.

I am aware that my participation in this study does not replace or constitute a complete eye examination in any way.  During the study and after completion of the scheduled study visits I agree to continue eye care at my regular eye care practitioner.

I am aware that my participation in this study is voluntary, but that following study procedures and attending scheduled sessions is important to the success of the research.  I am aware that the CCLR would appreciate notification if I am unable to attend a scheduled session, so that it can be rescheduled promptly.

I am aware that this study has been reviewed and received ethics clearance through the Office of Research Ethics, and that if I have any concerns or questions about my participation in this study, I may contact Dr Susan Sykes, the Director of the Office of Research Ethics at 519 – 888 - 4567 ext. 36005 or at ssykes@uwaterloo.ca.

With full knowledge of all foregoing, I agree, of my own free will, to participate in this study. I also consent to the release of information from the study, which may be relevant for my continued use of contact lenses, to my eye care practitioner.

I am aware that I will receive a copy of this information and consent letter. I am aware that by signing this form I do not waive my legal rights or release the investigator(s), and/or involved institution(s) from their legal and professional responsibilities.

_____         _____
Signature of participant                                      Date


_____
Printed name of participant


_____         _____
Signature of person explaining consent                Date


_____         _____
Signature of witness                           Date

## Appendix 4: Screening Form

Date _____Study _____ Participant _____ ID _____

<table>
<tr><td colspan="2"><strong>ICL Checklist for Prospective Participant (PP)</strong></td></tr>
<tr><td>☐</td><td>ICL given to PP</td></tr>
<tr><td>☐</td><td>PP given ample time to read ICL</td></tr>
<tr><td>☐</td><td>PP given opportunity to ask questions</td></tr>
<tr><td>☐</td><td>PP initialed all pages</td></tr>
<tr><td>☐</td><td>PP, investigator and witness correctly signed and dated ICL</td></tr>
<tr><td>☐</td><td>PP given copy of ICL</td></tr>
<tr><td>☐</td><td>PP forgot copy of ICL – copy has been mailed to address listed in pre-screening database</td></tr>
<tr><td>☐</td><td>PP took ICL home to discuss with family member(s) or friend(s)</td></tr>
</table>

## History:

Date of birth _____(DD/MM/YYYY)  Age_____      ☐ Female ☐ Male

Occupation_____

**Current Lens Wear:**

Current lens type: _____ Average wearing time: hours/day _____ days/week _____total # years wear _____

Replacement frequency: _____     Current care system: _____

Comfortable/tolerable wearing time: _____ hours/day  Comfortable wearing time less than average wearing time: ☐

Yes ☐ No

Presence of symptoms of dryness & discomfort:    ☐ Yes  ☐ No    Use of rewetting /lubricant drops:      ☐ Yes  ☐ No

If "Yes":  Current rewetting drops: _____     How often do you insert drops: ____ / day ____ / week

Other relevant history:


General Health _____ Medications _____ Allergies _____

Smoker?_____

OD                                                    OS

| INCLUSION / EXCLUSION CRITERIA | | | | |
|---|---|---|---|---|

**INCLUSION**

**Y   N**

☐ ☐  Is at least 17 years of age and has full legal capacity to volunteer

☐ ☐  Has read and signed the informed consent letter

☐ ☐  Is willing and able to follow instructions and maintain the appointment schedule

☐ ☐  Has been diagnosed with keratoconus or pellucid Marginal degeneration

☐ ☐  The patient is currently wearing his/her contact lenses or glasses to  improve his/her vision

**EXCLUSION**

**Y   N**

☐ ☐  Is participating in any concurrent clinical or research study

☐ ☐  Has any known active ocular disease and/or infection

☐ ☐  Has a systemic condition that may affect a study outcome variable

☐ ☐  Is using any systemic or topical medications that may affect a study outcome variable

☐ ☐  Has known sensitivity to the diagnostic pharmaceuticals to be used in the study

☐ ☐  Is aphakic

☐ ☐  Has taken part in another (pharmaceutical) research study within the last 30 days

☐ ☐  Has had any form of surgery for the correction of the keratoconus and pellucid marginal degeneration.

☐ ☐  Has undergone refractive surgery

**Based on the study inclusion/exclusion criteria, is the participant suitable for the study?**            ☐     **Yes**

                                                                        ☐     **No**

 **Participant to continue in study?**    ☐ **Yes**   ☐ **No**

**Date:**

**Investigator signature:** _____    _____

| **Signature of lead investigator (if not completing screening):** | **Date:** |
|---|---|

| Biomicroscopy-Ext. Adnexa Anomalies | OD | OS |
|---|---|---|
| Absent: ☐　　　Present ☐<br><br>Describe:_____<br><br>_____<br><br>_____ | | |

**HYPEREMIA**

**Bulbar**

negligible
trace
mild
moderate
severe

0_____|_____|_____|__|____100

| | | S | | | | S | |
|---|---|---|---|---|---|---|---|
| T | | | N | N | | | T |
| | | I | | | | I | |

**Limbal**

negligible　trace/localized
mild
moderate
severe

0_____|_____|_____
___|_____100

| | | S | | | | S | |
|---|---|---|---|---|---|---|---|
| T | | | N | N | | | T |
| | | I | | | | I | |

| CORNEA & ANTERIOR EYE | OD | OS |
|---|---|---|
| **Scars or other corneal observations:** | Absent ☐　Present ☐ & Describe: | Absent ☐　Present ☐ & Describe:<br>_____ |
| **Infiltrates:**<br><br>Size (diameter) of largest infiltrate<br>　0 = none　　　　　3 = 1 - 1.5mm<br>　1 = < 0.5mm　　　4 = >1.5mm<br>　2 = 0.5 - 1mm | Absent ☐　　Present ☐ | Absent ☐　　Present ☐ |
| **Endothelium abnormalities:** | Absent ☐　Present ☐ &<br>Describe: | Absent ☐　Present ☐ &<br>Describe: |
| **Anterior chamber reaction:** | Absent ☐　Present ☐ &<br>Describe: | Absent ☐　Present ☐ &<br>Describe: |
| **Other abnormalities:** | Absent ☐　Present ☐ &<br>Describe: | Absent ☐　Present ☐ &<br>Describe: |

| STAINING | OD | OS |
|---|---|---|

## Corneal Staining

**Type, T**
none   micropunctate   macropunctate   coalescence   patch
0 |_____|_____|_____| 100

**Extent, E:** grade as a % of each zone

**Depth, D:** 0 = none          3 = stromal (confined)
1 = epithelial     4 = stromal (diffuse)
2 = stromal (delayed)

**OD** — No staining in any zones ☐

| | SUPERIOR<br>None ☐<br>T<br>E<br>D | |
|---|---|---|
| **TEMPORAL**<br>None ☐<br>T<br>E<br>D | **CENTRAL**<br>None ☐<br>T<br>E<br>D | **NASAL**<br>None ☐<br>T<br>E<br>D |
| | INFERIOR<br>None ☐<br>T<br>E<br>D | |

**OS** — No staining in any zones ☐

| | SUPERIOR<br>None ☐<br>T<br>E<br>D | |
|---|---|---|
| **NASAL**<br>None ☐<br>T<br>E<br>D | **CENTRAL**<br>None ☐<br>T<br>E<br>D | **TEMPORAL**<br>None ☐<br>T<br>E<br>D |
| | INFERIOR<br>None ☐<br>T<br>E<br>D | |

## Mucin Ball Impressions

OD: None ☐   *or*   Count _____

OS: None ☐   *or*   Count _____

**Optional sketch of staining:**

## Conjunctival Staining

negligible   trace   mild   moderate   severe
0 |_____|_____|_____| 100

**OD** — No staining in any zones ☐

| | S | |
|---|---|---|
| T | | N |
| | I | |

**OS** — No staining in any zones ☐

| | S | |
|---|---|---|
| N | | T |
| | I | |

## Conjunctival Indentation

negligible   trace   mild   moderate   severe
0 |_____|_____|_____| 100

**OD** — No indentation in any zones ☐

| | S | |
|---|---|---|
| T | | N |
| | I | |

**OS** — No indentation in any zones ☐

| | S | |
|---|---|---|
| N | | T |
| | I | |

## Palpebral Conjunctiva

**Hyperemia, H**
negligible   trace   mild   moderate   severe
0 |_____|_____|_____| 100

**Papillae, P** *(Roughness)*
satin   uniform - small   non-uniform   uniform -large   ≥1.0mm
0 |_____|_____|_____| 100

| OD | OS |
|---|---|
| Upper central area<br>H<br>P | Upper central area<br>H<br>P |
| Lower central area<br>H<br>P | Lower central area<br>H<br>P |

**Comments:** None ☐

**Signature:** _____   **Date:** _____

150

## Appendix 5: Semi-scleral Fitting Forms-Fitting and Assessment 1

Date_____    Study: _____    Participant _____ ID _____ Visit 1-1

| Current Contact Lens VA | | OD | | OS | |
|---|---|---|---|---|---|
| **LogMAR chart (Mid Illumination)** | | HCVA | LCVA | HCVA | LCVA |
| | | | | | |

**Remove Lens (s)/Spectacle: Image with <u>Medmont (2X)</u> then, <u>Pentacam (2X)</u>, then, <u>UL-OCT (2X)</u> along both nasal and temporal and finally with the <u>Visante OCT</u> (both global pachymetry (2X) and two enhanced anterior segments i.e. at 090 and at 180 (1X each).**

| | OD: Pentacam | OD: Medmont | OS: Pentacam | OS: Medmont |
|---|---|---|---|---|
| **Simulated K readings Flat D/Steep D** | _____D/_____D | _____D/_____D | _____D/_____D | _____D/_____D |
| **Average K (D)** | | | | |
| **Steepest K reading(D) @ apex/thinnest point** | | | | |
| **Corneal cyl and axis** | _____X_____ | _____X_____ | _____X_____ | _____X_____ |
| **Cone diameter (apex and overall) mm** | _____/_____ | _____/_____ | _____/_____ | _____/_____ |
| **Cone type/severity Cen/Oval/PMD//Mi,M,S** | | | | |
| **Pachymetry (central and thinnest pt) µm** | _____/_____ | _____/_____ | _____/_____ | _____/_____ |
| **HVID (mm)** | | | | |
| **pupil diameter (mm)** | | | | |
| **e-value** | | | | |
| | Visante OCT | Medmont | Visante OCT | Medmont |
| **Sag @ 15mm (mm)090** | | | | |
| **Sag @ 15mm (mm)180** | | | | |
| **Sag @ 10mm (mm)090** | | | | |
| **Sag @ 10mm (mm)180** | | | | |
| | Visante OCT | | Visante OCT | |
| **Pachymetry-1** | Cent: | Thinnest: | Cent: | Thinnest: |
| **Pachymetry-2** | Cent: | Thinnest: | Cent: | Thinnest: |

|  | OD 2 | | OS 2 | |
| --- | --- | --- | --- | --- |
|  | **Pentacam** | **Medmont** | **Pentacam** | **Medmont** |
| **Simulated K readings Flat D/Steep D** | \_\_\_\_D/\_\_\_\_D | \_\_\_\_D/\_\_\_\_D | \_\_\_\_D/\_\_\_\_D | \_\_\_\_D/\_\_\_\_D |
| **Average K (D)** | | | | |
| **Steepest K reading(D) @ apex/thinnest point** | | | | |
| **Corneal cyl and axis** | \_\_\_\_X\_\_\_\_ | \_\_\_\_X\_\_\_\_ | \_\_\_\_X\_\_\_\_ | \_\_\_\_X\_\_\_\_ |
| **Cone diameter (apex and overall) mm** | \_\_\_/\_\_\_\_ | \_\_\_/\_\_\_\_ | \_\_\_/\_\_\_\_ | \_\_\_/\_\_\_\_ |
| **Cone type/severity Cen/Oval/PMD//Mi,M,S** | | | | |
| **Pachymetry (central and thinnest pt) μm** | \_\_\_/\_\_\_\_ | \_\_\_/\_\_\_\_ | \_\_\_/\_\_\_\_ | \_\_\_/\_\_\_\_ |
| **HVID (mm)** | | | | |
| **pupil diameter (mm)** | | | | |
| **e-value** | | | | |
|  | **Visante OCT** | **Medmont** | **Visante OCT** | **Medmont** |
| **Sag @ 15mm (mm)090** | | | | |
| **Sag @ 15mm (mm)180** | | | | |
| **Sag @ 10mm (mm)090** | | | | |
| **Sag @ 10mm (mm)180** | | | | |
|  | **Visante OCT** | | **Visante OCT** | |
| **Pachymetry-1** | Cent: | Thinnest: | Cent: | Thinnest: |
| **Pachymetry-2** | Cent: | Thinnest: | Cent: | Thinnest: |

**TOPOGRAPHIC PACHYMETRY: Visante™ OCT and Pentacam (Data packs on the instruments, repeatability 2X)-OD/OS 2X**

| | Inferior-1 | | | | | Superior-1 | | | | Inferior-2 | | | | | Superior-2 | | | |
|---|---|---|---|---|---|---|---|---|---|---|---|---|---|---|---|---|---|---|
| | -4 | -3 | -2 | -1 | 0 | +1 | +2 | +3 | +4 | -4 | -3 | -2 | -1 | 0 | +1 | +2 | +3 | +4 |
| Visante OCT @ 90 ($\mu$m) | | | | | | | | | | | | | | | | | | |
| Pentacam @ 90 ($\mu$m) | | | | | | | | | | | | | | | | | | |

| | Temporal-1 | | | | | Nasal-1 | | | | Temporal-2 | | | | | Nasal-2 | | | |
|---|---|---|---|---|---|---|---|---|---|---|---|---|---|---|---|---|---|---|
| | -4 | -3 | -2 | -1 | 0 | +1 | +2 | +3 | +4 | -4 | -3 | -2 | -1 | 0 | +1 | +2 | +3 | |
| Visante OCT @ 180 ($\mu$m) | | | | | | | | | | | | | | | | | | |
| Pentacam @180 ($\mu$m) | | | | | | | | | | | | | | | | | | |

| | Inf-Temp-1 | | | | | Sup-Nasal-1 | | | | Inf-Temp-2 | | | | | Sup-Nasal-2 | | | |
|---|---|---|---|---|---|---|---|---|---|---|---|---|---|---|---|---|---|---|
| | -4 | -3 | -2 | -1 | 0 | +1 | +2 | +3 | +4 | -4 | -3 | -2 | -1 | 0 | +1 | +2 | +3 | +4 |
| Visante OCT @ 045 ($\mu$m) | | | | | | | | | | | | | | | | | | |
| Pentacam @ 045 ($\mu$m) | | | | | | | | | | | | | | | | | | |

| | Inf-Temporal | | | | | Sup-Temporal | | | | Inf-Temporal | | | | | Sup-Temporal | | | |
|---|---|---|---|---|---|---|---|---|---|---|---|---|---|---|---|---|---|---|
| | -4 | -3 | -2 | -1 | 0 | 1 | 2 | 3 | 4 | -4 | -3 | -2 | -1 | 0 | 1 | 2 | 3 | 4 |
| Visante OCT @ 135 ($\mu$m) | | | | | | | | | | | | | | | | | | |
| Pentacam @ 135 ($\mu$m) | | | | | | | | | | | | | | | | | | |

**TOPOGRAPHIC KERATOMETRY: Medmont and Pentacam (Data hand written from the instrument: repeatability 2X)-OD/OS 2X**

| | Inferior-1 | | | | | Superior-1 | | | | Inferior-2 | | | | | Superior-2 | | | |
|---|---|---|---|---|---|---|---|---|---|---|---|---|---|---|---|---|---|---|
| | -4 | -3 | -2 | -1 | 0 | +1 | +2 | +3 | +4 | -4 | -3 | -2 | -1 | 0 | +1 | +2 | +3 | +4 |
| Visante OCT @ 90 ($\mu$m) | | | | | | | | | | | | | | | | | | |
| Pentacam @ 90 ($\mu$m) | | | | | | | | | | | | | | | | | | |
| | Temporal-1 | | | | | Nasal-1 | | | | Temporal-2 | | | | | Nasal-2 | | | |
| | -4 | -3 | -2 | -1 | 0 | +1 | +2 | +3 | +4 | -4 | -3 | -2 | -1 | 0 | +1 | +2 | +3 | |
| Visante OCT @ 180 ($\mu$m) | | | | | | | | | | | | | | | | | | |
| Pentacam @180 ($\mu$m) | | | | | | | | | | | | | | | | | | |
| | Inf-Temp-1 | | | | | Sup-Nasal-1 | | | | Inf-Temp-2 | | | | | Sup-Nasal-2 | | | |
| | -4 | -3 | -2 | -1 | 0 | +1 | +2 | +3 | +4 | -4 | -3 | -2 | -1 | 0 | +1 | +2 | +3 | +4 |
| Visante OCT @ 045 ($\mu$m) | | | | | | | | | | | | | | | | | | |
| Pentacam @ 045 ($\mu$m) | | | | | | | | | | | | | | | | | | |
| | Inf-Temporal | | | | | Sup-Temporal | | | | Inf-Temporal | | | | | Sup-Temporal | | | |
| | -4 | -3 | -2 | -1 | 0 | 1 | 2 | 3 | 4 | -4 | -3 | -2 | -1 | 0 | 1 | 2 | 3 | 4 |
| Visante OCT @ 135 ($\mu$m) | | | | | | | | | | | | | | | | | | |
| Pentacam @ 135 ($\mu$m) | | | | | | | | | | | | | | | | | | |

154

## Semi-scleral Fitting Forms-Fitting and Assessment 2

**Date_____ Study:              Participant _____ ID _____ Visit 1-1**

| Current Contact Lens VA | OD | | OS | |
|---|---|---|---|---|
| **LogMAR chart (Mid Illumination)** | HCVA | LCVA | HCVA | LCVA |
| | | | | |

Remove Lens (s)/Spectacle: Image with <u>Medmont (2X)</u> then, <u>Pentacam (2X)</u>, then, <u>UL-OCT (2X)</u> along both nasal and temporal and finally with the <u>Visante OCT</u> (both global pachymetry (2X) and two enhanced anterior segments i.e. at 090 and at 180 (1X each).

| | OD: Pentacam | OD: Medmont | OS: Pentacam | OS: Medmont |
|---|---|---|---|---|
| | _____D/_____D | _____D/_____D | _____D/_____D | _____D/_____D |
| **Simulated K readings Flat D/Steep D** | | | | |
| **Average K (D)** | | | | |
| **Steepest K reading(D) @ apex/thinnest point** | | | | |
| **Corneal cyl and axis** | _____X_____ | _____X_____ | _____X_____ | _____X_____ |
| **Cone diameter (apex and overall) mm** | _____/_____ | _____/_____ | _____/_____ | _____/_____ |
| **Cone type/severity Cen/Oval/PMD//Mi,M,S** | | | | |
| **Pachymetry (central and thinnest pt) μm** | _____/_____ | _____/_____ | _____/_____ | _____/_____ |
| **HVID (mm)** | | | | |
| **pupil diameter (mm)** | | | | |
| **e-value** | | | | |
| | Visante OCT | Medmont | Visante OCT | Medmont |
| **Sag @ 15mm (mm)090** | | | | |
| **Sag @ 15mm (mm)180** | | | | |
| **Sag @ 10mm (mm)090** | | | | |
| **Sag @ 10mm (mm)180** | | | | |
| | Visante OCT | | Visante OCT | |
| **Pachymetry-1** | Cent: | Thinnest: | Cent: | Thinnest: |
| **Pachymetry-2** | Cent: | Thinnest: | Cent: | Thinnest: |

|  | OD 2 | | OS 2 | |
|---|---|---|---|---|
|  | **Pentacam** | **Medmont** | **Pentacam** | **Medmont** |
| **Simulated K readings Flat D/Steep D** | _____D/_____D | _____D/_____D | _____D/_____D | _____D/_____D |
| **Average K (D)** |  |  |  |  |
| **Steepest K reading(D) @ apex/thinnest point** |  |  |  |  |
| **Corneal cyl and axis** | _____X_____ | _____X_____ | _____X_____ | _____X_____ |
| **Cone diameter (apex and overall) mm** | _____/_____ | _____/_____ | _____/_____ | _____/_____ |
| **Cone type/severity Cen/Oval/PMD//Mi,M,S** |  |  |  |  |
| **Pachymetry (central and thinnest pt) μm** | _____/_____ | _____/_____ | _____/_____ | _____/_____ |
| **HVID (mm)** |  |  |  |  |
| **pupil diameter (mm)** |  |  |  |  |
| **e-value** |  |  |  |  |
|  | **Visante OCT** | **Medmont** | **Visante OCT** | **Medmont** |
| **Sag @ 15mm (mm)090** |  |  |  |  |
| **Sag @ 15mm (mm)180** |  |  |  |  |
| **Sag @ 10mm (mm)090** |  |  |  |  |
| **Sag @ 10mm (mm)180** |  |  |  |  |
|  | **Visante OCT** |  | **Visante OCT** |  |
| **Pachymetry-1** | **Cent:** | **Thinnest:** | **Cent:** | **Thinnest:** |
| **Pachymetry-2** | **Cent:** | **Thinnest:** | **Cent:** | **Thinnest:** |

## SEMI-SCLERAL FITTING AND ASSESSMENT

| INSERTION OF THE SEMI-SCLERAL LENS | Use unpreserved saline | Use NaFl strip |
|---|---|---|
| | | |

**OD/OS**

| Randomized | Trial # 1 | Trial # 2 | Trial # 3 |
|---|---|---|---|
| Lens | | | |
| BC / Diam / Power / CT | /    /    / | /    /    / | /    /    / |

## FLUORESCEIN CHARACTERISTIC RATING @ 60 minutes
### OD/OS

| Fluorescein Rating | Lens # 1 | Lens # 2 | Lens # 3 |
|---|---|---|---|
| Central<br><br>-2 = flat, moderate dark touch area<br>-1 = slightly flat, small dark noticeable touch at centre<br>0 = alignment, even fluorescein across optic zone<br>+1 = slightly steep, noticeably brighter at centre<br>+2 = steep, clearly noticeable central pooling | -2  -1  0  +1  +2 | -2  -1  0  +1  +2 | -2  -1  0  +1  +2 |
| Mid Periphery (MP)<br><br>-2 = flat, fluorescein under MP merging into edge<br>-1 = slightly flat, slight fluorescein under MP<br>0 = alignment, smooth transition into edge<br>+1 = slightly tight, narrow or slight dark band before edge<br>+2 = tight, moderate pressure just before the edge lift | -2  -1  0  +1  +2 | -2  -1  0  +1  +2 | -2  -1  0  +1  +2 |
| Edge Width<br><br>-2 = wide<br>-1 = slightly wide<br>0 = optimal<br>+1 = slightly narrow<br>+2 = narrow | -2  -1  0  +1  +2 | -2  -1  0  +1  +2 | -2  -1  0  +1  +2 |
| Edge Clearance<br><br>-2 = excessive<br>-1 = slightly excessive<br>0 = optimal<br>+1 = slightly insufficient<br>+2 = insufficient | -2  -1  0  +1  +2 | -2  -1  0  +1  +2 | -2  -1  0  +1  +2 |

**LENS # 1**
**TOPOGRAPHIC CORNEAL CLEARANCE**
**<u>Method 2: UL-OCT 14mm (Y-scan)</u>** *Images taken every 10 minutes interval.*

**OD/OS**

| Photo | white@090 | white@090 | white@090 | white@090 | white@090 | white@090 | white@090 |
|---|---|---|---|---|---|---|---|
| | $\mu$m (0min) | $\mu$m(10min) | $\mu$m(20 min) | $\mu$m(30 min) | $\mu$m(40 min) | $\mu$m(50 min) | $\mu$m(60 min) |
| +7 Sup | | | | | | | |
| +6 Sup | | | | | | | |
| +5 Sup | | | | | | | |
| +4 Sup | | | | | | | |
| +3 Sup | | | | | | | |
| +2 Sup | | | | | | | |
| +1 Sup | | | | | | | |
| centre | | | | | | | |
| -1 Inf | | | | | | | |
| -2 Inf | | | | | | | |
| -3 Inf | | | | | | | |
| -4 Inf | | | | | | | |
| -5 Inf | | | | | | | |
| -6 Inf | | | | | | | |
| -7 Inf | | | | | | | |

**TOPOGRAPHIC CORNEAL CLEARANCE**

**Method 2: UL-OCT 14mm (Y-scan)** *Images taken every 10 minutes interval.*

**OD/OS**

| Photo | white@090 | white@090 | white@090 | white@090 | white@090 | white@090 | white@090 |
|---|---|---|---|---|---|---|---|
| | $\mu$m (0min) | $\mu$m(10min) | $\mu$m(20 min) | $\mu$m(30 min) | $\mu$m(40 min) | $\mu$m(50 min) | $\mu$m(60 min) |
| +7 Sup | | | | | | | |
| +6 Sup | | | | | | | |
| +5 Sup | | | | | | | |
| +4 Sup | | | | | | | |
| +3 Sup | | | | | | | |
| +2 Sup | | | | | | | |
| +1 Sup | | | | | | | |
| centre | | | | | | | |
| -1 Inf | | | | | | | |
| -2 Inf | | | | | | | |
| -3 Inf | | | | | | | |
| -4 Inf | | | | | | | |
| -5 Inf | | | | | | | |
| -6 Inf | | | | | | | |
| -7 Inf | | | | | | | |

**LENS # 3**
**TOPOGRAPHIC CORNEAL CLEARANCE**

**Method 2: UL-OCT 14mm (Y-scan)** *Images taken every 10 minutes interval.*

**OD/OS**

| Photo | white@090 | white@090 | white@090 | white@090 | white@090 | white@090 | white@090 |
|-------|-----------|-----------|-----------|-----------|-----------|-----------|-----------|
|       | $\mu$m (0min) | $\mu$m(10min) | $\mu$m(20 min) | $\mu$m(30 min) | $\mu$m(40 min) | $\mu$m(50 min) | $\mu$m(60 min) |
| +7 Sup | | | | | | | |
| +6 Sup | | | | | | | |
| +5 Sup | | | | | | | |
| +4 Sup | | | | | | | |
| +3 Sup | | | | | | | |
| +2 Sup | | | | | | | |
| +1 Sup | | | | | | | |
| centre | | | | | | | |
| -1 Inf | | | | | | | |
| -2 Inf | | | | | | | |
| -3 Inf | | | | | | | |
| -4 Inf | | | | | | | |
| -5 Inf | | | | | | | |
| -6 Inf | | | | | | | |
| -7 Inf | | | | | | | |

**OVER-REFRACTION/OVER-KERATOMETRY AND VA:** *at 60 minutes only*
**OD/OS**

| | Lens # 1 | | Lens # 2 | | Lens # 3 | |
|---|---|---|---|---|---|---|
| **Over-refraction** <br> **Sph/cyl/axis** | / / | | / / | | / / | |
| **Over-keratometry** <br> **Cyl/axis** | / | | / | | / | |
| **Best sphere correction** | | | | | | |
| **LogMAR VA** <br> **(HCVA & LCVA)** | | | | | | |

### SUBJECTIVE COMFORT RATING

The following questions are all of the comfort about each lens you are wearing in the study.

This is done at *60 minutes* only.

**Lens # 1.  How would you rate your <u>comfort</u> with your study lens?**

0                                                                          100

Very poor comfort |————————————————————————| excellent comfort

RE [ ]

LE [ ]

**Lens # 2.  How would you rate your <u>comfort</u> with your study lens?**

0                                                                          100

Very poor comfort |————————————————————————| excellent comfort

RE [ ]

LE [ ]

**Lens # 3.  How would you rate your <u>comfort</u> with your study lens?**

0                                                                          100

Very poor comfort |————————————————————————| excellent comfort

RE [ ]

LE [ ]

**Comments**

**Signature**_____          **Date**_____

## Appendix 6a: Results from Chapter 5 for Lens 1

**TCC (mm) at 1 hour for Lens 1.**

| | Lens 1 at 1 hour | | | | | | | | |
|---|---|---|---|---|---|---|---|---|---|
| | **Superior** | | | | **Location** | **Inferior** | | | |
| **ID** | **+4** | **+3** | **+2** | **+1** | **Centre** | **-1** | **-2** | **-3** | **-4** |
| 01 | 0.058 | 0.100 | 0.130 | 0.135 | 0.150 | 0.194 | 0.264 | 0.339 | 0.386 |
| 02 | 0.010 | 0.046 | 0.063 | 0.066 | 0.055 | 0.045 | 0.054 | 0.037 | 0.082 |
| 03 | 0.000 | -0.003 | -0.002 | 0.001 | 0.001 | -0.001 | 0.007 | 0.034 | 0.049 |
| 04 | 0.200 | 0.268 | 0.307 | 0.314 | 0.289 | 0.265 | 0.238 | 0.203 | 0.146 |
| 05 | 0.148 | 0.266 | 0.314 | 0.324 | 0.308 | 0.286 | 0.267 | 0.242 | 0.212 |
| 06 | 0.053 | 0.119 | 0.153 | 0.176 | 0.178 | 0.183 | 0.192 | 0.205 | 0.219 |
| 07 | 0.149 | 0.211 | 0.228 | 0.197 | 0.153 | 0.115 | 0.010 | 0.087 | 0.087 |
| 08 | 0.166 | 0.247 | 0.304 | 0.312 | 0.334 | 0.354 | 0.374 | 0.386 | 0.361 |
| 09 | 0.006 | 0.048 | 0.091 | 0.123 | 0.161 | 0.193 | 0.219 | 0.239 | 0.243 |
| 10 | 0.162 | 0.256 | 0.291 | 0.291 | 0.271 | 0.265 | 0.259 | 0.252 | 0.207 |
| 11 | 0.057 | 0.128 | 0.204 | 0.239 | 0.246 | 0.244 | 0.212 | 0.193 | 0.177 |
| 12 | 0.134 | 0.191 | 0.220 | 0.213 | 0.204 | 0.192 | 0.162 | 0.121 | 0.068 |
| 13 | 0.167 | 0.249 | 0.289 | 0.307 | 0.299 | 0.263 | 0.227 | 0.176 | 0.119 |
| 14 | 0.103 | 0.220 | 0.289 | 0.320 | 0.324 | 0.285 | 0.215 | 0.148 | 0.088 |
| 15 | 0.035 | 0.081 | 0.105 | 0.113 | 0.106 | 0.122 | 0.168 | 0.230 | 0.252 |
| 16 | 0.188 | 0.293 | 0.325 | 0.313 | 0.266 | 0.212 | 0.155 | 0.107 | 0.067 |
| 17 | 0.099 | 0.175 | 0.225 | 0.249 | 0.248 | 0.240 | 0.221 | 0.210 | 0.185 |
| 18 | 0.141 | 0.190 | 0.181 | 0.126 | 0.067 | 0.028 | 0.021 | 0.043 | 0.082 |
| 18 | 0.056 | 0.085 | 0.101 | 0.107 | 0.100 | 0.113 | 0.120 | 0.129 | 0.108 |
| 20 | 0.000 | 0.000 | 0.000 | 0.008 | 0.033 | 0.056 | 0.107 | 0.139 | 0.171 |
| **Mean** | **0.10** | **0.16** | **0.19** | **0.20** | **0.19** | **0.18** | **0.17** | **0.18** | **0.17** |
| **SD** | **0.07** | **0.09** | **0.11** | **0.11** | **0.10** | **0.10** | **0.10** | **0.09** | **0.10** |

**Note: The negative sign means area of touch on the cornea.**

**Appendix 6b: Results from Chapter 5 for Lens 1**

**TCC (mm) at Selected Time Interval for Lens 1.**

| | Lens 1 | | | | | | | | |
|---|---|---|---|---|---|---|---|---|---|
| | **Superior** | **20 min** | **Inferior** | **Inferior** | **40 min** | **Inferior** | **Inferior** | **60 min** | **Inferior** |
| **ID** | **+3** | **Centre** | **-3** | **+3** | **centre** | **-3** | **+3** | **Centre** | **-3** |
| **01** | -0.004 | 0.006 | 0.033 | 0.022 | 0.013 | 0.031 | 0.026 | 0.020 | 0.029 |
| **02** | 0.003 | 0.000 | -0.007 | 0.003 | 0.007 | 0.021 | 0.008 | 0.009 | 0.071 |
| **03** | -0.001 | -0.002 | -0.037 | 0.000 | -0.003 | -0.355 | 0.002 | -0.001 | -0.027 |
| **04** | -0.013 | 0.021 | 0.048 | 0.048 | 0.064 | 0.103 | 0.034 | 0.075 | 0.112 |
| **05** | 0.016 | -0.006 | -0.002 | 0.022 | -0.019 | -0.002 | 0.017 | -0.003 | 0.003 |
| **06** | -0.005 | 0.005 | 0.021 | -0.011 | 0.009 | 0.016 | -0.01 | 0.006 | 0.021 |
| **07** | 0.004 | 0.004 | 0.002 | 0.028 | 0.048 | 0.033 | 0.036 | 0.054 | 0.037 |
| **08** | -0.008 | 0.019 | 0.008 | 0.069 | 0.035 | 0.033 | -0.006 | 0.022 | 0.034 |
| **09** | -0.013 | -0.003 | 0.003 | 0.012 | 0.017 | 0.021 | 0.015 | 0.009 | 0.014 |
| **10** | 0.003 | -0.019 | 0.004 | 0.038 | -0.001 | 0.015 | 0.009 | 0.013 | 0.020 |
| **11** | 0.008 | 0.008 | 0.011 | 0.039 | 0.006 | 0.009 | 0.024 | 0.007 | 0.015 |
| **12** | 0.013 | 0.010 | -0.001 | 0.015 | 0.017 | 0.035 | 0.009 | 0.046 | 0.056 |
| **13** | 0.034 | 0.012 | -0.019 | 0.027 | 0.030 | 0.010 | 0.030 | 0.023 | 0.010 |
| **14** | -0.015 | -0.003 | -0.002 | 0.016 | 0.029 | 0.022 | -0.009 | 0.032 | 0.057 |
| **15** | 0.004 | 0.004 | 0.011 | 0.024 | 0.000 | 0.041 | 0.012 | -0.007 | -0.002 |
| **16** | 0.011 | 0.010 | 0.020 | 0.050 | -0.008 | -0.008 | -0.003 | 0.032 | 0.032 |
| **17** | 0.015 | 0.017 | 0.020 | 0.020 | 0.010 | -0.005 | 0.001 | 0.026 | 0.044 |
| **18** | 0.001 | 0.023 | 0.046 | 0.026 | 0.082 | 0.106 | 0.030 | 0.104 | 0.121 |
| **19** | 0.001 | 0.000 | 0.004 | 0.033 | 0.038 | 0.047 | 0.014 | 0.035 | 0.042 |
| **20** | -0.012 | -0.002 | -0.013 | 0.020 | 0.000 | -0.028 | 0.020 | 0.009 | -0.012 |
| **Mean** | **0.00** | **0.01** | **0.01** | **0.03** | **0.02** | **0.01** | **0.01** | **0.03** | **0.03** |
| **SD** | **0.01** | **0.01** | **0.02** | **0.02** | **0.03** | **0.09** | **0.01** | **0.03** | **0.04** |

**Appendix 7a: Results from Chapter 5 for Lens 2**

**TCC (mm) at 1 hour for Lens 2.**

| | | | | | Lens 2 at 1 hour | | | | |
|---|---|---|---|---|---|---|---|---|---|
| | **Superior** | | | | **Location** | **Inferior** | | | |
| **ID** | **+4** | **+3** | **+2** | **+1** | **Centre** | **-1** | **-2** | **-3** | **-4** |
| **01** | 0.063 | 0.104 | 0.132 | 0.140 | 0.151 | 0.201 | 0.268 | 0.340 | 0.385 |
| **02** | 0.141 | 0.243 | 0.296 | 0.322 | 0.334 | 0.336 | 0.347 | 0.346 | 0.323 |
| **03** | 0.070 | 0.141 | 0.179 | 0.197 | 0.207 | 0.224 | 0.235 | 0.226 | 0.208 |
| **04** | 0.311 | 0.434 | 0.493 | 0.528 | 0.512 | 0.500 | 0.465 | 0.403 | 0.336 |
| **05** | 0.239 | 0.364 | 0.435 | 0.454 | 0.448 | 0.420 | 0.387 | 0.350 | 0.300 |
| **06** | 0.109 | 0.216 | 0.337 | 0.409 | 0.453 | 0.479 | 0.505 | 0.517 | 0.525 |
| **07** | 0.188 | 0.329 | 0.406 | 0.420 | 0.398 | 0.358 | 0.314 | 0.270 | 0.206 |
| **08** | 0.202 | 0.327 | 0.405 | 0.446 | 0.476 | 0.497 | 0.505 | 0.519 | 0.476 |
| **09** | 0.068 | 0.145 | 0.240 | 0.317 | 0.374 | 0.415 | 0.432 | 0.447 | 0.434 |
| **10** | 0.281 | 0.422 | 0.517 | 0.550 | 0.544 | 0.537 | 0.503 | 0.452 | 0.380 |
| **11** | 0.118 | 0.234 | 0.322 | 0.363 | 0.379 | 0.367 | 0.308 | 0.270 | 0.291 |
| **12** | 0.195 | 0.294 | 0.363 | 0.406 | 0.406 | 0.399 | 0.371 | 0.332 | 0.269 |
| **13** | 0.164 | 0.185 | 0.187 | 0.187 | 0.159 | 0.132 | 0.115 | 0.078 | 0.064 |
| **14** | 0.139 | 0.294 | 0.400 | 0.469 | 0.494 | 0.456 | 0.400 | 0.303 | 0.241 |
| **15** | 0.168 | 0.265 | 0.326 | 0.363 | 0.373 | 0.388 | 0.437 | 0.465 | 0.446 |
| **16** | 0.196 | 0.349 | 0.433 | 0.460 | 0.411 | 0.392 | 0.328 | 0.263 | 0.194 |
| **17** | 0.055 | 0.107 | 0.161 | 0.171 | 0.180 | 0.178 | 0.189 | 0.204 | 0.215 |
| **18** | 0.212 | 0.347 | 0.405 | 0.409 | 0.380 | 0.351 | 0.343 | 0.329 | 0.324 |
| **19** | 0.161 | 0.264 | 0.328 | 0.364 | 0.376 | 0.383 | 0.381 | 0.351 | 0.319 |
| **20** | 0.068 | 0.099 | 0.116 | 0.136 | 0.151 | 0.174 | 0.187 | 0.215 | 0.230 |
| **Mean** | **0.16** | **0.26** | **0.32** | **0.36** | **0.36** | **0.36** | **0.35** | **0.33** | **0.31** |
| **SD** | **0.07** | **0.10** | **0.12** | **0.13** | **0.12** | **0.12** | **0.11** | **0.11** | **0.11** |

# Appendix 7b: Results from Chapter 5 for Lens 2

**TCC (mm) at Selected Time Interval for Lens 2.**

| | Superior | 20 min | Inferior | Superior | 40 min | Inferior | Superior | 60 min | Inferior |
|---|---|---|---|---|---|---|---|---|---|
| **ID** | +3 | Centre | -3 | +3 | Centre | -3 | +3 | Centre | -3 |
| **01** | -0.020 | -0.010 | -0.001 | 0.184 | 0.247 | 0.185 | 0.189 | 0.255 | 0.187 |
| **02** | 0.016 | -0.002 | -0.012 | -0.020 | 0.001 | 0.009 | -0.023 | -0.009 | -0.022 |
| **03** | -0.033 | -0.003 | 0.007 | -0.039 | 0.002 | 0.017 | -0.028 | 0.012 | 0.028 |
| **04** | 0.005 | 0.006 | 0.009 | -0.043 | -0.003 | 0.007 | -0.066 | -0.004 | 0.044 |
| **05** | -0.004 | 0.010 | 0.006 | 0.007 | -0.014 | -0.027 | 0.003 | -0.009 | -0.021 |
| **06** | -0.031 | 0.003 | 0.010 | -0.025 | 0.007 | 0.005 | 0.049 | 0.034 | 0.037 |
| **07** | 0.035 | 0.017 | 0.014 | 0.022 | 0.052 | 0.041 | 0.071 | 0.050 | 0.039 |
| **08** | 0.007 | 0.002 | 0.014 | 0.028 | 0.049 | 0.031 | 0.054 | 0.047 | 0.043 |
| **09** | -0.001 | 0.005 | 0.021 | -0.006 | 0.003 | 0.023 | 0.055 | 0.033 | 0.029 |
| **10** | -0.006 | -0.018 | -0.016 | 0.036 | -0.020 | -0.020 | 0.016 | -0.001 | 0.001 |
| **11** | 0.029 | 0.015 | 0.012 | 0.015 | 0.021 | 0.032 | 0.015 | 0.019 | 0.074 |
| **12** | 0.155 | -0.048 | 0.264 | 0.147 | -0.041 | 0.273 | 0.185 | -0.035 | 0.262 |
| **13** | 0.020 | 0.036 | 0.051 | 0.042 | 0.082 | 0.085 | 0.054 | 0.101 | 0.117 |
| **14** | 0.043 | 0.025 | -0.009 | -0.006 | 0.024 | 0.019 | 0.024 | 0.025 | 0.044 |
| **15** | 0.082 | 0.042 | 0.017 | 0.073 | 0.045 | 0.019 | 0.034 | 0.026 | 0.011 |
| **16** | -0.040 | -0.013 | -0.009 | -0.016 | 0.010 | 0.012 | 0.023 | 0.008 | -0.028 |
| **17** | 0.066 | 0.024 | 0.043 | 0.052 | 0.025 | 0.014 | 0.033 | 0.024 | 0.032 |
| **18** | 0.042 | 0.009 | 0.022 | 0.028 | 0.028 | 0.038 | 0.055 | 0.050 | 0.047 |
| **19** | 0.024 | 0.005 | 0.034 | 0.015 | 0.031 | 0.054 | 0.019 | 0.040 | 0.075 |
| **20** | 0.015 | 0.003 | 0.001 | -0.008 | -0.004 | 0.003 | 0.005 | 0.024 | 0.049 |
| **Mean** | **0.02** | **0.01** | **0.02** | **0.02** | **0.03** | **0.04** | **0.04** | **0.03** | **0.05** |
| **SD** | **0.04** | **0.02** | **0.06** | **0.06** | **0.06** | **0.07** | **0.06** | **0.06** | **0.07** |

## Appendix 8a: Results from Chapter 5 for Lens 3

**TCC (mm) at 1 hour for Lens 3.**

| ID | Superior | | | | Location | Inferior | | | |
|---|---|---|---|---|---|---|---|---|---|
| | +4 | +3 | +2 | +1 | Centre | -1 | -2 | -3 | -4 |
| 01 | 0.201 | 0.321 | 0.406 | 0.447 | 0.455 | 0.447 | 0.434 | 0.405 | 0.355 |
| 02 | 0.140 | 0.262 | 0.363 | 0.430 | 0.459 | 0.471 | 0.478 | 0.467 | 0.422 |
| 03 | 0.147 | 0.237 | 0.322 | 0.349 | 0.368 | 0.389 | 0.400 | 0.390 | 0.351 |
| 04 | 0.293 | 0.460 | 0.575 | 0.640 | 0.660 | 0.649 | 0.629 | 0.571 | 0.500 |
| 05 | 0.201 | 0.321 | 0.406 | 0.447 | 0.455 | 0.447 | 0.434 | 0.405 | 0.355 |
| 06 | 0.204 | 0.339 | 0.447 | 0.514 | 0.540 | 0.542 | 0.527 | 0.491 | 0.448 |
| 07 | 0.176 | 0.270 | 0.308 | 0.289 | 0.251 | 0.204 | 0.182 | 0.150 | 0.104 |
| 08 | 0.210 | 0.303 | 0.391 | 0.440 | 0.459 | 0.486 | 0.499 | 0.503 | 0.462 |
| 09 | 0.043 | 0.097 | 0.160 | 0.213 | 0.251 | 0.29 | 0.320 | 0.332 | 0.332 |
| 10 | 0.209 | 0.324 | 0.391 | 0.416 | 0.397 | 0.370 | 0.363 | 0.333 | 0.290 |
| 11 | 0.249 | 0.441 | 0.560 | 0.635 | 0.661 | 0.649 | 0.601 | 0.542 | 0.458 |
| 12 | 0.312 | 0.465 | 0.583 | 0.650 | 0.670 | 0.654 | 0.620 | 0.544 | 0.431 |
| 13 | 0.306 | 0.405 | 0.462 | 0.493 | 0.479 | 0.440 | 0.383 | 0.307 | 0.223 |
| 14 | 0.310 | 0.513 | 0.656 | 0.736 | 0.753 | 0.721 | 0.641 | 0.524 | 0.394 |
| 15 | 0.068 | 0.137 | 0.186 | 0.210 | 0.214 | 0.219 | 0.250 | 0.297 | 0.306 |
| 16 | 0.289 | 0.519 | 0.659 | 0.709 | 0.694 | 0.639 | 0.556 | 0.449 | 0.324 |
| 17 | 0.180 | 0.284 | 0.368 | 0.406 | 0.424 | 0.409 | 0.388 | 0.369 | 0.339 |
| 18 | 0.175 | 0.263 | 0.279 | 0.254 | 0.190 | 0.161 | 0.155 | 0.167 | 0.196 |
| 19 | 0.179 | 0.255 | 0.300 | 0.317 | 0.332 | 0.347 | 0.374 | 0.391 | 0.353 |
| 20 | 0.132 | 0.206 | 0.290 | 0.351 | 0.385 | 0.413 | 0.441 | 0.454 | 0.454 |
| **Mean** | **0.20** | **0.32** | **0.41** | **0.45** | **0.45** | **0.45** | **0.43** | **0.40** | **0.35** |
| **SD** | **0.08** | **0.12** | **0.14** | **0.16** | **0.17** | **0.16** | **0.14** | **0.12** | **0.10** |

## Appendix 8b: Results from Chapter 5 for Lens 3

**TCC (mm) at Selected Time Interval for Lens 3.**

| | Superior | 20 min | Inferior | Superior | 40 min | Inferior | Superior | 60 min | Inferior |
|---|---|---|---|---|---|---|---|---|---|
| ID | +3 | Centre | -3 | +3 | Centre | -3 | +3 | Centre | -3 |
| 01 | -0.005 | 0.006 | 0.023 | 0.012 | 0.022 | 0.033 | 0.033 | 0.041 | 0.052 |
| 02 | 0.059 | 0.009 | -0.014 | -0.003 | -0.004 | -0.005 | 0.033 | 0.023 | 0.029 |
| 03 | 0.025 | -0.002 | 0.028 | 0.040 | 0.020 | 0.051 | 0.053 | 0.032 | 0.065 |
| 04 | -0.023 | 0.003 | 0.033 | -0.008 | 0.007 | 0.039 | 0.023 | 0.007 | 0.029 |
| 05 | -0.004 | 0.006 | 0.023 | 0.012 | 0.022 | 0.033 | 0.033 | 0.041 | 0.052 |
| 06 | -0.035 | -0.004 | 0.004 | -0.014 | 0.002 | -0.023 | 0.048 | 0.003 | -0.042 |
| 07 | 0.010 | 0.023 | 0.012 | 0.019 | 0.065 | 0.051 | 0.026 | 0.061 | 0.049 |
| 08 | -0.050 | -0.039 | -0.016 | -0.013 | 0.003 | 0.022 | 0.012 | 0.025 | 0.052 |
| 09 | 0.010 | 0.020 | 0.028 | 0.006 | 0.021 | 0.035 | 0.034 | 0.057 | 0.057 |
| 10 | -0.016 | 0.006 | 0.027 | 0.022 | 0.034 | 0.053 | 0.019 | 0.030 | 0.053 |
| 11 | -0.004 | 0.012 | 0.032 | 0.049 | 0.026 | 0.027 | 0.037 | 0.030 | 0.043 |
| 12 | 0.001 | 0.018 | 0.011 | -0.001 | 0.026 | 0.037 | -0.008 | 0.041 | 0.089 |
| 13 | 0.009 | 0.033 | 0.063 | 0.036 | 0.056 | 0.089 | 0.037 | 0.072 | 0.098 |
| 14 | 0.030 | 0.004 | -0.012 | -0.008 | 0.025 | 0.039 | 0.054 | 0.019 | -0.008 |
| 15 | 0.041 | 0.030 | 0.052 | 0.038 | 0.027 | 0.054 | 0.060 | 0.032 | 0.059 |
| 16 | -0.102 | 0.041 | 0.098 | -0.018 | 0.041 | 0.056 | 0.004 | 0.025 | 0.065 |
| 17 | -0.003 | -0.033 | -0.036 | 0.039 | -0.002 | -0.018 | -0.013 | -0.015 | 0.023 |
| 18 | 0.015 | -0.019 | 0.034 | 0.002 | 0.004 | 0.029 | 0.022 | 0.006 | 0.029 |
| 19 | -0.016 | 0.025 | 0.063 | -0.023 | 0.014 | 0.046 | 0.106 | 0.251 | 0.208 |
| 20 | -0.034 | -0.014 | -0.001 | 0.048 | 0.031 | 0.019 | 0.054 | 0.047 | 0.043 |
| **Mean** | **0.00** | **0.01** | **0.02** | **0.01** | **0.02** | **0.03** | **0.03** | **0.04** | **0.05** |
| **SD** | **0.03** | **0.02** | **0.03** | **0.02** | **0.02** | **0.03** | **0.03** | **0.05** | **0.05** |

# Copyright Permissions

## Contact Lens and Anterior Eye

This is a License Agreement between heinz otchere ("You") and Elsevier ("Elsevier") provided by Copyright Clearance Center ("CCC"). The license consists of your order details, the terms and conditions provided by Elsevier, and the payment terms and conditions.

**All payments must be made in full to CCC. For payment instructions, please see information listed at the bottom of this form.**

| | |
|---|---|
| Supplier | Elsevier Limited<br>The Boulevard,Langford Lane<br>Kidlington,Oxford,OX5 1GB,UK |
| Registered Company Number | 1982084 |
| Customer name | heinz otchere |
| Customer address | School of optometry and Vision Science<br>Waterloo, ON N2L 3G1 |
| License number | 3179020756621 |
| License date | Jun 30, 2013 |
| Licensed content publisher | Elsevier |
| Licensed content publication | Contact Lens and Anterior Eye |
| Licensed content title | Pellucid corneal marginal degeneration: A review |
| Licensed content author | Amit Jinabhai,Hema Radhakrishnan,Clare O'Donnell |
| Licensed content date | April 2011 |
| Licensed content volume number | 34 |
| Licensed content issue number | 2 |
| Number of pages | 8 |
| Start Page | 56 |
| End Page | 63 |
| Type of Use | reuse in a thesis/dissertation |
| Portion | figures/tables/illustrations |
| Number of figures/tables/illustrations | 1 |
| Format | electronic |
| Are you the author of this Elsevier article? | No |
| Will you be translating? | No |

169

Order reference number

Title of your thesis/dissertation      Use of OCT and Oculus Pentacam HR as aids to semi-scleral
contact lens fitting

Expected completion date      Jul 2013

Estimated size (number of pages)      200

Elsevier VAT number      GB 494 6272 12

Permissions price      0.00 USD

VAT/Local Sales Tax      0.00 USD / 0.00 GBP

Total      0.00 USD

Terms and Conditions

**Journal of Histochemistry and Cytochemistry**

**Eye and Contact Lens**

My Orders > Orders > All Orders

## License Details

This is a License Agreement between heinz otchere ("You") and Wolters Kluwer Health ("Wolters Kluwer Health"). The license consists of your order details, the terms and conditions provided by Wolters Kluwer Health, and the payment terms and conditions.

Get the printable license.

| | |
|---|---|
| License Number | 3179040510900 |
| License date | Jun 30, 2013 |
| Licensed content publisher | Wolters Kluwer Health |
| Licensed content publication | Eye & Contact Lens: Science and Clinical Practice |
| Licensed content title | Corneal Nerve Structure and Function in Keratoconus: A Case Report. |
| Licensed content author | Mannion, Luisa; Tromans, Cindy; O'Donnell, Clare |
| Licensed content date | Jan 1, 2007 |
| Volume number | 33 |
| Issue Number | 2 |
| Type of Use | Dissertation/Thesis |
| Requestor type | Individual Account |
| Author of this Wolters Kluwer article | No |
| Title of your thesis / dissertation | Use of OCT and Oculus Pentacam HR as aids to semi-scleral contact lens fitting |
| Expected completion date | Jul 2013 |
| Estimated size(pages) | 200 |
| **Total** | **0.00 USD** |

◄ Back

**Contact Lens and Anterior Eye**

Copyright Clearance Center RightsLink®

Home | Account Info | Help

Title: Keratoconus: A review
Author: Miguel Romero-Jiménez,Jacinto Santodomingo-Rubido,James S. Wolffsohn
Publication: Contact Lens and Anterior Eye
Publisher: Elsevier
Date: August 2010
Copyright © 2010, Elsevier

## Order Completed

Thank you very much for your order.

This is a License Agreement between heinz otchere ("You") and Elsevier ("Elsevier"). The license consists of your order details, the terms and conditions provided by Elsevier, and the payment terms and conditions.

Get the printable license.

| License Number | 3179050027134 |
|---|---|
| License date | Jun 30, 2013 |
| Licensed content publisher | Elsevier |
| Licensed content publication | Contact Lens and Anterior Eye |
| Licensed content title | Keratoconus: A review |
| Licensed content author | Miguel Romero-Jiménez,Jacinto Santodomingo-Rubido,James S. Wolffsohn |
| Licensed content date | August 2010 |
| Licensed content volume number | 33 |
| Licensed content issue number | 4 |
| Number of pages | 10 |
| Type of Use | reuse in a thesis/dissertation |
| Portion | figures/tables/illustrations |

# References

## References for Chapter 1

1.      Grzybowski A, McGhee CN. The early history of keratoconus prior to Nottingham's landmark 1854 treatise on conical cornea: A review. Clin Exp Optom 2013;

2.      Rabinowitz YS. Keratoconus. Surv Ophthalmol 1998;42:297-319.

3.      Krachmer JH, Feder RS, Belin MW. Keratoconus and related noninflammatory corneal thinning disorders. Surv Ophthalmol 1984;28:293-322.

4.      Vanathi M. Keratoconus: Prevalence and associations. Expert Rev Ophthalmol 2012;7:529-531.

5.      Romero-Jimenez M, Santodomingo-Rubido J, Wolffsohn JS. Keratoconus: a review. Cont Lens Anterior Eye 2010;33:157-66.

6.      Sugar J, MacSai MS. What causes keratoconus? Cornea 2012;31:716-719.

7.      Chopra I, Jain AK. Between eye asymmetry in keratoconus in an Indian population. Clin Exp Optom 2005;88:146-152.

8.      Li Y, Wei RH, Zhao SZ. Clinical characteristics and diagnosis of keratoconus. Int J Ophthalmol 2011;11:270-272.

9.      Piñero DP, Nieto JC, Lopez-Miguel A. Characterization of corneal structure in keratoconus. J Cataract Refract Surg 2012;38:2167-2183.

10.     Kenney MC, Brown DJ, Rajeev B. Everett Kinsey lecture. The elusive causes of keratoconus: a working hypothesis. The CLAO J 2000;26:10-13.

11.     Li Y, Tan O, Brass R, Weiss JL, Huang D. Corneal epithelial thickness mapping by fourier-domain optical coherence tomography in normal and keratoconic eyes. Ophthalmology 2012;119:2425-2433.

12.     Piñero DP, Alió JL, Alesón A, Vergara ME, Miranda M. Corneal volume, pachymetry, and correlation of anterior and posterior corneal shape in subclinical and different stages of clinical keratoconus. J Cataract Refract Surg 2010;36:814-825.

13.     Gosavi VV, Hardten DR. Developments in diagnostic tools for corneal ectasia. Expert Rev Ophthalmol 2010;5:475-481.

14. Sanchis-Gimeno JA, Herrera M, Lleó-Pérez A, Alonso L, Rahhal MS, Martínez-Soriano F. Anatomic differences between a normal and two keratoconus corneas. Eur J Anat 2007;11:31-35.

15. Souza MB, Medeiros FW, Souza DB, Garcia R, Alves MR. Evaluation of machine learning classifiers in keratoconus detection from orbscan ii examinations. Clinics 2010;65:1223-1228.

16. Tananuvat N, Leeungurasatien P, Wiriyaluppa C. Superior keratoconus with hydrops. Int Ophthalmol 2009;29:419-421.

17. Chan JS, Mandell RB, Fusaro RE. Keratoconus changes with your view point. Invest Ophthalmol Vis Sci 1996;37:

18. Prisant O, Legeais JM, Renard G. Superior keratoconus. Cornea 1997;16:693-694.

19. Weed KH, McGhee CNJ, MacEwen CJ. Atypical unilateral superior keratoconus in young males. Cont Lens Anterior Eye 2005;28:177-179.

20. Rahman W, Anwar S. An unusual case of keratoconus. J Pediatr Ophthalmol Strabismus 2006;43:373-375.

21. Tenkman LR, Price MO, Price Jr FW. Keratoconus onset after age 50. J Refract Surg 2012;28:436-438.

22. Li X, Rabinowitz YS, Rasheed K, Yang H. Longitudinal study of the normal eyes in unilateral keratoconus patients. Ophthalmology 2004;111:440-446.

23. Shen X, Xu G, Jiao Q, Shi R, Li X. Ocular complications in atopic dermatitis. Chinese Ophthalmic Res 2007;25:544-546.

24. Akova YA, Rodriguez A, Foster CS. Atopic keratoconjunctivitis. Ocul Immunol Inflamm 1994;2:125-144.

25. Garrity JA, Liesegang TJ. Ocular complications of atopic dermatitis. Can J Ophthalmol 1984;19:21-24.

26. Khan MD, Kundi N, Saeed N, Gulab A, Nazeer AF. Incidence of keratoconus in spring catarrh. Br J Ophthalmol 1988;72:41-43.

27. Rao M, Victoria MS, Jabbar H, Steiner P. Atopic dermatitis, asthma and eye changes in children. J Asthma Res 1981;18:47-48.

28.     Tuft SJ, Kemeny DM, Dart JKG, Buckley RJ. Clinical features of atopic keratoconjunctivitis. Ophthalmology 1991;98:150-158.

29.     Culbertson WW, Tseng SCG. Corneal disorders in floppy eyelid syndrome. Cornea 1994;13:33-42.

30.     Ezra DG, Beaconsfield M, Collin R. Floppy Eyelid Syndrome: Stretching the Limits. Surv Ophthalmol 2010;55:35-46.

31.     Ezra DG, Beaconsfield M, Sira M, Bunce C, Wormald R, Collin R. The Associations of Floppy Eyelid Syndrome: A Case Control Study. Ophthalmology 2010;117:831-838.

32.     Fowler AM, Dutton JJ. Floppy eyelid syndrome as a subset of lax eyelid conditions: Relationships and clinical relevance (an ASOPRS thesis). Ophthalmic Plast Reconstr Surg 2010;26:195-204.

33.     Hirunwiwatkul P, Puangsricharern V, Sothornwit N, Pongpun PR, Sawatdiwithayayong J. Eye diseases associated with obstructive sleep apnea syndrome in an Asian population. Asian Biomed 2010;4:645-650.

34.     Mojon DS, Goldblum D, Fleischhauer J, Chiou AGY, Frueh BE, Hess CW, Gugger M, Bassetti C, Boehnke M, Mathis J. Eyelid, conjunctival, and corneal findings in sleep apnea syndrome. Ophthalmology 1999;106:1182-1185.

35.     Negris R. Floppy eyelid syndrome associated with keratoconus. J Am Optom Assoc 1992;63:316-319.

36.     Bielory B, Bielory L. Atopic dermatitis and keratoconjunctivitis. Immunol Allerg Clin North Am 2010;30:323-336.

37.     McMonnies CW. Management of chronic habits of abnormal eye rubbing. Cont Lens Anterior Eye 2008;31:95-102.

38.     Nemet AY, Vinker S, Bahar I, Kaiserman I. The association of keratoconus with immune disorders. Cornea 2010;29:1261-1264.

39.     Patel D, McGhee C. Understanding keratoconus: What have we learned from the New Zealand perspective? Clin Exp Optom 2012;

40.     Tuft SJ, Hassan H, George S, Frazer DG, Willoughby CE, Liskova P. Keratoconus in 18 pairs of twins. Acta Ophthalmol 2012;90:e482-e486.

41.  Kenney MC, Brown DJ. The cascade hypothesis of keratoconus. Cont Lens Anterior Eye 2003;26:139-146.

42.  Fimiani F, Iovine A, Carelli R, Pansini M, Sebastio G, Magli A. Incidence of ocular pathologies in Italian children with Down syndrome. Eur J Ophthalmol 2007;17:817-822.

43.  Grünauer-Kloevekorn C, Duncker GIW. Keratoconus: Epidemiology, risk factors and diagnosis. Klin Monbl Augenheilkd 2006;223:493-502.

44.  Liza-Sharmini AT, Azlan ZN, Zilfalil BA. Ocular findings in Malaysian children with Down syndrome. Singapore Med J 2006;47:14-19.

45.  Wroblewski KJ, Mader TH, Torres MF, Parmley VC, Rotkis WM. Long-term graft survival in patients with Down syndrome after penetrating keratoplasty. Cornea 2006;25:1026-1028.

46.  Liza-Sharmini AT, Azlan ZN, Zilfalil BA. Ocular findings in Malaysian children with Down syndrome. Singapore Med J 2006;47:14-19.

47.  Mohd-Ali B, Mohammed Z, Norlaila MD, Mohd-Fadzil N, Rohani CJC, Mohidin N. Visual and binocular status of down syndrome children in Malaysia. Clin Exp Optom 2006;89:150-154.

48.  Godel V, Blumenthal M, Iaina A. Congenital Leber amaurosis, keratoconus, and mental retardation in familial juvenile nephronophthisis. J Pediatr Ophthalmol Strabismus 1978;15:89-91.

49.  Flanders M, Lapointe ML, Brownstein S, Little JM. Keratoconus and Leber's congenital amaurosis: A clinicopathological correlation. Can J Ophthalmol 1984;19:310-314.

50.  Kuming BS, Joffe L. Ehlers-Danlos syndrome associated with keratoconus: a case report. S Afr Med J 1977;52:403-405.

51.  May MA, Beauchamp GR. Collagen maturation defects in Ehlers-Danlos ketatopathy. J Pediatr Ophthalmol Strabismus 1987;24:78-82.

52.  McDermott ML, Holladay J, Liu D, Puklin JE, Shin DH, Cowden JW. Corneal topography in Ehlers-Danlos syndrome. J Cataract Refract Surg 1998;24:1212-1215.

53.  Gregoratos ND, Bartsocas CS, Papas K. Blue sclerae with keratoglobus and brittle cornea. Br J Ophthalmol 1971;55:424-426.

54.     Hyams SW, Kar H, Neumann E. Blue sclerae and keratoglobus. Ocular signs of a systemic connective tissue disorder. Br J Ophthalmol 1969;53:53-58.

55.     Jinabhai A, Radhakrishnan H, O'Donnell C. Pellucid corneal marginal degeneration: A review. Cont Lens Anterior Eye 2011;34:56-63.

56.     Al-Torbak AA. Deep anterior lamellar keratoplasty for pellucid marginal degeneration. Saudi J Ophthalmol. 2013;27:11-14.

57.     Walker RN, Khachikian SS, Belin MW. Scheimpflug photographic diagnosis of pellucid marginal degeneration. Cornea 2008;27:963-966.

58.     Belin MW, Asota IM, Ambrosio Jr R, Khachikian SS. What's in a name: Keratoconus, pellucid marginal degeneration, and related thinning disorders. Am J Ophthalmol 2011;152:157-162.e1.

59.     Millar MJ, Maloof A. Deep lamellar keratoplasty for pellucid marginal degeneration: Review of management options for corneal perforation. Cornea 2008;27:953-956.

60.     Etzine S. Corneal thinning syndrome: keratoleptynsis. Ophthalmol 1969;157:263-267.

61.     Karabatsas CH, Cook SD. Topographic analysis in pellucid marginal corneal degeneration and keratoglobus. Eye 1996;10:451-455.

62.     Sridhar MS, Mahesh S, Bansal AK, Nutheti R, Rao GN. Pellucid marginal corneal degeneration. Ophthalmology 2004;111:1102-1107.

63.     Bower KS, Dhaliwal DK, Barnhorst DAJ, Warnicke J. Pellucid Marginal Degeneration with Superior Corneal Thinning. Cornea 1997;16:483-485.

64.     Nowak DM, Gajecka M. The genetics of keratoconus. Middle East Afr J Ophthalmol 2011;18:2-6.

65.     Mackey DA. Genetic eye research in Tasmania: A historical overview. Clin Exp Ophthalmol 2012;40:205-210.

66.     Mishra A, Yazar S, Hewitt AW, Mountain JA, Ang W, Pennell CE, Martin NG, Montgomery GW, Hammond CJ, Young TL, Macgregor S, Mackey DA. Genetic variants near PDGFRA are associated with corneal curvature in Australians. Invest Ophthalmol Vis Sci 2012;53:7131-7136.

67.     Burdon KP, Vincent AL. Insights into keratoconus from a genetic perspective. Clin Exp Optom 2013;

68. Nielsen K, Hjortdal J, Pihlmann M, Corydon TJ. Update on the keratoconus genetics. Acta Ophthalmol 2013;91:106-113.

69. Nielsen K, Hjortdal J, Pihlmann M, Corydon TJ. Update on the keratoconus genetics. Act Ophthalmol 2013;91:106-113.

70. Gonzalez V, McDonnell PJ. Computer-assisted corneal topography in parents of patients with keratoconus. Arch Ophthalmol 1992;110:1412-1414.

71. Wang Y, Rabinowitz YS, Rotter JI, Yang H. Genetic epidemiological study of keratoconus: Evidence for major gene determination. Am J Med Genet 2000;93:403-409.

72. Hammerstein W. Genetics of conical cornea. Albrecht Von Graefes .Arch Klin Exp Ophthalmol 1974;190:293-308.

73. Weed KH, MacEwen CJ, McGhee CNJ. The variable expression of keratoconus within monozygotic twins: Dundee University Scottish Keratoconus Study (DUSKS). Cont Lens Anterior Eye 2006;29:123-126.

74. Bourne WM, Michels VV. Keratoconus in one identical twin. Cornea 1982;1:35-37.

75. Itoi M HM, Tsuda N, et al. Corneal shape of familial members of keratoconis patients. Fort Lauderdale. A1082–D706 Presented at: 2011 ARVO Annual Meeting; April 30April 30 to May 5, 2011;

76. Barraquer Somers E, Chan CC, Green WR. Corneal epithelial iron deposition. Ophthalmology 1983;90:729-734.

77. Davis LJ, Barr JT, Vanotteren D. Transient rigid lens-induced striae in keratoconus. Optom Vis Sci 1993;70:216-219.

78. Belin MW, Asota IM, Ambrosio R, Jr., Khachikian SS. What's in a name: keratoconus, pellucid marginal degeneration, and related thinning disorders. Am J Ophthalmol 2011;152:157-162.

79. Varley GA, Macsai MS, Krachmer JH. The results of penetrating keratoplasty for pellucid marginal corneal degeneration. Am J Ophthalmol 1990;110:149-152.

80. Kayazawa F, Nishimura K, Kodama Y, Tsuji T, Itoi M. Keratoconus with pellucid marginal corneal degeneration. Arch Ophthalmol 1984;102:895-6.

81. Ljubic AD. Keratoconus and its prevalence in Macedonia. Macedonian J Med Sci 2009;2:58-62.

82. Kok YO, Ling Tan GF, Loon SC. Review: Keratoconus in Asia. Cornea 2012;31:581-593.

83. Nielsen K, Hjortdal J, Nohr EA, Ehlers N. Incidence and prevalence of keratoconus in Denmark. Act Ophthalmol Scand 2007;85:890-892.

84. Kennedy RH, Bourne WM, Dyer JA. A 48-year clinical and epidemiologic study of keratoconus. Am J Ophthalmol 1986;101:267-273.

85. Pearson AR, Soneji B, Sarvananthan N, Sanford-Smith JH. Does ethnic origin influence the incidence or severity of keratoconus? Eye 2000;14:625-628.

86. Tanabe U, Fujiki K, Ogawa A, Ueda S, Kanai A. Prevalence of keratoconus patients in Japan. J Jpn Ophthlmol Soc 1985;89:407-411.

87. Jonas JB, Nangia V, Matin A, Kulkarni M, Bhojwani K. Prevalence and Associations of Keratoconus in Rural Maharashtra in Central India: The Central India Eye and Medical Study. Am J Ophthalmol 2009;148:760-765.

88. Ihalainen A. Clinical and epidemiological features of keratoconus genetic and external factors in the pathogenesis of the disease. Act Ophthalmol 1986;178:1-64.

89. Robin JB, Schanzlin DJ, Verity SM, Barron BA, Arffa RC, Suarez E, Kaufman HE. Peripheral corneal disorders. Surv Ophthalmol 1986;31:1-36.

90. Millodot M, Shneor E, Albou S, Atlani E, Gordon-Shaag A. Prevalence and associated factors of keratoconus in jerusalem: A cross-sectional study. Ophthalmic Epidemiol 2011;18:91-97.

91. Owens H, Gamble G. A profile of keratoconus in New Zealand. Cornea 2003;22:122-125.

92. Ertan A, Muftuoglu O. Keratoconus clinical findings according to different age and gender groups. Cornea 2008;27:1109-1113.

93. Fink BA, Wagner H, Steger-May K, Rosenstiel C, Roediger T, McMahon TT, Gordon MO, Zadnik K. Differences in keratoconus as a function of gender. Am J Ophthalmol 2005;140:459.e1-459.11.

94.    Lim N, Vogt U. Characteristics and functional outcomes of 130 patients with keratoconus attending a specialist contact lens clinic. Eye 2002;16:54-59.

95.    Abu Ameerh MA, Al Refai RM, Al Bdour MD. Keratoconus patients at Jordan University Hospital: A descriptive study. Clin Ophthalmol 2012;6:1895-1899.

96.    Fan Gaskin JC, Good WR, Jordan CA, Patel DV, McGhee CN. The Auckland keratoconus study: Identifying predictors of acute corneal hydrops in keratoconus. Clin Exp Optom 2013;

97.    Barr JT, Zadnik K, Wilson BS, Edrington TB, Everett DF, Fink BA, Shovlin JP, Weissman BA, Siegmund K, Gordon MO. Factors associated with corneal scarring in the collaborative longitudinal evaluation of keratoconus (CLEK) study. Cornea 2000;19:501-507.

98.    Khor WB, Wei RH, Lim L, Chan CM, Tan DT. Keratoconus in Asians: Demographics, clinical characteristics and visual function in a hospital-based population. Clin Exp Ophthalmol 2011;39:299-307.

99.    Mohd-Ali B, Abdu M, Yaw CY, Mohidin N. Clinical characteristics of keratoconus patients in Malaysia: A review from a cornea specialist centre. J Optom 2012;5:38-42.

100.    Cozma I, Atherley C, James NJ, Georgiou T, Funnell CL, Cassels-Brown A, O'Conor R. Influence of ethnic origin on the incidence of keratoconus and associated atopic disease in Asian and white patients (multiple letters) [7]. Eye 2005;19:924-926.

101.    Georgiou T, Funnell CL, Cassels-Brown A, O'Conor R. Influence of ethnic origin on the incidence of keratoconus and associated atopic disease in Asians and white patients. Eye 2004;18:379-383.

102.    Banitt MR, Romano A, Iragavarapu S, Budenz DL, Lee RK. Forme fruste anterior segment dysgenesis. Br J Ophthalmol 2011;95:1756-7.

103.    Doane JF. Keratoconus and forme fruste keratoconus. Cataract Refract Surg Today 2005;38.

104.    Koller T, Iseli HP, Donitzky C, Ing D, Papadopoulos N, Seiler T. Topography-Guided Surface Ablation for Forme Fruste Keratoconus. Ophthalmology 2006;113:2198-2202.

105.    Li SW, Li ZX, Shi WY, Zeng QY, Jin XM. Clinical features of 233 cases of keratoconus. Chinese J Ophthalmol 2005;41:610-613.

106.    Bron AJ. Keratoconus. Cornea 1988;7:163-169.

107. Romero-Jiménez M, Santodomingo-Rubido J, Wolffsohn JS. Keratoconus: A review. Cont Lens Anterior Eye 2010;33:157-166.

108. Edrington TB, Zadnik K, Barr JT. Keratoconus. Optom Clin : the official publication of the Prentice Society 1995;4:65-73.

109. Mocan MC, Yilmaz PT, Irkec M, Orhan M. The significance of Vogt's striae in keratoconus as evaluated by in vivo confocal microscopy. Clin Exp Ophthalmol 2008;36:329-334.

110. Mannion LS, Tromans C, O'Donnell C. Corneal nerve structure and function in keratoconus: A case report. Eye Contact Lens 2007;33:106-108.

111. Basu S, Mukhopadhyay S. Acute corneal hydrops. Ophthalmology 2012;119:2197-2197.e1.

112. Bilgin B, Ünal B, Ünal M, Doĝan E, Çetinkaya A, Akyol M, Yücel T, Akar Y, Apaydin C, Ilhan D. Keratoconus presenting with bilateral simultaneous acute corneal hydrops. Cont Lens Anterior Eye 2013;36:98-100.

113. Ch'ng SW, Pillai MB, Aazeem S, Tu KL. Acute corneal hydrops mimicking full thickness perforation. BMJ case reports 2012;2012:

114. Fan Gaskin JC, Good WR, Jordan CA, Patel DV, McGhee CN. The Auckland keratoconus study: Identifying predictors of acute corneal hydrops in keratoconus. Clin Exp Optom 2013;

115. Güell JL, Verdaguer P, Elies D, Gris O, Manero F. Acute corneal hydrops after intrastromal corneal ring segment implantation for keratoconus. J Cataract Refract Surg 2012;38:2192-2195.

116. Palioura S, Chodosh J, Pineda R. A novel approach to the management of a progressive descemet membrane tear in a patient with keratoglobus and acute hydrops. Cornea 2013;32:355-358.

117. Weichenthal L, Monarrez L. Acute vision loss. Keratoconus with acute corneal hydrops. Ann Emerg Med 2012;59:

118. Barbara A, Shehadeh-Masha'our R, Zvi F, Garzozi HJ. Management of pellucid marginal degeneration with intracorneal ring segments. J Refract Surg 2005;21:296-298.

119.  Tzelikis PF, Cohen EJ, Rapuano CJ, Hammersmith KM, Laibson PR. Management of pellucid marginal corneal degeneration. Cornea 2005;24:555-560.

120.  Tang M, Shekhar R, Miranda D, Huang D. Characteristics of keratoconus and pellucid marginal degeneration in mean curvature maps. Am J Ophthalmol 2005;140:993-1001.e1.

121.  Parker DL, McDonnell PJ, Barraquer J, Green WR. Pellucid marginal corneal degeneration. Cornea 1986;5:115-123.

122.  Dundar H, Kara N, Kaya V, Bozkurt E, Yazici AT, Hekimhan PK. Unilateral superior pellucid marginal degeneration in a case with ichthyosis. Cont Lens Anterior Eye 2011;34:45-48.

123.  Sridhar MS, Mahesh S, Bansal AK, Rao GN. Superior pellucid marginal corneal degeneration. Eye 2004;18:393-399.

124.  Taglia DP, Sugar J. Superior pellucid marginal corneel degeneration with hydrops. Arch Ophthalmol 1997;115:274-275.

125.  Gruenauer-Kloevekorn C, Fischer U, Kloevekorn-Norgall K, Duncker GIW. Pellucid marginal corneal degeneration: Evaluation of the corneal surface and contact lens fitting. Br J Ophthalmol 2006;90:318-323.

126.  Lee BW, Jurkunas UV, Harissi-Dagher M, Poothullil AM, Tobaigy FM, Azar DT. Ectatic Disorders Associated With a Claw-shaped Pattern on Corneal Topography. Am J Ophthalmol 2007;144:154-156.e3.

127.  Randleman JB. Ectatic Disorders Associated with a Claw-shaped Pattern on Corneal Topography. Am J Ophthalmol 2007;144:977-978.

128.  Aldave AJ, Mabon M, Hollander DA, McLeod SD, Spencer WH, Abbott RL. Spontaneous corneal hydrops and perforation in keratoconus and pellucid marginal degeneration. Cornea 2003;22:169-174.

129.  Forooghian F, Assaad D, Dixon WS. Successful conservative management of hydrops with perforation in pellucid marginal degeneration. Can J Ophthalmol 2006;41:74-77.

130.  Hsu HY, Phillips NJ, Harocopos GJ. Secondary amyloidosis in the hydrops lesion of a patient with pellucid marginal degeneration. Cornea 2007;26:992-994.

131. Ramamurthy B, Mittal V, Rani A, Ram M, Sangwan VS. Spontaneneous hydrops in pellucid marginal degeneration: Documentation by OCT-III. Clin Exp Ophthalmol 2006;34:616-617.

132. Tsumamoto Y, Okada K, Nakamoto H, Tsukamoto H, Mishima HK. A case of pellucid marginal corneal degeneration diagnosed ten years after acute hydrops. Jpn Ophthalmol 2000;51:865-869.

133. Toriyama K, Inoue T, Suzuki T, Higashiura R, Maeda N, Ohashi Y. Spontaneous bleb formation in a presumed pellucid marginal corneal degeneration with acute hydrops. Cornea 2013;

134. Ambrósio Jr R, Caiado ALC, Guerra FP, Louzada R, Roy AS, Luz A, Dupps WJ, Belin MW. Novel pachymetric parameters based on corneal tomography for diagnosing keratoconus. J Refract Surg 2011;27:753-758.

135. Della Vecchia MA, Lamkin-Kennard K. Corneal modeling for analysis of photorefractive keratectomy. 1997.

136. Douthwaite WA, Parkinson A. Precision of Orbscan II assessment of anterior corneal curvature and asphericity. J Refract Surg. 2009;25:435-443.

137. Karimian F, Feizi S, Doozandeh A, Faramarzi A, Yaseri M. Comparison of corneal tomography measurements using Galilei,,Orbscan II,and placido disk-based topographer systems. J Refract Surg 2011;27:502-508.

138. Tajbakhsh Z, Salouti R, Nowroozzadeh MH, Aghazadeh-Amiri M, Tabatabaee S, Zamani M. Comparison of keratometry measurements using the Pentacam HR, the Orbscan IIz, and the TMS-4 topographer. Ophthalmic Physiol Opt 2012;32:539-546.

139. Taneja M, Ashar JN, Mathur A, Vaddavalli PK, Rathi V, Sangwan V, Murthy S. Measure of keratoconus progression in patients with vernal keratoconjunctivitis using scanning slit topography. Cont Lens Anterior Eye 2013;36:41-44.

140. Tummanapalli SS, Maseedupally V, Mandathara P, Rathi VM, Sangwan VS. Evaluation of corneal elevation and thickness indices in pellucid marginal degeneration and keratoconus. J Cataract Refract Surg 2013;39:56-65.

141. Faramarzi A, Karimian F, Jafarinasab MR, Jabbarpoor Bonyadi MH, Yaseri M. Central corneal thickness measurements after myopic photorefractive keratectomy using Scheimpflug imaging, scanning-slit topography, and ultrasonic pachymetry. J Cataract Refract Surg 2010;36:1543-1549.

142. Guilbert E, Saad A, Grise-Dulac A, Gatinel D. Corneal thickness, curvature, and elevation readings in normal corneas: Combined Placido-Scheimpflug system versus combined Placido-scanning-slit system. J Cataract Refract Surg 2012;38:1198-1206.

143. Tajbakhsh Z, Salouti R, Nowroozzadeh MH, Aghazadeh-Amiri M, Tabatabaee S, Zamani M. Comparison of keratometry measurements using the Pentacam HR, the Orbscan IIz, and the TMS-4 topographer. Ophthal Physiol Opt 2012;32:539-546.

144. Brautaset RL, Nilsson M, Miller WL, Leach NE, Tukler JH, Bergmanson JPG. Central and peripheral corneal thinning in keratoconus. Cornea 2013;32:257-261.

145. Bueno-Gimeno I, España-Gregori E, Gené-Sampedro A, Lanzagorta-Aresti A, Dualde-Beltrán C. Anterior chamber depth measurement in teenagers. Comparison of two techniques. J Optom. 2013;

146. Dutta D, Rao HL, Addepalli UK, Vaddavalli PK. Corneal Thickness in Keratoconus. Comparing Optical, Ultrasound, and Optical Coherence Tomography Pachymetry. Ophthalmology 2012;

147. Hamard P, El Maftouhi A, Baudouin C. Molteno implant and the vicryl tie technique: Role of Visante anterior segment OCT. J Fr Ophtalmol 2013;

148. Nemeth G, Hassan Z, Szalai E, Berta A, Modis Jr L. Anterior segment parameters measured with 2 optical devices compared to ultrasonic data. Eur J Ophthalmol 2013;23:177-182.

149. Rama P, Knutsson KA, Razzoli G, Matuska S, Viganò M, Paganoni G. Deep anterior lamellar keratoplasty using an original manual technique. Br J Ophthalmol 2013;97:23-27.

150. Vega-Estrada A, Alió JL, Plaza Puche AB, Marshall J. Outcomes of a new microwave procedure followed by accelerated cross-linking for the treatment of keratoconus: A pilot study. J Refract Surg 2012;28:787-792.

151. Alhassan MB, Rabiu M, Agbabiaka IO. Interventions for Mooren's ulcer. Cochrane database of systematic reviews (Online) 2011;

152. Fan W, Xiao X, Chen C, Xing Y. Cause analysis of corneal perforation in central China. Med J Wuhan Univ 2012;33:134-136.

153. Hatou S, Dogru M, brahim OMA, Wakamatsu T, Sato EA, Shimmura S, Negishi K, Tsubota K. The application of in vivo confocal scanning laser microscopy in the

diagnosis and evaluation of treatment responses in mooren's ulcer. Invest Ophthalmol Vis Sci 2011;52:6680-6689.

154.    Mathur A, Ashar J, Sangwan V. Mooren's ulcer in children. Br J Ophthalmol 2012;96:796-800.

155.    Meskin SW, Carlson EM. Mooren's-type ulceration associated with severe hidradenitis suppurativa: A case report and literature review. Ocul Immunol Inflamm 2011;19:340-342.

156.    Shoaib KK. Mooren's ulcer or peripheral ulcerative keratitis. Bri J Ophthalmol 2012;96:1146.

157.    Zelefsky JR, Srinivasan M, Cunningham ET. Mooren's ulcer. Expert Rev Ophthalmol 2011;6:461-467.

158.    Huang T, Wang YJ, Ji JP, Gao N, Chen JQ. Lamellar keratoplasty for treatment of peripheral corneal perforation. Chinese J Ophthalmol 2008;44:104-110.

159.    Jain K, Kumar S, Jain C, Malik VK. Terrien's marginal degeneration: an unusual presentation in an indian female. Nepalese J Ophthalmol 2009;1:141-142.

160.    Kawamoto K, Nishida T. Terrien's marginal corneal degeneration. Jpn J Clin Ophthalmol 2005;59:170-173.

161.    Liang LY, Liu ZG, Chen JQ, Huang T, Wang ZC, Zou WJ, Chen LS, Zhou SY, Lin AH. Keratoplasty in the management of Terrien' s marginal degeneration. Chinese J Ophthalmol 2008;44:116-121.

162.    Shimazaki J, Yang HY, Shimmura S, Tsubota K. Terrien's marginal degeneration associated with erythema elevatum diutinum. Cornea 1998;17:342-344.

163.    Wagoner MD, Teichmann KD. Terrien's marginal degeneration associated with posterior polymorphous dystrophy. Cornea 1999;18:612-615.

164.    Zare M, Javadi MA, Einollahi B, Baradaran-Rafii A, Ghanavati SZ, Jamshidi Farsani MR, Mohammadi P, Feizi S. Indications for corneal transplantation at a tertiary referral center in Tehran. J Ophthalmic Vis Res 2010;5:82-86.

165.    Corredor-Osorio R, Corredor-Osorio M, Corredor-Osorio A, Perez-Balbuena AL. Terrien's marginal degeneration. Case and literature report. Ann Ophthalmol 1998;72:297-301.

166. Lampé Z, Békési L, Csutak A, Berta A. Two cases of terrien's marginal degeneration treated with peripherial full thickness keratectomy, and followed-up by computer-assisted corneal topography. Klin Monbl Augenheilkd 2003;220:404-410.

167. Wilson SE, Lin DTC, Klyce SD, Insler MS. Terrien's marginal degeneration: Corneal topography. Refract Corneal Surg 1990;6:15-20.

168. Ahmadi Hosseini SM, Mohidin N, Abolbashari F, Mohd-Ali B, Santhirathelagan CT. Corneal thickness and volume in subclinical and clinical keratoconus. Int Ophthalmol 2012;1-7.

169. Tummanapalli SS, Maseedupally V, Mandathara P, Rathi VM, Sangwan VS. Evaluation of corneal elevation and thickness indices in pellucid marginal degeneration and keratoconus. J Cataract Refract Surg 2013;39:56-65.

170. Saad A, Gatinel D. Topographic and tomographic properties of forme fruste keratoconus corneas. Invest Ophthalmol Vis Sci 2010;51:5546-5555.

171. Prakash G, Agarwal A, Mazhari AI, Kumar G, Desai P, Kumar DA, Jacob S. A new, pachymetry-based approach for diagnostic cutoffs for normal, suspect and keratoconic cornea. Eye 2012;26:650-657.

172. Schlegel Z, Hoang-Xuan T, Gatinel D. Comparison of and correlation between anterior and posterior corneal elevation maps in normal eyes and keratoconus-suspect eyes. J Cataract Refract Surg 2008;34:789-795.

173. Piñero DP, Alió JL, Alesón A, Vergara ME, Miranda M. Corneal volume, pachymetry, and correlation of anterior and posterior corneal shape in subclinical and different stages of clinical keratoconus. J Cataract Refract Surg 2010;36:814-825.

174. Uçakhan OO, Çetinkor V, Özkan M, Kanpolat A. Evaluation of Scheimpflug imaging parameters in subclinical keratoconus, keratoconus, and normal eyes. J Cataract Refract Surg 2011;37:1116-1124.

175. Al-Farhan HM, Almutairi RN. Anterior segment biometry using ultrasound biomicroscopy and the artemis-2 very high frequency ultrasound scanner. Clin Ophthalmol 2012;7:141-147.

176. Al-Farhan HM, Al-Otaibi WM. Comparison of central corneal thickness measurements using ultrasound pachymetry, ultrasound biomicroscopy, and the Artemis-2 VHF scanner in normal eyes. Clin Ophthalmol 2012;6:1037-1043.

177. Gemoules G. A novel method of fitting scleral lenses using high resolution optical coherence tomography. Eye Contact Lens 2008;34:80-83.

178. Szalai E, Berta A, Hassan Z, Módis Jr L. Reliability and repeatability of swept-source Fourier-domain optical coherence tomography and Scheimpflug imaging in keratoconus. J Cataract Refract Surg 2012;38:485-494.

179. Jahadi Hosseini HR, Katbab A, Khalili MR, Abtahi MB. Comparison of corneal thickness measurements using Galilei, HR Pentacam, and ultrasound. Cornea 2010;29:1091-1095.

180. Oliveira CM, Ribeiro C, Franco S. Corneal imaging with slit-scanning and Scheimpflug imaging techniques. Clin Exp Optom 2011;94:33-42.

181. Park SH, Choi SK, Lee D, Jun EJ, Kim JH. Corneal thickness measurement using orbscan, pentacam, galilei, and ultrasound in normal and post-femtosecond laser in situ keratomileusis eyes. Cornea 2012;31:978-982.

182. Sorbara L, Maram J, Fonn D, Woods C, Simpson T. Metrics of the normal cornea: Anterior segment imaging with the Visante OCT. Clin Exp Optom 2010;93:150-156.

183. Sorbara L MJ, Mueller K. Use of the Visante™ OCT anterior segment image to measure the saggital depth of keratoconus corneae compared to normal's at a 15mm chord length. Br Contact lens Assoc 2011;

184. Kompella VB, Aasuri MK, Rao GN. Management of pellucid marginal corneal degeneration with rigid gas permeable contact lenses. CLAO J 2002;28:140-145.

185. Jinabhai A, Radhakrishnan H, O'Donnell C. Corneal changes after suspending contact lens wear in early pellucid marginal corneal degeneration and moderate keratoconus. Eye Contact Lens 2011;37:99-105.

186. Looi ALG, Lim L, Tan DTH. Visual rehabilitation with new-age rigid gas-permeable scleral contact lenses - A case series. Ann Acad Med Singapore 2002;31:234-237.

187. Oliveira CM, Ferreira A, Franco S. Wavefront analysis and Zernike polynomial decomposition for evaluation of corneal optical quality. J Cataract Refract Surg 2012;38:343-356.

188. Pullum KW, Buckley RJ. A study of 530 patients referred for rigid gas permeable scleral contact lens assessment. Cornea 1997;16:612-622.

189. Ward HJ, Watanabe RK. Aspheric multifocal RGP lenses in a pellucid marginal degeneration patient. Optom Vis Sci 2000;77:167.

190. Zadnik K, Barr JT, Steger-May K, Edrington TB, McMahon TT, Gordon MO. Comparison of flat and steep rigid contact lens fitting methods in keratoconus. Optom Vis Sci 2005;82:1014-1021.

191. Garcia-Lledo M, Feinbaum C, Alio JL. Contact lens fitting in keratoconus. Compr Ophthalmol Update 2006;7:47-52.

192. Yanai R, Ueda K, Sonoda KH. Bevel toric multicurve rigid gas-permeable lens for keratoconus. Japanese J Ophthalmol 2012;1-7.

193. Hwang JS, Lee JH, Wee WR, Kim MK. Effects of multicurve RGP contact lens use on topographic changes in keratoconus. Korean J Ophthalmol 2010;24:201-206.

194. Kok JH. A European fitting philosophy for aspheric, high-Dk RGP contact lenses. CLAO J 1992;18:232-6.

195. Wasserman D, Itzkowitz J, Kamenar T, Asbell PA. Corneal topographic data: its use in fitting aspheric contact lenses. CLAO J 1992;18:83-5.

196. Dominguez CE, Shah A, Weissman BA. Bitoric gas-permeable contact lens application in pellucid marginal corneal degeneration. Eye Contact Lens 2005;31:241-243.

197. Gruenauer-Kloevekorn C, Fischer U, Kloevekorn-Norgall K, Duncker GIW. Pellucid marginal corneal degeneration: Evaluation of the corneal surface and contact lens fitting. Br J Ophthalmol 2006;90:318-323.

198. Nejabat M, Khalili MR, Dehghani C. Cone location and correction of keratoconus with rigid gas-permeable contact lenses. Cont Lens Anterior Eye 2012;35:17-21.

199. Betts AM, Mitchell GL, Zadnik K. Visual performance and comfort with the Rose K lens for keratoconus. Optom Vis Sci 2002;79:493-501.

200. Fatima T, Acharya MC, Mathur U, Barua P. Demographic profile and visual rehabilitation of patients with keratoconus attending contact lens clinic at a tertiary eye care centre. Cont Lens Anterior Eye 2010;33:19-22.

201. Fernandez-Velazquez FJ. Kerasoft IC compared to Rose-K in the management of corneal ectasias. Cont Lens Anterior Eye 2012;35:175-179.

202. Jain AK, Sukhija J. Rose-K contact lens for keratoconus. Indian J Ophthalmol 2007;55:121-5.

203. Mandathara Sudharman P, Rathi V, Dumapati S. Rose K lenses for keratoconus--an Indian experience. Eye Contact Lens 2010;36:220-2.

204. Ozkurt YB, Sengor T, Kurna S, Evciman T, Acikgoz S, Haboglu M, Aki S. Rose K contact lens fitting for keratoconus. Int Ophthalmol 2008;28:395-8.

205. Zhang Q, Xie PY. RGPCL fitting techniques for keratoconus. Int J Ophthalmol 2005;5:313-317.

206. Elbendary AM, Abou Samra W. Evaluation of rigid gas permeable lens fitting in keratoconic patients with optical coherence tomography. Graefes Arch Clin Exp Ophthalmol 2013;1-6.

207. Barnett M, Mannis MJ. Contact lenses in the management of keratoconus. Cornea 2011;30:1510-1516.

208. Biswas S, Brahma A, Tromans C, Ridgway A. Management of pellucid marginal corneal degeneration. Eye 2000;14:629-634.

209. Oriowo OM, Briggs ST. Contact lens management of pellucid marginal corneal degeneration in a Saudi Arabia teaching hospital. Int Contact Lens Clin 1994;21:147-150.

210. Liu J, Leach NE, Bergmanson JPG. Reverse-geometry gas-permeable lens design for pellucid marginal degeneration. Eye Contact Lens 2005;31:127-129.

211. Hu CY, Tung HC. Managing keratoconus with reverse-geometry and dual-geometry contact lenses: A case report. Eye Contact Lens 2008;34:71-75.

212. Jae LL, Kim MK. Clinical performance and fitting characteristics with a multicurve lens for keratoconus. Eye Contact Lens 2004;30:20-24.

213. Hwang JS, Lee JH, Wee WR, Kim MK. Effects of multicurve RGP contact lens use on topographic changes in keratoconus. Korean J Ophthalmol 2010;24:201-206.

214. Yanai R, Ueda K, Sonoda KH. Bevel toric multicurve rigid gas-permeable lens for keratoconus. Jpn J Ophthalmol 2012;1-7.

215. Mahadevan R, Amudhaoli A, Valarmathi A. Retrospective study of contact lens fitting in pellucid marginal degeneration. Eye Contact Lens 2008;34:207-210.

216. Katsoulos C, Karageorgiadis L, Vasileiou N, Mousafeiropoulos T, Asimellis G. Customized hydrogel contact lenses for keratoconus incorporating correction for vertical coma aberration. Ophthalmic Physiol Opt 2009;29:321-329.

217. Marsack JD, Parker KE, Applegate RA. Performance of wavefront-guided soft lenses in three keratoconus subjects. Optom Vis Sci 2008;85:E1172-E1178.

218. Fernandez-Velazquez FJ. Response to Comment to "Kerasoft IC compared to Rose-K in the management of corneal ectasias". Cont Lens Anterior Eye 2013;

219. Abdalla YF, Elsahn AF, Hammersmith KM, Cohen EJ. Synergeyes lenses for keratoconus. Cornea 2010;29:5-8.

220. Bromley JG, Randleman JB. Treatment strategies for corneal ectasia. Curr Opin Ophthalmol. 2010;21:255-258.

221. Donshik PC, Luistro E. Hybrid gas permeable - Soft contact lens. Contactologia1990;12:32-34.

222. Owens H, Watters G, Gamble G. Effect of SoftPerm lens wear on corneal thickness and topography: A comparison between keratoconic and normal corneae. CLAO J 2002;28:83-87.

223. Pilskalns B, Fink BA, Hill RM. Oxygen demands with hybrid contact lenses. Optom Vis Sci 2007;84:334-342.

224. Rubinstein MP, Sud S. The use of hybrid lenses in management of the irregular cornea. Cont Lens Anterior Eye 1999;22:87-90.

225. Tan DTH, Pullum KW, Buckley RJ. Medical applications of scleral contact lenses: 1. A retrospective analysis of 343 cases. Cornea 1995;14:121-129.

226. Nau AC. A comparison of Synergeyes versus traditional rigid gas permeable lens designs for patients with irregular corneas. Eye Contact Lens 2008;34:198-200.

227. Sengor T, Kurna SA, Aki S, Özkurt Y. High Dk piggyback contact lens system for contact lens-intolerant keratoconus patients. Clin Ophthalmol 2011;5:331-335.

228. Gould HL. Management of keratoconus with corneal and scleral lenses. Am J Ophthalmol 1970;70:624-629.

229. Gungor I, Schor K, Rosenthal P, Jacobs DS. The Boston Scleral Lens in the treatment of pediatric patients. J AAPOS 2008;12:263-267.

230. Pearson RM. The sämisch case and the müllers of wiesbaden. Optom Vis Sci 2009;86:157-164.

231. Pullum KW, Whiting MA, Buckley RJ. Scleral contact lenses: The expanding role. Cornea 2005;24:269-277.

232. Romero-Jiménez M, Flores-Rodríguez P. Utility of a semi-scleral contact lens design in the management of the irregular cornea. Cont Lens Anterior Eye 2013;

233. Schornack MM, Patel SV. Scleral lenses in the management of keratoconus. Eye Contact Lens 2010;36:39-44.

234. Segal O, Barkana Y, Hourovitz D, Behrman S, Kamun Y, Avni I, Zadok D. Scleral contact lenses may help where other modalities fail. Cornea 2003;22:308-310.

235. Severinsky B, Millodot M. Current applications and efficacy of scleral contact lenses - A retrospective study. J Optom 2010;3:158-163.

236. Shneor E, Millodot M, Blumberg S, Ortenberg I, Behrman S, Gordon-Shaag A. Characteristics of 244 patients with keratoconus seen in an optometric contact lens practice. Clin Exp Optom 2012;

237. Visser ES, Visser R, Van Lier HJJ, Otten HM. Modern scleral lenses part II: Patient satisfaction. Eye Contact Lens 2007;33:21-25.

238. Tan DTH, Pullum KW, Buckley RJ. Medical applications of scleral contact lenses: 2. Gas-permeable scleral contact lenses. Cornea 1995;14:130-137.

239. Jhanji V, Sharma N, Vajpayee RB. Management of keratoconus: Current scenario. Br J Ophthalmol 2011;95:1044-1050.

240. Dalton K, Sorbara L. Fitting an MSD (Mini Scleral Design) rigid contact lens in advanced keratoconus with INTACS. Cont Lens Anterior Eye 2011;34:274-281.

241. Visser ES, Visser R, Van Lier HJJ, Otten HM. Modern scleral lenses part I: Clinical features. Eye Contact Lens 2007;33:13-20.

242. Schornack MM, Baratz KH, Patel SV, Maguire LJ. Jupiter scleral lenses in the management of chronic graft versus host disease. Eye Contact Lens 2008;34:302-305.

243. Tappin MJ, Pullum KW, Buckley RJ. Scleral contact lenses for overnight wear in the management of ocular surface disorders. Eye 2001;15:168-172.

244.    Smiddy WE, Hamburg TR, Kracher GP, Gottsch JD, Stark WJ. Therapeutic contact lenses. Ophthalmology 1990;97:291-295.

245.    Foss AJE, Trodd TC, Dart JKG. Current indications for scleral contact lenses. CLAO J 1994;20:115-118.

246.    Schornack MM, Patel SV. Relationship between corneal topographic indices and scleral lens base curve. Eye Contact Lens 2010;36:330-333.

247.    Hostetter TA. Learning the "numbers game" of today's contact lens fitting: clinical and business pearls. J Ophthalmic Nurs Technol 1996;15:148-152.

248.    Sorbara L, Dalton K. The use of video-keratoscopy in predicting contact lens parameters for keratoconic fitting. Cont Lens Anterior Eye 2010;33:112-118.

249.    Michaud L, van der Worp E, Brazeau D, Warde R, Giasson CJ. Predicting estimates of oxygen transmissibility for scleral lenses. Cont Lens Anterior Eye 2012;35:266-271.

250.    Organization IS. Ophthalmic optics–Contact lenses and contact lens care products-Guidance for clinical investigations. 1997;

251.    Ozkurt Y, Atakan M, Gencaga T, Akkaya S. Contact lens visual rehabilitation in keratoconus and corneal keratoplasty. J Ophthalmol 2012;2012:

252.    Biswas S, Brahma A, Tromans C, Ridgway A. Management of pellucid marginal corneal degeneration. Eye 2000;14:629-34.

253.    Jhanji V, Sharma N, Vajpayee RB. Management of keratoconus: Current scenario. Br J Ophthalmol 2011;95:1044-1050.

254.    Pramanik S, Musch DC, Sutphin JE, Farjo AA. Extended Long-term Outcomes of Penetrating Keratoplasty for Keratoconus. Ophthalmology 2006;113:1633-1638.

255.    Böhringer D, Reinhard T. Long-term keratoplasty graft survival. Ophthalmology 2013;120:216.

256.    Bhatt UK, Faraj LA, Dhillon V, Dua HS. Visual outcomes in corneal transplantation. Br J Ophthalmol 2013;97:5-6.

257.    Bhatt UK, Faraj LA, Dhillon V, Dua HS. Visual outcomes in corneal transplantation. Br J Ophthalmol. 2013;97:5-6.

258. Bahar I, Kaiserman I, Srinivasan S, Ya-Ping J, Slomovic AR, Rootman DS. Comparison of Three Different Techniques of Corneal Transplantation for Keratoconus. Am J Ophthalmol. 2008;146:905-912.e1.

259. Reinhart WJ, Musch DC, Jacobs DS, Lee WB, Kaufman SC, Shtein RM. Deep anterior lamellar keratoplasty as an alternative to penetrating keratoplasty: A report by the American academy of ophthalmology. Ophthalmology 2011;118:209-218.

260. Amayem AF, Hamdi IM, Hamdi MM. Refractive and visual outcomes of penetrating keratoplasty versus deep anterior lamellar keratoplasty with hydrodissection for treatment of keratoconus. Cornea 2012;

261. Cohen E. Comparison of outcomes of lamellar keratoplasty and penetrating keratoplasty in keratoconus. Evidence-Based Ophthalmol 2010;11:82-83.

262. Jones MNA, Armitage WJ, Ayliffe W, Larkin DF, Kaye SB. Penetrating and deep anterior lamellar keratoplasty for keratoconus: A comparison of graft outcomes in the United Kingdom. Invest Ophthalmol Vis Sci 2009;50:5625-5629.

263. Kiliç Uzbek A, Müftüočlu O. Advances in keratoconus treatment. Expert Rev Ophthalmol 2011;6:95-103.

264. Kim KH, Choi SH, Ahn K, Chung ES, Chung TY. Comparison of refractive changes after deep anterior lamellar keratoplasty and penetrating keratoplasty for keratoconus. Jpn J Ophthalmol 2011;55:93-97.

265. Kubaloglu A, Coskun E, Sari ES, Gune AS, Cinar Y, Piero DP, Kutluturk I, Ozerturk Y. Comparison of astigmatic keratotomy results in deep anterior lamellar keratoplasty and penetrating keratoplasty in keratoconus. Am J Ophthalmol 2011;151:637-643.

266. Motlagh BF, Sedghipoor MR, Abroon G, Sadigh AL. Outcomes of penetrating keratoplasty and deep anterior Lamellar keratoplasty for Keratoconus in a university teaching hospital. Iran J Ophthalmol 2012;24:52-56.

267. Sari ES, Kubaloğlu A, Ünal M, Llorens DP, Koytak A, Ofluoğlu AN, Özertürk Y. Penetrating keratoplasty versus deep anterior lamellar keratoplasty: Comparison of optical and visual quality outcomes. Br J Ophthalmol 2012;96:1063-1067.

268. Shi JL, Feng YF, Yu JG, Wang QM. Meta analysis of deep lamellar keratoplasty and penetrating keratoplasty for keratoconus. Chinese J Exp Ophthalmol 2012;30:926-931.

269. Feizi S, Javadi MA, Kanavi MR. Recurrent keratoconus in a corneal graft after deep anterior lamellar keratoplasty. J Ophthal Vis Res 2012;7:328-331.

270. Ting DSJ, Ramaesh K, Srinivasan S, Sau CY, Mantry S, Roberts F. Deep anterior lamellar keratoplasty: Challenges in histopathological examination. Br J Ophthalmol 2012;96:1510-1512.

271. Razmju H, Shams M, Abtahi MA, Abtahi SH. Comparison of deep lamellar keratoplasty and penetrating keratoplasty in patients with keratoconus: A clinical trial study. J Isfahan Med Sch 2011;29:

272. Koh S, Maeda N, Nakagawa T, Nishida K. Quality of vision in eyes after selective lamellar keratoplasty. Cornea 2012;31:S45-S49.

273. Tan BU, Purcell TL, Torres LF, Schanzlin DJ. New surgical approaches to the management of keratoconus and post-LASIK ectasia. Trans Am Ophthalmol Soc 2006;104:212-218.

274. Alessio G, L'Abbate M, Boscia F, Sborgia C, La Tegola MG. Excimer Laser-Assisted Lamellar Keratoplasty and the Corneal Endothelium. Am J Ophthalmol. 2010;150:88-96.e1.

275. Alio JL, Shah S, Barraquer C, Bilgihan K, Anwar M, Melles GRJ. New techniques in lamellar keratoplasty. Curr Opin Ophthalmol. 2002;13:224-229.

276. Bilgihan K, Özdek SC, Sari A, Hasanreisoğlu B. Excimer laser-assisted anterior lamellar keratoplasty for keratoconus, corneal problems after laser in situ keratomileusis, and corneal stromal opacities. J Cataract Refract Surg. 2006;32:1264-1269.

277. O'Keefe M, Kirwan C. Laser epithelial keratomileusis in 2010 - a review. Clin Exp Ophthalmol 2010;38:183-191.

278. Spadea L. Collagen crosslinking for ectasia following PRK performed in excimer laser-assisted keratoplasty for keratoconus. Eur J Ophthalmol 2012;22:274-277.

279. Xu K, McKee HD, Jhanji V. Changing perspective of reasons for not performing laser-assisted in situ keratomileusis among candidates in a university eye clinic. Clin Exp Optom 2013;96:20-24.

280. Greenbaum A, Kaiserman I, Avni I. Long-term reversibility of epikeratophakia. Cornea 2007;26:1210-1212.

281. Javadi MA, Kanavi MR, Ahmadi M, Yazdani S. Outcomes of epikeratoplasty for advanced keratoglobus. Cornea 2007;26:154-157.

282.  Panda A, Gupta A, Sharma N, Nindrakrishna S, Vajpayee R. Anatomical and functional graft survival, 10 years after epikeratoplasty in keratoconus. Indian J Ophthalmol 2013;61:18-22.

283.  Zare MA, Hashemi H, Salari MR. Intracorneal ring segment implantation for the management of keratoconus: Safety and efficacy. J ataract Refract Surg 2007;33:1886-1891.

284.  Piñero DP, Alio JL. Intracorneal ring segments in ectatic corneal disease - a review. Clin Exp Ophthalmol 2010;38:154-167.

285.  Shetty R, Kurian M, Anand D, Mhaske P, Narayana KM, Shetty BK. Intacs in advanced keratoconus. Cornea 2008;27:1022-1029.

286.  Siganos CS, Kymionis GD, Kartakis N, Theodorakis MA, Astyrakakis N, Pallikaris IG. Management of keratoconus with Intacs. Am J Ophthalmol 2003;135:64-70.

287.  Tomalla M, Cagnolati W. Modern treatment options for the therapy of keratoconus. Cont Lens Anterior Eye 2007;30:61-66.

288.  Mularoni A, Torreggiani A, Di Biase A, Laffi GL, Tassinari G. Conservative treatment of early and moderate pellucid marginal degeneration: A new refractive approach with intracorneal rings. Ophthalmology 2005;112:660-666.

289.  Jabbarvand M, Amanzadeh K, Rahimi F, Kheirkhah A, Hashemi H. Visual outcome after implantation of intracorneal ring segments for pellucid marginal degeneration. Iran J Ophthalmol 2010;22:41-45.

290.  Barbara A, Shehadeh-Masha'our R, Zvi F, Garzozi HJ. Management of pellucid marginal degeneration with intracorneal ring segments. J Refract Surg. 2005;21:296-298.

291.  Ertan A, Bahadir M. Intrastromal ring segment insertion using a femtosecond laser to correct pellucid marginal corneal degeneration. J Cataract Refract Surg 2006;32:1710-1716.

292.  Ertan A, Bahadir M. Management of superior pellucid marginal degeneration with a single intracorneal ring segment using femtosecond laser. J Refract Surg 2007;23:205-208.

293.  Kymionis GD, Aslanides IM, Siganos CS, Pallikaris IG. Intacs for early pellucid marginal degeneration. J Cataract Refract Surg 2004;30:230-233.

294.  Piñero DP, Alio JL. Intracorneal ring segments in ectatic corneal disease - a review. Clin Exp Ophthalmol 2010;38:154-167.

295.  Rodriguez-Prats J, Galal A, Garcia-Lledo M, De La Hoz F, Alió JL. Intracorneal rings for the correction of pellucid marginal degeneration. J Cataract Refract Surg 2003;29:1421-1424.

296.  Koller T, Seiler T. Therapeutic cross-linking of the cornea using riboflavin/UVA. Klin Monbl Augenheilkd 2007;224:700-706.

297.  Spoerl E, Mrochen M, Sliney D, Trokel S, Seiler T. Safety of UVA-riboflavin cross-linking of the cornea. Cornea 2007;26:385-389.

298.  Wollensak G. Crosslinking treatment of progressive keratoconus: New hope. Curr Opin Ophthalmol 2006;17:356-360.

299.  Asri D, Touboul D, Fournié P, Malet F, Garra C, Gallois A, Malecaze F, Colin J. Corneal collagen crosslinking in progressive keratoconus: Multicenter results from the French National Reference Center for Keratoconus. J Cataract Refract Surg. 2011;37:2137-2143.

300.  Tahzib NG, van der Leij AG. Corneal crosslinking as treatment for progressive keratoconus. Ned Tijdschr Geneeskd. 2011;155:

301.  Vanathi M, Bypareddy R, Panda A. Corneal collagen crosslinking using UVA light and riboflavin for keratoconus. Expert Rev Ophthalmol 2012;7:33-44.

302.  Wollensak G. Crosslinking treatment of progressive keratoconus: New hope. Curr Opin Ophthalmol 2006;17:356-360.

303.  Spadea L. Corneal collagen cross-linking with riboflavin and UVA irradiation in pellucid marginal degeneration. J Refract Surg 2010;26:375-377.

304.  Gasson A. Andrew Gasson. Contact Lenses. 1998-2013;
305.  Rosenthal P. Clinincal performance and fitting principles of "rigid" super permeable contact lenses. J Br Contact Lens Assoc 1986;1986:88-90,91.

306.  Sorbara L, Chong T, Fonn D. Visual acuity, lens flexure, and residual astigmatism of keratoconic eyes as a function of back optic zone radius of rigid lenses. Cont Lens Anterior Eye 2000;23:48-52.

307.  Wechsler S. Effects of rigid lens flexure on vision. J Am Optom Assoc 1979;50:327-328.

308. Alipour F, Kheirkhah A, Jabarvand Behrouz M. Use of mini scleral contact lenses in moderate to severe dry eye. Cont Lens Anterior Eye 2012;35:272-276.

309. Gan Jh, Zhang J, Lü Hb. Clinical application and follow-up of new-type HD soft hydrophilic contact lenses. Chinese J Tissue Eng Res 2012;16:5506-5510.

310. Guillon M. Are silicone hydrogel contact lenses more comfortable than hydrogel contact lenses? Eye Contact Lens 2013;39:86-92.

311. Jacob JT. Biocompatibility in the development of silicone-hydrogel lenses. Eye Contact Lens 2013;39:13-19.

312. Keir N, Jones L. Wettability and silicone hydrogel lenses: A review. Eye Contact Lens 2013;39:100-108.

313. Sankaridurg P, Lazon De La Jara P, Holden B. The future of silicone hydrogels. Eye Contact Lens 2013;39:125-129.

314. Wang H, Guo YZ. Curative effect of rigid gas permeable contact lens for adults with high ametropic amblyopia. Int Eye Sci 2012;12:2237-2238.

315. Berry M, Purslow C, Murphy PJ, Pult H. Contact lens materials, mucin fragmentation and relation to symptoms. Cornea 2012;31:770-776.

316. Diec J, De La Jara PL, Willcox M, Holden BA. The clinical performance of lenses disposed of daily can vary considerably. Eye Contact Lens 2012;38:313-318.

317. Diec J, Evans VE, Tilia D, Naduvilath T, Holden BA, De La Jara PL. Comparison of ocular comfort, vision, and SICS during silicone hydrogel contact lens daily wear. Eye Contact Lens 2012;38:2-6.

318. Guillon M. Are silicone hydrogel contact lenses more comfortable than hydrogel contact lenses? Eye Contact Lens 2013;39:86-92.

319. Jacob JT. Biocompatibility in the development of silicone-hydrogel lenses. Eye Contact Lens 2013;39:13-19.

320. Keir N, Jones L. Wettability and silicone hydrogel lenses: A review. Eye Contact Lens 2013;39:100-108.

321. Sankaridurg P, Lazon De La Jara P, Holden B. The future of silicone hydrogels. Eye Contact Lens 2013;39:125-129.

322. Wang H, Guo YZ. Curative effect of rigid gas permeable contact lens for adults with high ametropic amblyopia. Int Eye Sci 2012;12:2237-2238.

323. Lembach RG. Use of contact lenses for management of keratoconus. Ophthalmol Clin North Am 2003;16:383-394.

324. Rengstorff RH, Odby A. Adaptation to Paraperm extended wear lenses: a clinical study in Sweden. J Am Optom Assoc 1986;57:600-603.

325. Szczotka-Flynn LB, Patel S. Menicon Z rigid gas permeable lenses for keratoconus and irregular corneas: a retrospective case series. Eye Contact Lens 2008;34:254-260.

326. Elbendary A, Abou Samra W. Evaluation of rigid gas permeable lens fitting in keratoconic patients with optical coherence tomography. Graefes Arch Clin Exp Ophthalmol 2013;1-6.

327. Fonn D, Holden BA. Rigid gas-permeable vs. hydrogel contact lenses for extended wear. Am J Optom Physiol Opt 1988;65:536-544.

328. Polse KA, Graham AD, Fusaro RE, Gan CM, Rivera RK, Chan JS, McNamara NA, Sanders TS. Predicting RGP daily wear success. CLAO J 1999;25:152-158.

329. Fortuin MF, Schilperoort J, Evans BJ, Edgar DF, Manon HM, Kiers H. Randomised controlled study comparing comfort-related outcomes between two rigid gas permeable (RGP) lenses with different sessile drop contact angles. Ophthalmic Physiol Opt 2011;31:190-9.

330. van der Worp E. Comfort O2 RGP material study. Glob Contact Lens 2006;34–38.

331. van der Worp E. Comfort O2; an independent clinical evaluation. Optom Today 2005;23 30-32.

332. Tromans C, Bullock JM, Ridgway AEA, Tullo AB. Evaluation of gas permeable scleral contact lenses. Invest Ophthalmol Vis Sci 1996;37:

333. Liesegang TJ. Physiologic changes of the cornea with contact lens wear. CLAO J 2002;28:12-27.

334. Polse KA, Brand R, Mandell R, Vastine D, Demartini D, Flom R. Age differences in corneal hydration control. Invest Ophthalmol Vis Sci 1989;30:392-399.

335. Iskeleli G, Karakoç Y, Aydin Ö, Yetik H, Uslu H, Kizilkaya M. Comparison of Tear-Film Osmolarity in Different Types of Contact Lenses. CLAO J 2002;28:174-176.

336. Maldonado-Codina C, Morgan PB, Efron N, Efron S. Comparative clinical performance of rigid versus soft hyper Dk contact lenses used for continuous wear. Optom Vis Sci 2005;82:536-548.

337. Graham AD, Fusaro RE, Polse KA, Lin Meng C, Giasson CJ. Predicting extended wear complications from overnight corneal swelling. Invest Ophthalmol Vis Sci 2001;42:3150-3157.

338. Leung BK, Bonanno JA, Radke CJ. Oxygen-deficient metabolism and corneal edema. Prog Retin Eye Res 2011;30:471-492.

339. Forister JFY, Forister EF, Yeung KK, Ye P, Chung MY, Tsui A, Weissman BA. Prevalence of contact lens-related complications: UCLA contact lens study. Eye Contact Lens 2009;35:176-180.

340. Pullum KW, Stapleton FJ. Scleral lens induced corneal swelling: What is the effect of varying Dk and lens thickness? CLAO J 1997;23:259-263.

341. Smith GT, Mireskandari K, Pullum KW. Corneal Swelling with Overnight Wear of Scleral Contact Lenses. Cornea 2004;23:29-34.

342. Staarmann MT, Schoessler JP. Contact lenses and eye closure: Comparative analysis using three different methods to induce corneal swelling. Optom Vis Sci 1991;68:374-379.

343. Efron N. Intersubject variability in corneal swelling response to anoxia. Acta Ophthalmol 1986;64:302-305.

344. Wang Q, Savini G, Hoffer KJ, Xu Z, Feng Y, Wen D, Hua Y, Yang F, Pan C, Huang J. A Comprehensive Assessment of the Precision and Agreement of Anterior Corneal Power Measurements Obtained Using 8 Different Devices. PLoS One 2012;7:

345. Cho P, Lam AKC, Mountford J, Ng L. The performance of four different corneal topographers on normal human corneas and its impact on orthokeratology lens fitting. Optom Vis Sci 2002;79:175-183.

346. Buehl W, Stojanac D, Sacu S, Drexler W, Findl O. Comparison of three methods of measuring corneal thickness and anterior chamber depth. Am J Ophthalmol 2006;141:7-12.e1.

347. Shankar H, Taranath D, Santhirathelagan CT, Pesudovs K. Repeatability of corneal first-surface wavefront aberrations measured with Pentacam corneal topography. J Cataract Refract Surg 2008;34:727-734.

348.    Miranda MA, O'Donnell C, Radhakrishnan H. Repeatability of corneal and ocular aberration measurements and changes in aberrations over one week. Clin Exp Optom 2009;92:253-266.

349.    Salouti R, Nowroozzadeh MH, Zamani M, Ghoreyshi M. Comparison of anterior chamber depth measurements using Galilei, HR Pentacam, and Orbscan II. Optometry 2010;81:35-39.

350.    Ahmadi Hosseini SM, Abolbashari F, Mohidin N. Anterior segment parameters in Indian young adults using the Pentacam. Int Ophthalmol 2013;1-6.

351.    Aptel F, Chiquet C, Beccat S, Denis P. Biometric evaluation of anterior chamber changes after physiologic pupil dilation using Pentacam and anterior segment optical coherence tomography. Invest Ophthalmol Vis Sci 2012;53:4005-4010.

352.    Koç M, Özülken K, Ayar O, Karakurt A. Measurement of the anterior chamber angle according to quadrants and age groups using pentacam scheimpflug camera. J Glaucoma 2013;22:226-229.

353.    Lam AK, Tse JS. Pentacam anterior chamber parameters in young and middle-aged Chinese. Clin Exp Optom 2013;96:85-91.

354.    Nakakura S, Mori E, Nagatomi N, Tabuchi H, Kiuchi Y. Comparison of anterior chamber depth measurements by 3-dimensional optical coherence tomography, partial coherence interferometry biometry, Scheimpflug rotating camera imaging, and ultrasound biomicroscopy. J Cataract Refract Surg 2012;38:1207-1213.

355.    Rossi GCM, Scudeller L, Delfino A, Raimondi M, Pezzotta S, Maccarone M, Antoniazzi E, Pasinetti GM, Bianchi PE. Pentacam sensitivity and specificity in detecting occludable angles. Eur J Ophthalmol 2012;22:701-708.

356.    Chen X, Ji YH, Jiang YX, Luo Y, Jiang CH, Lu Y. Clinical study of intraocular lens power calculation methods after cornea refractive surgery. Chinese J Ophthalmol 2010;46:518-524.

357.    Norrby S. Pentacam keratometry and IOL power calculation. J Cataract Refract Surg 2008;34:3.

358.    Savini G, Barboni P, Carbonelli M, Hoffer KJ. Accuracy of Scheimpflug corneal power measurements for intraocular lens power calculation. J Cataract Refract Surg 2009;35:1193-1197.

359. Savini G, Barboni P, Carbonelli M, Hoffer KJ. Comparison of methods to measure corneal power for intraocular lens power calculation using a rotating Scheimpflug camera. J Cataract Refract Surg 2013;

360. Mohamed S, Lee GKY, Rao SK, Wong AL, Cheng ACK, Li EYM, Chi SCC, Lam DSC. Repeatability and reproducibility of pachymetric mapping with Visante Anterior Segment-Optical Coherence Tomography. Invest Ophthalmol Vis Sci 2007;48:5499-5504.

361. Wells M, Wu N, Kokkinakis J, Sutton G. Correlation of central corneal thickness measurements using Topcon TRK-1P, Zeiss Visante AS-OCT and DGH Pachmate 55 handheld ultrasonic pachymeter. Clin Exp Optom 2013;

362. Li Y, Meisler DM, Tang M, Lu ATH, Thakrar V, Reiser BJ, Huang D. Keratoconus Diagnosis with Optical Coherence Tomography Pachymetry Mapping. Ophthalmology 2008;115:2159-2166.

363. Li Y, Shekhar R, Huang D. Corneal Pachymetry Mapping with High-speed Optical Coherence Tomography. Ophthalmology 2006;113:799.e1-799.e2.

364. Cui L, Wang J, Perez VL, Shen M, Yuan Y, Wang MR. Visualization of the precorneal tear film using ultrahigh resolution optical coherence tomography in dry eye. Eye Contact Lens 2012;38:240-244.

365. Chen F, Shen M, Chen W, Wang J, Li M, Yuan Y, Lu F. Tear meniscus volume in dry eye after punctal occlusion. Invest Ophthalmol Vis Sci. 2010;51:1965-1969.

366. Li M, Du C, Zhu D, Shen M, Cui L, Wang J. Daytime variations of tear osmolarity and tear meniscus volume. Eye and Contact Lens 2012;38:282-287.

367. Li M, Wang J, Shen M, Cui L, Tao A, Chen Z, Ge L, Lu F. Effect of punctal occlusion on tear menisci in symptomatic contact lens wearers. Cornea 2012;31:1014-1022.

368. Palakuru JR, Wang J, Aquavella JV. Effect of Blinking on Tear Volume After Instillation of Midviscosity Artificial Tears. Am J Ophthalmol 2008;146:920-924.

369. Li J, Shen M, Wang J, Ma H, Tao A, Xu S, Lu F. Clinical significance of tear menisci in dry eye. Eye Contact Lens 2012;38:183-187.

370. Wang J, Cui L, Shen M, Perez VL, Wang MR. Ultra-high resolution optical coherence tomography for monitoring tear meniscus volume in dry eye after topical cyclosporine treatment. Clin Ophthalmol 2012;6:933-938.

371. Shen M, Wang J, Tao A, Chen Q, Lin S, Qu J, Lu F. Diurnal Variation of Upper and Lower Tear Menisci. Am J Ophthalmol 2008;145:801-806.e2.

372. Wang J, Palakuru JR, Aquavella JV. Correlations Among Upper and Lower Tear Menisci, Noninvasive Tear Break-up Time, and the Schirmer Test. Am J Ophthalmol 2008;145:795-800.e1.

373. Wang J, Fonn D, Simpson TL, Jones L. Precorneal and pre- and postlens tear film thickness measured indirectly with optical coherence tomography. Invest Ophthalmol Vis Sci 2003;44:2524-2528.

374. Kieval JZ, Karp CL, Shousha MA, Galor A, Hoffman RA, Dubovy SR, Wang J. Ultra-high resolution optical coherence tomography for differentiation of ocular surface squamous neoplasia and pterygia. Ophthalmology 2012;119:481-486.

375. Abou Shousha M, Karp CL, Canto AP, Hodson K, Oellers P, Kao AA, Bielory B, Matthews J, Dubovy SR, Perez VL, Wang J. Diagnosis of Ocular Surface Lesions Using Ultra–High-Resolution Optical Coherence Tomography. Ophthalmology

376. Ge L, Yuan Y, Shen M, Tao A, Wang J, Lu F. The role of axial resolution of optical coherence tomography on the measurement of corneal and epithelial thicknesses. Invest Ophthalmol Vis Sci 2012;

377. Ge L, Shen M, Tao A, Wang J, Dou G, Lu F. Automatic segmentation of the central epithelium imaged with three optical coherence tomography devices. Eye Contact Lens 2012;38:150-157.

378. Du C, Wang J, Cui L, Shen M, Yuan Y. Vertical and horizontal corneal epithelial thickness profiles determined by ultrahigh resolution optical coherence tomography. Cornea 2012;31:1036-1043.

379. Wang J, Fonn D, Simpson TL, Jones L. Measurement of corneal epithelial thickness using optical coherence tomography in response to hypoxia induced by soft contact lens and eye closure. Optom Vis Sci 2000;77:170.

380. Wang J, Thomas J, Cox I, Rollins A. Noncontact measurements of central corneal epithelial and flap thickness after laser in situ keratomileusis. InvestOphthalmol Vis Sci 2004;45:1812-1816.

381. Wang J, Simpson TL, Fonn D. Objective measurements of corneal light-backscatter during corneal swelling, by optical coherence tomography. Invest Ophthalmol Vis Sci 2004;45:3493-3498.

382. Wang J, Fonn D, Simpson TL, Sorbara L, Kort R, Jones L. Topographical Thickness of the Epithelium and Total Cornea after Overnight Wear of Reverse-Geometry Rigid Contact Lenses for Myopia Reduction. Invest Ophthalmol Vis Sci 2003;44:4742-4746.

383. Wang J, Fonn D, Simpson TL. Topographical thickness of the epithelium and total cornea after hydrogel and PMMA contact lens wear with eye closure. Invest Ophthalmol Vis Sci 2003;44:1070-1074.

384. Wang J, Fonn D, Simpson TL, Jones L. Relation between optical coherence tomography and optical pachymetry measurements of corneal swelling induced by hypoxia. Am J Ophthalmol 2002;134:93-98.

385. Lu F, Xu S, Qu J, Shen M, Wang X, Fang H, Wang J. Central Corneal Thickness and Corneal Hysteresis During Corneal Swelling Induced by Contact Lens Wear With Eye Closure. Am J Ophthalmol 2007;143:616-622.e2.

386. Shen M, Fan F, Xue A, Wang J, Zhou X, Lu F. Biomechanical properties of the cornea in high myopia. Vis Res 2008;48:2167-2171.

387. Du C, Shen M, Li M, Zhu D, Wang MR, Wang J. Anterior segment biometry during accommodation imaged with ultralong scan depth optical coherence tomography. Ophthalmology 2012;119:2479-2485.

388. Yuan Y, Chen F, Shen M, Lu F, Wang J. Repeated measurements of the anterior segment during accommodation using long scan depth optical coherence tomography. Eye Contact Lens 2012;38:102-108.

389. Zhou C, Wang J, Jiao S. Dual channel dual focus optical coherence tomography for imaging accommodation of the eye. Opt Express 2009;17:8947-8955.

390. Leng T, Lujan BJ, Yoo SH, Wang J. Three-dimensional spectral domain optical coherence tomography of a clear corneal cataract incision. Ophthalmic Surg Lasers and Imaging 2008;39:S132-S134.

391. Shousha MA, Perez VL, Wang J, Ide T, Jiao S, Chen Q, Chang V, Buchser N, Dubovy SR, Feuer W, Yoo SH. Use of Ultra-High-Resolution Optical Coherence Tomography to Detect In Vivo Characteristics of Descemet's Membrane in Fuchs' Dystrophy. Ophthalmology 2010;117:1220-1227.

392. Ide T, Wang J, Tao A, Leng T, Kymionis GD, O'Brien TP, Yoo SH. Intraoperative use of three-dimensional spectral-domain optical coherence tomography. Ophthalmic Surg Lasers and Imaging 2010;41:250-254.

393.    Cui L, Shen M, Wang MR, Wang J. Micrometer-Scale Contact Lens Movements Imaged by Ultrahigh-resolution Optical Coherence Tomography. Am J Ophthalmol 2012;153:275-283.e1.

394.    Shen M, Wang MR, Wang J, Yuan Y, Chen F. Entire contact lens imaged in vivo and in vitro with spectral domain optical coherence tomography. Eye Contact Lens 2010;36:73-76.

395.    Wang J, Jiao S, Ruggeri M, Shousha MA, Chen Q. In situ visualization of tears on contact lens using ultra high resolution optical coherence tomography. Eye Contact Lens 2009;35:44-49.

396.    Wang J, Aquavella J, Palakuru J, Chung S, Feng C. Relationships between central tear film thickness and tear menisci of the upper and lower eyelids. Invest Ophthalmol Vis Sci 2006;47:4349-4355.

397.    Chen Q, Wang J, Tao A, Shen M, Jiao S, Lu F. Ultrahigh-resolution measurement by optical coherence tomography of dynamic tear film changes on contact lenses. Invest Ophthalmol Vis Sci 2010;51:1988-1993.

398.    Wang J, Aquavella J, Palakuru J, Chung S. Repeated measurements of dynamic tear distribution on the ocular surface after instillation of artificial tears. Invest Ophthalmol Vis Sci 2006;47:3325-3329.

## References for Chapter 2

1.      Chen D, Lam AKC. Reliability and repeatability of the Pentacam on corneal curvatures. Clin Exp Optom 2009;92:110-118.

2.      Varssano D, Rapuano CJ, Luchs JI. Comparison of keratometric values of healthy and diseased eyes measured by Javal keratometer, EyeSys, and PAR. J Cataract Refract Surg 1997;23:419-422.

3.      Dastjerdi MH, Hashemi H. A quantitative corneal topography index for detection of keratoconus. J Refract Surg 1998;14:427-436.

4.      Yan J, Meng P, Zhao J. Research of curvature measuring system of eyes cornea. J Basic Sci Eng 2011;19:254-261.

5.      Swartz T, Marten L, Wang M. Measuring the cornea: The latest developments in corneal topography. Curr Opin Ophthalmol 2007;18:325-333.

6.      Buehren T, Collins MJ, Iskander DR, Davis B, Lingelbach B. The stability of corneal topography in the post-blink interval. Cornea 2001;20:826-833.

7.      Cronje-Dunn S, Harris WF. Keratometric variation: The influence of a fluid layer. Ophthalmic Physiol Opt 1996;16:234-236.

8.      Németh J, Erdélyi B, Csákány B. Corneal topography changes after a 15 second pause in blinking. J Cataract Refract Surg 2001;27:589-592.

9.      Tsubota K, Hata S, Okusawa Y, Egami F, Ohtsuki T, Nakamori K. Quantitative videographic analysis of blinking in normal subjects and patients with dry eye. Arch Ophthalmol 1996;114:715-720.

10.     Maldonado MJ, Nieto JC, Díez-Cuenca M, Piñero DP. Repeatability and Reproducibility of Posterior Corneal Curvature Measurements by Combined Scanning-Slit and Placido-Disc Topography after LASIK. Ophthalmology 2006;113:1918-1926.

11.     Jonuscheit S, Doughty MJ. Regional repeatability measures of corneal thickness: Orbscan II and ultrasound. Optom Vis Sci 2007;84:52-58.

12.     Cairns G, McGhee CNJ. Orbscan computerized topography: Attributes, applications, and limitations. J Cataract Refract Surg 2005;31:205-220.

13. Wegener A, Laser-junga H. Photography of the anterior eye segment according to Scheimpflug's principle: Options and limitations - A review. Clin Exp Ophthalmol 2009;37:144-154.

14. Grewal DS, Grewal SPS. Clinical applications of Scheimpflug imaging. Expert Rev Ophthalmol 2009;4:243-258.

15. Kawamorita T, Uozato H, Kamiya K, Bax L, Tsutsui K, Aizawa D, Shimizu K. Repeatability, reproducibility, and agreement characteristics of rotating Scheimpflug photography and scanning-slit corneal topography for corneal power measurement. J Cataract Refract Surg 2009;35:127-133.

16. Jain R, Dilraj G, Grewal SPS. Repeatability of corneal parameters with Pentacam after laser in situ keratomileusis. Indian J Ophthalmol 2007;55:341-347.

17. Eysteinsson T, Jonasson F, Sasaki H, Arnarsson A, Sverrisson T, Sasaki K, Stefánsson E. Central corneal thickness, radius of the corneal curvature and intraocular pressure in normal subjects using non-contact techniques: Reykjavik eye study. Acta Ophthalmol Scand 2002;80:11-15.

18. Dubbelman M, Weeber HA, Van Der Heijde RGL, Völker-Dieben HJ. Radius and asphericity of the posterior corneal surface determined by corrected Scheimpflug photography. Acta Ophthalmol Scand 2002;80:379-383.

19. Dubbelman M, Sicam VADP, Van Der Heijde GL. The shape of the anterior and posterior surface of the aging human cornea. Vis Res 2006;46:993-1001.

20. Hashemi H, Yazdani K, Mehravaran S, Khabazkhoob M, Mohammad K, Parsafar H, Fotouhi A. Corneal thickness in a population-based, cross-sectional study: The tehran eye study. Cornea 2009;28:395-400.

21. Miháltz K, Kovács I, Takács Á, Nagy ZZ. Evaluation of keratometric, pachymetric, and elevation parameters of keratoconic corneas with pentacam. Cornea 2009;28:976-980.

22. Zhang Z, Wang J, Niu W, Ma M, Jiang K, Zhu P, Ke B. Corneal asphericity and its related factors in 1052 Chinese subjects. Optom Vis Sci 2011;88:1232-1239.

23. Lackner B, Schmidinger G, Pieh S, Funovics MA, Skorpik C. Repeatability and reproducibility of central corneal thickness measurement with pentacam, orbscan, and ultrasound. Optom Vis Sci 2005;82:892-899.

24. Amano S, Honda N, Amano Y, Yamagami S, Miyai T, Samejima T, Ogata M, Miyata K. Comparison of Central Corneal Thickness Measurements by Rotating Scheimpflug

Camera, Ultrasonic Pachymetry, and Scanning-Slit Corneal Topography. Ophthalmology 2006;113:937-941.

25. González-Pérez J, González-Méijome JM, Rodríguez Ares MT, Parafita MA. Central corneal thickness measured with three optical devices and ultrasound pachometry. Eye Contact Lens 2011;37:66-70.

26. O'Donnell C, Maldonado-Codina C. Agreement and repeatability of central thickness measurement in normal corneas using ultrasound pachymetry and the OCULUS Pentacam. Cornea 2005;24:920-924.

27. Savant V, Chavan R, Pushpoth S, Ilango B. Comparability and intra-/interobserver reliability of anterior chamber depth measurements with the Pentacam and IOLMaster. J Refract Surg 2008;24:615-618.

28. Lackner B, Schmidinger G, Skorpik C. Validity and repeatability of anterior chamber depth measurements with pentacam and orbscan. Optom Vision Sci 2005;82:858-861.

29. Oliveira CM, Ribeiro C, Franco S. Corneal imaging with slit-scanning and Scheimpflug imaging techniques. Clin Exp Optom 2011;94:33-42.

30. Piñero DP, Alió JL, Alesón A, Escaf M, Miranda M. Pentacam posterior and anterior corneal aberrations in normal and keratoconic eyes. Clin Exp Optom 2009;92:297-303.

31. Gobbe M, Guillon M. Corneal wavefront aberration measurements to detect keratoconus patients. Cont Lens Anterior Eye 2005;28:57-66.

32. Onay MP, Eğilmez S, Üretmen Ö, Yağci A, Köse S. Evaluation of cornea and anterior chamber using pentacam in pediatric cases. Turk Ophthamol Soc 2011;41:133-137.

33. Mannion LS, Tromans C, O'Donnell C. Reduction in corneal volume with severity of keratoconus. Curr Eye Res 2011;36:522-527.

34. Zare MA, Hashemi H, Jamali M, Tafti MF, Hashemian MN, Kheirkhah A, Z-Mehrjardi H, Mohammadpour M. Comparison of corneal and anterior chamber parameters following myopic laser in situ keratomileusis and photorefractive keratectomy by pentacam as a new imaging technique. Iran J Ophthalmol 2011;23:27-32.

35. Borasio E, Stevens J, Smith GT. Estimation of true corneal power after keratorefractive surgery in eyes requiring cataract surgery: BESSt formula. J Cataract Refract Surg 2006;32:2004-2014.

36. Chen X, Ji YH, Jiang YX, Luo Y, Jiang CH, Lu Y. Clinical study of intraocular lens power calculation methods after cornea refractive surgery. Chinese J Ophthalmol 2010;46:518-524.

37. Turner SJ, Lee EJK, Hu V, Hollick EJ. Scheimpflug imaging to determine intraocular lens power in vivo. J Cataract Refract Surg 2007;33:1041-1044.

38. Tang Q, Hoffer KJ, Olson MD, Miller KM. Accuracy of Scheimpflug Holladay equivalent keratometry readings after corneal refractive surgery. J Cataract Refract Surg 2009;35:1198-1203.

39. Ho JD, Tsai CY, Tsai RJF, Kuo LL, Tsai IL, Liou SW. Validity of the keratometric index: Evaluation by the Pentacam rotating Scheimpflug camera. J Cataract Refract Surg 2008;34:137-145.

40. Tsukiyama J, Miyamoto Y, Higaki S, Fukuda M, Shimomura Y. Changes in the anterior and posterior radii of the corneal curvature and anterior chamber depth by orthokeratology. Eye Contact Lens 2008;34:17-20.

41. Queirós A, Villa-Collar C, Gutiérrezá AR, Jorge J, Ribeiro-Queirós MS, Peixoto-De-Matos SC, González-Méijome JM. Anterior and posterior corneal elevation after orthokeratology and standard and customized lasik surgery. Eye Contact Lens 2011;37:354-358.

42. Chen D, Lam AKC, Cho P. Posterior corneal curvature change and recovery after 6 months of overnight orthokeratology treatment. Ophthalmic Physiol Opt 2010;30:274-280.

43. Bland JM, Altman DG. Statistical methods for assessing agreement between two methods of clinical measurement. Int J Nurs Stud 2010;47:931-936.

44. Vieira S, Corrente JE. Statistical methods for assessing agreement between double readings of clinical measurements. J Appl Oral Sci 2011;19:488-492.

45. Ho T, Cheng ACK, Rao SK, Lau S, Leung CKS, Lam DSC. Central corneal thickness measurements using Orbscan II, Visante, ultrasound, and Pentacam pachymetry after laser in situ keratomileusis for myopia. J Cataract Refract Surg 2007;33:1177-1182.

46. Potvin RJ, Fonn D, Sorbara L. Comparison of polycarbonate and steel test surfaces for videokeratography. J Refract Surg 1995;11:89-91.

47.	McCarey BE, Zurawski CA, O'Shea DS. Practical aspects of a corneal topography system. CLAO J 1992;18:248-254

## References for Chapter 3

1.    Garcia-Resua C, Blanco A, Miñones M, Yebra-Pimentel E, Jesus Giraldez M. Accuracy and repeatability of a new tono-pachymeter for measuring central corneal thickness. Eye Contact Lens 2012;38:158-163.

2.    Pang C, Song X, Wang L, Liu S, Nie X. Comparison of orbscan II and ultrasound methods measuring corneal thickness and anterior chamber depth. Chinese Ophthalmic Res 2008;26:780-783.

3.    Al-Mohtaseb ZN, Wang L, Weikert MP. Repeatability and comparability of corneal thickness measurements obtained from Dual Scheimpflug Analyzer and from ultrasonic pachymetry. Graefes Arch Clin Exp Ophthalmol 2013;1-6.

4.    Cheng SM, Li Y, Huang JH, Zhou X, Xu L. Meta analysis of comparison of central corneal thickness measurement between Pentacam and A-scan in normal people. Chinese J Exp Ophthalmol 2013;31:172-176.

5.    Seyeddain O, Bachernegg A, Riha W, Rückl T, Reitsamer H, Grabner G, Dexl AK. Femtosecond laser-assisted small-aperture corneal inlay implantation for corneal compensation of presbyopia: Two-year follow-up. J Cataract Refract Surg 2013;39:234-241.

6.    Brautaset RL, Nilsson M, Miller WL, Leach NE, Tukler JH, Bergmanson JPG. Central and peripheral corneal thinning in keratoconus. Cornea 2013;32:257-261.

7.    Du XL, Chen M, Ma L, Wang XX, Xie LX. Comparison of Pentacam and Orbscan II systems for the diagnosis of keratoconus suspects. Chinese J Ophthalmol 2012;48:323-329.

8.    Elbaz U, Zadok D, Frenkel S, Pokroy R, Orucoglu F, Caspi Z, Landau D, Strassman E, Perry JF. Mathematical approximation of orbscan II central corneal thickness to contact ultrasound. Cornea 2012;

9.    Fares U, Otri AM, Al-Aqaba MA, Dua HS. Correlation of central and peripheral corneal thickness in healthy corneas. Cont Lens Anterior Eye 2012;35:39-45.

10.   Manassakorn A, Chaidaroon W. Effects of 0.5% tetracaine hydrochloride on central corneal thickness and intraocular pressure. Asian Biomed 2012;6:291-296.

11.   Ou TH, Lai IC, Teng MC. Comparison of central corneal thickness measurements by ultrasonic pachymetry, Orbscan II, and SP3000P in eyes with glaucoma or glaucoma suspect. Med J 2012;35:255-262.

12. Sanchis-Gimeno JA, Palanca-Sanfrancisco JM, García-Lázaro S, Madrid-Costa D, Cerviño A. The effect of anesthetic eye drop instillation on the distribution of corneal thickness. Cornea 2012;

13. Tummanapalli SS, Maseedupally V, Mandathara P, Rathi VM, Sangwan VS. Evaluation of corneal elevation and thickness indices in pellucid marginal degeneration and keratoconus. J Cataract Refract Surg 2013;39:56-65.

14. Barkana Y, Gerber Y, Elbaz U, Schwartz S, Ken-Dror G, Avni I, Zadok D. Central corneal thickness measurement with the Pentacam Scheimpflug system, optical low-coherence reflectometry pachymeter, and ultrasound pachymetry. J Cataract Refract Surg 2005;31:1729-1735.

15. Bourges JL, Alfonsi N, Laliberté JF, Chagnon M, Renard G, Legeais JM, Brunette I. Average 3-Dimensional Models for the Comparison of Orbscan II and Pentacam Pachymetry Maps in Normal Corneas. Ophthalmology 2009;116:2064-2071.

16. Agarwal T, Bhartiya S, Dada T, Panda A, Jhanji V, Yu M. Agreement of corneal thickness measurement using slitlamp and ultrasound pachymetry. Eye Contact Lens 2012;38:231-233.

17. Iyamu E, Iyamu JE, Amadasun G. Central corneal thickness and axial length in an adult Nigerian population. J Optom 2013;6:154-160

18. Al-Farhan HM, Al-Otaibi WM. Comparison of central corneal thickness measurements using ultrasound pachymetry, ultrasound biomicroscopy, and the Artemis-2 VHF scanner in normal eyes. Clin Ophthalmol 2012;6:1037-1043.

19. Iyamu E, Iyamu JE, Amadasun G. Central corneal thickness and axial length in an adult Nigerian population. J Optom 2013;6:154-160

20. Nemeth G, Hassan Z, Szalai E, Berta A, Modis Jr L. Anterior segment parameters measured with 2 optical devices compared to ultrasonic data. Eur J Ophthalmol 2013;23:177-182.

21. Thapa SS, Paudyal I, Khanal S, Paudel N, Mansberger SL, Van Rens GHMB. Central corneal thickness and intraocular pressure in a nepalese population: The bhaktapur glaucoma study. J Glaucoma 2012;21:481-485.

22. Bovelle R, Kaufman SC, Thompson HW, Hamano H. Corneal thickness measurements with the Topcon SP-2000P specular microscope and an ultrasound pachymeter. Arch Ophthalmol 1999;117:868-870.

23.  Lincoln VAC, Ventura L, Faria E Sousa SJ. Critical evaluation of the ultrasonic pachymetry for "in vitro" corneas. 2011.

24.  Whitacre MM, Stein RA, Hassanein K. The effect of corneal thickness on applanation tonometry. Am J Ophthalmol 1993;115:592-596.

25.  Garcia-Medina JJ, Garcia-Medina M, Garcia-Maturana C, Zanon-Moreno V, Pons-Vazquez S, Pinazo-Duran MD. Comparative study of central corneal thickness using fourier-domain optical coherence tomography versus ultrasound pachymetry in primary open-angle glaucoma. Cornea 2013;32:9-13.

26.  Hua YJ, Huang JH, Wang QM. Clinical meaning of corneal thickness and progress of corneal pachymetry. Int J Ophthalmol 2011;11:1376-1378.

27.  Huang J, Savini G, Hu L, Hoffer KJ, Lu W, Feng Y, Yang F, Hu X, Wang Q. Precision of a new Scheimpflug and Placido-disk analyzer in measuring corneal thickness and agreement with ultrasound pachymetry. J Cataract Refract Surg 2013;39:219-224.

28.  Jorge J, Rosado JL, Díaz-Rey JA, González-Méijome JM. Central corneal thickness and anterior chamber depth measurement by sirius® Scheimpfug tomography and ultrasound. Clin Ophthalmol 2013;7:417-422.

29.  Rao HL, Pahuja S, Murthy SI, Senthil S. Central corneal thickness measurement. Ophthalmology 2011;118:1010.

30.  Salz JJ, Azen SP, Berstein J, Caroline P, Villasenor RA, Schanzlin DJ. Evaluation and comparison of sources of variability in the measurement of corneal thickness with ultrasonic and optical pachymeters. Ophthalmic Surg 1983;14:750-754.

31.  Bechmann M, Thiel MJ, Neubauer AS, Ullrich S, Ludwig K, Kenyon KR, Ulbig MW. Central corneal thickness measurement with a retinal optical coherence tomography device versus standard ultrasonic pachymetry. Cornea 2001;20:50-54.

32.  Gordon A, Boggess EA, Molinari JF. Variability of ultrasonic pachometry. Optom Vis Sci 1990;67:162-165.

33.  Dutta D, Rao HL, Addepalli UK, Vaddavalli PK. Corneal Thickness in Keratoconus. Comparing Optical, Ultrasound, and Optical Coherence Tomography Pachymetry. Ophthalmology 2012;

34.  Reinstein DZ, Archer TJ, Gobbe M. Epithelial thickness up to 26 years after radial keratotomy: Three-dimensional display with artemis very high-frequency digital ultrasound. J Refract Surg 2011;27:618-624.

35.  Reinstein DZ, Archer TJ, Gobbe M, Silverman RH, Coleman DJ. Epithelial thickness in the normal cornea: Three-dimensional display with artemis very high-frequency digital ultrasound. J Refract Surg 2008;24:571-581.

36.  Li HF, Petroll WM, Møller-Pedersen T, Maurer JK, Cavanagh HD, Jester JV. Epithelial and corneal thickness measurements by in vivo confocal microscopy through focusing (CMTF). Curr Eye Res 1997;16:214-221.

37.  Sorbara L, Maram J, Fonn D, Woods C, Simpson T. Metrics of the normal cornea: Anterior segment imaging with the Visante OCT. Clin Expl Optom 2010;93:150-156.

38.  Piñero DP, Nieto JC, Lopez-Miguel A. Characterization of corneal structure in keratoconus. J Cataract Refract Surg 2012;38:2167-2183.

39.  Wells M, Wu N, Kokkinakis J, Sutton G. Correlation of central corneal thickness measurements using Topcon TRK-1P, Zeiss Visante AS-OCT and DGH Pachmate 55 handheld ultrasonic pachymeter. Clin Exp Optom 2013;

40.  Nam SM, Im CY, Lee HK, Kim EK, Kim TI, Seo KY. Accuracy of RTVue optical coherence tomography, Pentacam, and ultrasonic pachymetry for the measurement of central corneal thickness. Ophthalmology 2010;117:2096-103.

41.  Nasser CK, Singer R, Barkana Y, Zadok D, Avni I, Goldich Y. Repeatability of the sirius imaging system and agreement with the pentacam HR. J Refract Surg 2012;28:499-502.

42.  Oliveira CM, Ribeiro C, Franco S. Corneal imaging with slit-scanning and Scheimpflug imaging techniques. Clinical and Experimental Optometry 2011;94:33-42.

43.  Fercher AF, Drexler W, Hitzenberger CK, Lasser T. Optical coherence tomography - Principles and applications. Rep Prog Phys 2003;66:239-303.

44.  Boppart SA. Optical coherence tomography: Principles applications and advances. Minerva Biotecnol 2004;16:211-237.

45.  Mencucci R, Paladini I, Virgili G, Giacomelli G, Menchini U. Corneal thickness measurements using time-domain anterior segment OCT, ultrasound, and Scheimpflug tomographer pachymetry before and after corneal cross-linking for keratoconus. J Refract Surg 2012;28:562-6.

46.  Amato D, Lombardo M, Oddone F, Nubile M, Colabelli Gisoldi RAM, Villani CM, Yoo S, Parel JM, Pocobelli A. Evaluation of a new method for the measurement of

corneal thickness in eye bank posterior corneal lenticules using anterior segment optical coherence tomography. Br J Ophthalmol 2011;95:580-584.

47.    Ge L, Yuan Y, Shen M, Tao A, Wang J, Lu F. The role of axial resolution of optical coherence tomography on the measurement of corneal and epithelial thicknesses. Invest Ophthalmol Vis Sci 2013;54:746-755.

48.    Ursea R, Feng M, Urs R, RoyChoudhury A, Silverman RH. Comparison of Artemis 2 ultrasound and visante optical coherence tomography corneal thickness profiles. J Refract Surg 2013;29:36-41.

49.    Mohamed S, Lee GKY, Rao SK, Wong AL, Cheng ACK, Li EYM, Chi SCC, Lam DSC. Repeatability and reproducibility of pachymetric mapping with Visante Anterior Segment-Optical Coherence Tomography. Invest Ophthalmol Vis Sci 2007;48:5499-5504.

50.    Ahmadi Hosseini SM, Mohidin N, Abolbashari F, Mohd-Ali B, Santhirathelagan CT. Corneal thickness and volume in subclinical and clinical keratoconus. Int Ophthalmol 2012;9:9.

51.    Belin MW. Topography and Scheimpflug Imaging: pearls for refractive surgery screening and keratoconus detection. Cataract Retract Surg Today 2006;48-50.

52.    Amano S, Honda N, Amano Y, Yamagami S, Miyai T, Samejima T, Ogata M, Miyata K. Comparison of Central Corneal Thickness Measurements by Rotating Scheimpflug Camera, Ultrasonic Pachymetry, and Scanning-Slit Corneal Topography. Ophthalmology 2006;113:937-941.

53.    Lackner B, Schmidinger G, Skorpik C. Validity and repeatability of anterior chamber depth measurements with pentacam and orbscan. Optom Vis Sci 2005;82:858-861.

54.    Hao GS, Zeng L, Li YR, Shui D. Agreement and repeatability of central corneal thickness measurement using the Pentacam and ultrasound pachymetry. Chinese J Ophthalmol 2011;47:142-5.

55.    Huang J, Pesudovs K, Yu A, Wright T, Wen D, Li M, Yu Y, Wang Q. A comprehensive comparison of central corneal thickness measurement. Optom Vis Sci 2011;88:940-9.

56.    Lackner B, Schmidinger G, Pieh S, Funovics MA, Skorpik C. Repeatability and reproducibility of central corneal thickness measurement with Pentacam, Orbscan, and ultrasound. Optom Vis Sci 2005;82:892-9.

57. Modis L, Jr., Szalai E, Nemeth G, Berta A. Reliability of the corneal thickness measurements with the Pentacam HR imaging system and ultrasound pachymetry. Cornea 2011;30:561-6.

58. Montalbán R, Alió JL, Javaloy J, Piñero DP. Intrasubject repeatability in keratoconus-eye measurements obtained with a new Scheimpflug photography-based system. J Cataract Refract Surg 2013;39:211-218.

59. Oliveira CM, Ribeiro C, Franco S. Corneal imaging with slit-scanning and Scheimpflug imaging techniques. Clin Exp Optom 2011;94:33-42.

60. Miranda MA, Radhakrishnan H, O'Donnell C. Repeatability of corneal thickness measured using an oculus pentacam. Optom Vis Sci 2009;86:266-272.

61. Sedaghat MR, Daneshvar R, Kargozar A, Derakhshan A, Daraei M. Comparison of central corneal thickness measurement using ultrasonic pachymetry, rotating scheimpflug camera, and scanning-slit topography. Am J Ophthalmol 2010;150:780-789.

62. de Sanctis U, Missolungi A, Mutani B, Richiardi L, Grignolo FM. Reproducibility and Repeatability of Central Corneal Thickness Measurement in Keratoconus Using the Rotating Scheimpflug Camera and Ultrasound Pachymetry. Am J Ophthalmol 2007;144:712-718.e1.

63. Institution BS. Accuracy (trueness and Precision) of Measurement Methods and Results: Implementation of ISO 5725-1:1994. Part 1. General principles and definitions. BSI; 2000.

64. Leung DYL, Lam DKT, Yeung BYM, Lam DSC. Comparison between central corneal thickness measurements by ultrasound pachymetry and optical coherence tomography. Clin Exp Ophthalmol 2006;34:751-754.

65. Basmak H, Sahin A, Yildirim N. The reliability of central corneal thickness measurements by ultrasound and by Orbscan system in schoolchildren. Curr Eye Res 2006;31:569-575.

66. Li Y, Meisler DM, Tang M, Lu ATH, Thakrar V, Reiser BJ, Huang D. Keratoconus Diagnosis with Optical Coherence Tomography Pachymetry Mapping. Ophthalmology 2008;115:2159-2166.

67. Li Y, Shekhar R, Huang D. Corneal Pachymetry Mapping with High-speed Optical Coherence Tomography. Ophthalmology 2006;113:799.e1-799.e2.

68.     Li Y, Wei RH, Zhao SZ. Clinical characteristics and diagnosis of keratoconus. Int J Ophthalmol 2011;11:270-272.

69.     Büyük K, Bozkurt B, Kamiş Ü, Özkağnici A, Okudan S. Comparison of central corneal thickness measurements in normal and keratoconic eyes using ultrasonic pachymetry and OCULUS pentacam. Turk J Ophthalmol 2011;41:104-107.

70.     Prospero Ponce CM, Rocha KM, Smith SD, Krueger RR. Central and peripheral corneal thickness measured with optical coherence tomography, Scheimpflug imaging, and ultrasound pachymetry in normal, keratoconus-suspect, and post-laser in situ keratomileusis eyes. J Cataract Refract Surg 2009;35:1055-1062.

71.     Uçakhan OO, Çetinkor V, Özkan M, Kanpolat A. Evaluation of Scheimpflug imaging parameters in subclinical keratoconus, keratoconus, and normal eyes. J Cataract Refract Surg 2011;37:1116-1124.

72.     Ahmadi Hosseini SM, Mohidin N, Abolbashari F, Mohd-Ali B, Santhirathelagan CT. Corneal thickness and volume in subclinical and clinical keratoconus. Int Ophthalmol 2012;1-7.

73.     Li EYM, Mohamed S, Leung CKS, Rao SK, Cheng ACK, Cheung CYL, Lam DSC. Agreement among 3 Methods to Measure Corneal Thickness: Ultrasound Pachymetry, Orbscan II, and Visante Anterior Segment Optical Coherence Tomography. Ophthalmology 2007;114:1842-1847.e2.

74.     Wong ACM, Wong CC, Yuen NSY, Hui SP. Correlational study of central corneal thickness measurements on Hong Kong Chinese using optical coherence tomography, Orbscan and ultrasound pachymetry. Eye 2002;16:715-721.

75.     Ishibazawa A, Igarashi S, Hanada K, Nagaoka T, Ishiko S, Ito H, Yoshida A. Central corneal thickness measurements with fourier-domain optical coherence tomography versus ultrasonic pachymetry and rotating scheimpflug camera. Cornea 2011;30:615-619.

76.     Park SH, Choi SK, Lee D, Jun EJ, Kim JH. Corneal thickness measurement using orbscan, pentacam, galilei, and ultrasound in normal and post-femtosecond laser in situ keratomileusis eyes. Cornea 2012;31:978-982.

77.     Avitabile T, Marano F, Uva MG, Reibaldi A. Evaluation of central and peripheral corneal thickness with ultrasound biomicroscopy in normal and keratoconic eyes. Cornea 1997;16:639-644.

78.    Lam AK, Chen D. Pentacam pachometry: Comparison with non-contact specular microscopy on the central cornea and inter-session repeatability on the peripheral cornea. Clin Exp Optom 2007;90:108-114.

79.    Potvin RJ, Fonn D, Sorbara L. Comparison of polycarbonate and steel test surfaces for videokeratography. J Refract Surg 1995;11:89-91.

# References for Chapter 4

1.      González-Méijome JM, Jorge J, Queiros A, Almeida JB, Parafita MA. A comparison of the ARK-700A autokeratometer and Medmont E300 corneal topographer when measuring peripheral corneal curvature. Ophthalmic Physiol Opt 2004;24:391-398.

2.      Huang J, Pesudovs K, Yu A, Wright T, Wen D, Li M, Yu Y, Wang Q. A comprehensive comparison of central corneal thickness measurement. Optom Vis Sci 2011;88:940-949.

3.      Wang Q, Savini G, Hoffer KJ, Xu Z, Feng Y, Wen D, Hua Y, Yang F, Pan C, Huang J. A Comprehensive Assessment of the Precision and Agreement of Anterior Corneal Power Measurements Obtained Using 8 Different Devices. PLos One 2012;7:

4.      Jin H, Auffarth GU, Guo H, Zhao P. Corneal power estimation for intraocular lens power calculation after corneal laser refractive surgery in Chinese eyes. J Cataract Refract Surg 2012;38:1749-1757.

5.      Lee A, Qazi M, Pepose J. Biometry and intraocular lens power calculation. Curr Opin Ophthalmol. 2008;19:13-7.

6.      Sahin A, Hamrah P. Clinically relevant biometry. Curr Opin Ophthalmol 2012;23:47-53.

7.      Chastang PJ, Borderie VM, Carvajal-Gonzalez S, Rostène W, Laroche L. Automated keratoconus detection using the EyeSys videokeratoscope. J Cataract Refract Surg. 2000;26:675-683.

8.      Yebra-Pimentel E, Giráldez MJ, Arias FL, González J, González JM, Parafita MA, Febrero M. Rigid gas permeable contact lens and corneal topography. Ophthalmic Physiol Opt 2001;21:236-242.

9.      González-Méijome JM, González-Pérez J, Cerviño A, Yebra-Pimentel E, Parafita MA. Changes in corneal structure with continuous wear of high-Dk soft contact lenses: A pilot study. Optom Vis Sci 2003;80:440-446.

10.     Cho P, Lam AKC, Mountford J, Ng L. The performance of four different corneal topographers on normal human corneas and its impact on orthokeratology lens fitting. Optom Vis Sci. 2002;79:175-183.

11.     Srivannaboon S, Reinstein DZ, Sutton HFS, Holland SP. Accuracy of Orbscan total optical power maps in detecting refractive change after myopic laser in situ keratomileusis. J Cataract Refract Surg 1999;25:1596-1599.

12.     Wolffsohn JS, Safeen S, Shah S, Laiquzzaman M. Changes of corneal biomechanics with keratoconus. Cornea 2012;31:849-854.

13.     Carvalho LA, Stefani M, Romão AC, Carvalho L, De Castro JC, Tonissi Jr S, Schor P, Chamon W. Videokeratoscopes for dioptric power measurement during surgery. J Cataract Refract Surg. 2002;28:2006-2016.

14.     Read SA, Collins MJ, Iskander DR, Davis BA. Corneal topography with Scheimpflug imaging and videokeratography: Comparative study of normal eyes. J Cataract Refract Surg 2009;35:1072-1081.

15.     Chan B, Cho P, Mountford J. Relationship between corneal topographical changes and subjective myopic reduction in overnight orthokeratology: A retrospective study. Clin Exp Optom. 2010;93:237-242.

16.     Lu F, Simpson T, Sorbara L, Fonn D. Malleability of the ocular surface in response to mechanical stress induced by orthokeratology contact lenses. Cornea 2008;27:133-141.

17.     Lui WO, Edwards MH, Cho P. Contact lenses in myopia reduction - From orthofocus to accelerated orthokeratology. Cont Lens Anterior Eye 2000;23:68-76.

18.     Queirós A, González-Méijome JM, Jorge J, Villa-Collar C, Gutiérrez AR. Peripheral refraction in myopic patients after orthokeratology. Optom Vis Sci 2010;87:323-329.

19.     Soni PS, Nguyen TT, Bonanno JA. Overnight orthokeratology: Visual and corneal changes. Eye Contact Lens 2003;29:137-145.

20.     Sridharan R, Swarbrick H. Corneal response to short-term orthokeratology lens wear. Optom Vis Sci 2003;80:200-206.

21.     Tang W, Collins MJ, Carney L, Davis B. The accuracy and precision performance of four videokeratoscopes in measuring test surfaces. Optom Vis Sci 2000;77:483-491.

22.     Carvalho LA. Absolute accuracy of placido-based videokeratographs to measure the optical aberrations of the cornea. Optom Vis Sci. 2004;81:616-628.

23.     Courville CB, Smolek MK, Klyce SD. Contribution of the ocular surface to visual optics. Exp Eye Res. 2004;78:417-425.

24.     Chen D, Lam AKC. Reliability and repeatability of the Pentacam on corneal curvatures. Clin Exp Optom. 2009;92:110-118.

25. Keller PR, van Saarloos PP. Perspectives on corneal topography: a review of videokeratoscopy. Clin Exp Optom 1997;80:18-30.

26. Belin MW, Ratliff CD. Evaluating data acquisition and smoothing functions of currently available videokeratoscopes. J Cataract Refract Surg. 1996;22:421-426.

27. Markakis G, et al.,. Comparison of topographic technologies in anterior surface mapping of keratoconus using two display algorithms and six corneal topography devices. Int. J Kerat Ect Cor Dis 2012;1:153-157.

28. Roberts C. Analysis of the inherent error of the TMS-1 topographic modeling system in mapping a radially aspheric surface. Cornea 1995;14:258-265.

29. Franklin RJ, Morelande MR, Iskander DR, Collins MJ, Davis BA. Combining central and peripheral videokeratoscope maps to investigate total corneal topography. Eye Contact Lens 2006;32:27-32.

30. Wilson SE, Ambrosio R. Computerized corneal topography and its importance to wavefront technology. Cornea 2001;20:441-454.

31. Applegate RA, Nunez R, Buettner J, Howland HC. How accurately can videokeratographic systems measure surface elevation? Optom Vis Sci. 1995;72:785-792.

32. Mattioli R, Tripoli NK. Corneal geometry reconstruction with the Keratron videokeratographer. Optom Vis Sci 1997;74:881-894.

33. Tomidokoro A, Oshika T, Amano S, Higaki S, Maeda N, Miyata K. Changes in anterior and posterior corneal curvatures in keratoconus. Ophthalmology 2000;107:1328-1332.

34. McMahon TT, Anderson RJ, Joslin CE, Rosas GA. Precision of three topography instruments in keratoconus subjects. Optom Vis Sci 2001;78:599-604.

35. Greivenkamp JE, Mellinger MD, Snyder RW, Schwiegerling JT, Lowman AE, Miller JM. Comparison of three videokeratoscopes in measurement of toric test surfaces. J Refract Surg 1996;12:229-239.

36. Tripoli NK, Cohen KL, Holmgren DE, Coggins JM. Assessment of radial aspheres by the arc-step algorithm as implemented by the Keratron keratoscope. Am J Ophthalmol 1995;120:658-664.

37. Savini G, Carbonelli M, Sbreglia A, Barboni P, Deluigi G, Hoffer KJ. Comparison of anterior segment measurements by 3 Scheimpflug tomographers and 1 Placido corneal topographer. J Cataract Refract Surg 2011;37:1679-1685.

38. Oliveira CM, Ribeiro C, Franco S. Corneal imaging with slit-scanning and Scheimpflug imaging techniques. Clin Exp Optom 2011;94:33-42.

39. Li Y, Cheng SM, Yang X, Huang JH, Wang QM. Comparison of anterior chamber depth and central corneal thickness measuring values between Sirius and Pentacam. Chinese J Exp Ophthalmol 2012;30:262-265.

40. Feng MT, Belin MW, Ambrósio R, Grewal SPS, Yan W, Shaheen MS, McGhee C, Maeda N, Neuhann TH, Burkhard Dick H, Alageel SA, Steinmueller A. Anterior chamber depth in normal subjects by rotating scheimpflug imaging. Saudi J Ophthalmol. 2011;25:255-259.

41. Jia L, Li JK, Zhang C, Mi SJ, Duan YH. Measuring central corneal thickness and anterior chamber depth in myopia with Pentacam Scheimpflug imaging system. Int J Ophthalmol 2011;11:148-149.

42. Henriquez MA, Izquierdo Jr L, Mannis MJ. Intereye asymmetry detected by Scheimpflug imaging in subjects with normal corneas and keratoconus. Cornea 2012;

43. Omura T, Tanito M, Doi R, Ishida R, Ohira A. Anterior chamber parameters measured using the Pentacam Scheimpflug imaging device before and after cataract surgery in eyes with primary angle closure. Act Ophthalmol 2012;90:e654-e655.

44. Ahmadi Hosseini SM, Mohidin N, Abolbashari F, Mohd-Ali B, Santhirathelagan CT. Corneal thickness and volume in subclinical and clinical keratoconus. Int Ophthalmol. 2012;1-7.

45. Módis L, Szalai E, Németh G, Berta A. Reliability of the corneal thickness measurements with the pentacam HR imaging system and uiltrasound pachymetry. Cornea 2011;30:561-566.

46. Otchere H, Sorbara L, Jones, L. Repeatability and accuracy of the Oculus Pentacam HR® corneal topographer in measuring radius of curvature and shape factor. GSLS 2013;Abstract:

47. Swartz T, Marten L, Wang M. Measuring the cornea: The latest developments in corneal topography. Curr Opin Ophthalmol 2007;18:325-333.

48. Kawamorita T, Nakayama N, Uozato H. Repeatability and reproducibility of corneal curvature measurements using the Pentacam and Keratron topography systems. J Refract Surg 2009;25:539-544.

49. Amano S, Honda N, Amano Y, Yamagami S, Miyai T, Samejima T, Ogata M, Miyata K. Comparison of Central Corneal Thickness Measurements by Rotating Scheimpflug Camera, Ultrasonic Pachymetry, and Scanning-Slit Corneal Topography. Ophthalmology 2006;113:937-941.

50. Buehl W, Stojanac D, Sacu S, Drexler W, Findl O. Comparison of three methods of measuring corneal thickness and anterior chamber depth. Am J Ophthalmol 2006;141:7-12.e1.

51. Yazici AT, Bozkurt E, Alagoz C, Alagoz N, Pekel G, Kaya V, Yilmaz OF. Central corneal thickness, anterior chamber depth, and pupil diameter measurements using visante OCT, orbscan, and pentacam. J Refract Surg 2010;26:127-133.

52. Kawamorita T, Uozato H, Kamiya K, Bax L, Tsutsui K, Aizawa D, Shimizu K. Repeatability, reproducibility, and agreement characteristics of rotating Scheimpflug photography and scanning-slit corneal topography for corneal power measurement. J Cataract Refract Surg 2009;35:127-133.

53. Doors M, Cruysberg LPJ, Berendschot TTJM, Brabander J, Verbakel F, Webers CAB, Nuijts RMMA. Comparison of central corneal thickness and anterior chamber depth measurements using three imaging technologies in normal eyes and after phakic intraocular lens implantation. Graefes Arch Clin Exp Ophthalmol 2009;247:1139-1146.

54. Hall LA, Young G, Wolffsohn JS, Riley C. The influence of corneoscleral topography on soft contact lens fit. Invest Ophthalmol Vis Sci 2011;52:6801-6806.

55. Fink BA, Mitchell GL, Hill RM. Rigid gas-permeable contact lens base curve radius and transmissibility effects on corneal oxygen uptake. Optom Vis Sci 2006;83:740-744.

56. Jongsma FHM, De Brabander J, Hendrikse F, Stultiens BAT. Development of a wide field height eye topographer: Validation on models of the anterior eye surface. Optom Vis Sci 1998;75:69-77.

57. Lin MC, Chen YQ, Polse KA. The effects of ocular and lens parameters on the postlens tear thickness. Eye Contact Lens 2003;29:S33-36; discussion S57-59, S192-194.

58. Sorbara L, Luong J. Contact lens fitting guidelines for the keratoconic patient using videokeratographic data. Pract Optom 1999;10:238-243.

59.     Szczotka LB, Thomas J. Comparison of axial and instantaneous videokeratographic data in keratoconus and utility in contact lens curvature prediction. CLAO J 1998;24:22-28.

60.     Holmes-Higgin DK, Baker PC, Burris TE, Silvestrini TA. Characterization of the aspheric corneal surface with intrastromal corneal ring segments. J Refract Surg 1999;15:520-528.

61.     Klonos GG, Pallikaris J, Fitzke FW. A computer model for predicting image quality after photorefractive keratectomy. J Refract Surg 1996;12:S280-S284.

62.     Ortiz D, Anera RG, Saiz JM, Jiménez JR, Moreno F, Del Barco LJ, González F. Corneal changes induced by laser ablation: Study of the visual-quality evolution by a customized eye model. J Mod Opt 2006;53:1605-1618.

63.     Patel S, Marshall J, Fitzke Iii FW. Model for predicting the optical performance of the eye in refractive surgery. Refract Cor Surg 1993;9:366-375.

64.     Dorronsoro C, Remon L, Merayo-Lloves J, Marcos S. Experimental evaluation of optimized ablation patterns for laser refractive surgery. Opt Express 2009;17:15292-15307.

65.     Cerviño A, Gonzalez-Meijome JM, Ferrer-Blasco T, Garcia-Resua C, Montes-Mico R, Parafita M. Determination of corneal volume from anterior topography and topographic pachymetry: Application to healthy and keratoconic eyes. Ophthalmic and Physiol Opt. 2009;29:652-660.

66.     Karnowski K, Kaluzny BJ, Szkulmowski M, Gora M, Wojtkowski M. Corneal topography with high-speed swept source OCT in clinical examination. Biomed Opt Express 2011;2:2709-2720.

67.     Mutti DO, Mitchell GL, Sinnott LT, Jones-Jordan LA, Moeschberger ML, Cotter SA, Kleinstein RN, Manny RE, Twelker JD, Zadnik K. Corneal and crystalline lens dimensions before and after myopia onset. Optom Vis Sci 2012;89:251-262.

68.     Rodrigues EB, Johanson M, Penha FM. Anterior segment tomography with the cirrus optical coherence tomography. J Ophthalmol 2012;2012:

69.     Chan KY, Cheung SW, Cho P. Clinical performance of an orthokeratology lens fitted with the aid of a computer software in Chinese children. Cont Lens Anterior Eye 2012;35:180-184.

70. Gifford P, Alharbi A, Swarbrick HA. Corneal thickness changes in hyperopic orthokeratology measured by optical pachometry. Invest Ophthalmol Vis Sci 2011;52:3648-3653.

71. Kirkwood BJ, Rees IH. Central corneal iron line arising from hyperopic orthokeratology. Clin Exp Optom 2011;94:376-379.

72. Kojima T, Hasegawa A, Hara S, Horai R, Yoshida Y, Nakamura T, Dogru M, Ichikawa K. Quantitative evaluation of night vision and correlation of refractive and topographical parameters with glare after orthokeratology. Graefes Arch Clin Exp Ophthalmol 2011;249:1519-1526.

73. Lian Y, Shen M, Jiang J, Mao X, Lu P, Zhu D, Chen Q, Wang J, Lu F. Vertical and horizontal thickness profiles of the corneal epithelium and Bowman's layer after orthokeratology. Invest Ophthalmol Vis Sci 2013;54:691-696.

74. Ma W, Liao M, Jin HZ, Liu LQ. Evaluation of visual quality after overnight orthokeratology in pre-adolescent myopes. Chinese J Exp Ophthalmol 2012;30:1104-1109.

75. Nieto-Bona A, González-Mesa A, Nieto-Bona MP, Villa-Collar C, Lorente-Velázquez A. Short-term effects of overnight orthokeratology on corneal cell morphology and corneal thickness. Cornea 2011;30:646-654.

76. Özyol P, Uçakhan-Gündüz O, Özyol E, Kanpolat A. Overnight orthokeratology with two brands of reverse-geometry contact lenses. Cont Lens Anterior Eye 2012;

77. Yoon JH, Swarbrick HA. Posterior corneal shape changes in myopic overnight orthokeratology. Optom Vis Sci 2013;90:196-204.

78. Zhai Z, Yang X, Wang HR, Fang BL, Dai ZY, Wei L. The short-term effects of orthokeratologic lens on central and peripheral corneal thickness. Ophthalmol China 2012;21:376-380.

79. Miháltz K, Kovács I, Takács Á, Nagy ZZ. Evaluation of keratometric, pachymetric, and elevation parameters of keratoconic corneas with pentacam. Cornea 2009;28:976-980.

80. Modis L, Jr., Szalai E, Kolozsvari B, Nemeth G, Vajas A, Berta A. Keratometry evaluations with the Pentacam high resolution in comparison with the automated keratometry and conventional corneal topography. Cornea 2012;31:36-41.

81.   De Stefano VS, Junior LASM, Mallmann F, Schor P. Interchangeability between Placido disc and Scheimpflug system: Quantitative and qualitative analysis. Arq Bras Oftalmol 2010;73:363-366.

82.   McGhee C. Keratoconus: the arc of past, present and future. Clin Exp Optom. 2013 Mar;96(2):137-9. doi: 10.1111/cxo.12043

83.   Choi JA, Kim MS. Progression of keratoconus by longitudinal assessment with corneal topography. Invest Ophthalmol Vis Sci. 2012;53:927-935.

84.   Jones-Jordan LA, Walline JJ, Sinnott LT, Kymes SM, Zadnik K. Asymmetry in keratoconus and vision-related quality of life. Cornea 2013;32:267-272.

85.   McMahon TT, Edrington TB, Szczotka-Flynn L, Olafsson HE, Davis LJ, Schechtman KB, Zadnik K. Longitudinal changes in corneal curvature in keratoconus. Cornea 2006;25:296-305.

86.   Ambrósio Jr R, Klyce SD, Wilson SE. Corneal topographic and pachymetric screening of keratorefractive patients. J Refract Surg. 2003;19:24-29.

87.   Bilgihan K, Özdek SC, Konuk O, Akata F, Hasanreisoglu B. Results of photorefractive keratectomy in keratoconus suspects at 4 years. J Refract Surg. 2000;16:438-443.

88.   Nesburn AB, Bahri S, Salz J, Rabinowitz YS, Maguen E, Hofbauer J, Berlin M, Macy JI. Keratoconus detected by videokeratography in candidates for photorefractive keratectomy. J Refract Surg 1995;11:194-201.

89.   Agrawal VB. Characteristics of Keratoconus patients at a tertiary eye center in India. J Ophthalmic Vis Res. 2011;6:87-91.

90.   Baum J. On the location of the cone and the etiology of keratoconus. Cornea 1995;14:142-143.

91.   Ertan A, Kamburoglu G, Colin J. Location of steepest corneal area of cone in keratoconus stratified by age using Pentacam. J Refract Surg. 2009;25:1012-1016.

92.   Mahmoud AM, Roberts CJ, Lembach RG, Twa MD, Herderick EE, McMahon TT. CLMI: The cone location and magnitude index. Cornea 2008;27:480-487.

93.   McMahon TT, Robin JB, Scarpulla KM, Putz JL. The spectrum of topography found in keratoconus. CLAO J 1991;17:198-204.

94.     Nejabat M, Khalili MR, Dehghani C. Cone location and correction of keratoconus with rigid gas-permeable contact lenses. Cont Lens Anterior Eye 2012;35:17-21.

95.     Schwiegerling J. Cone dimensions in keratoconus using Zernike polynomials. Optom Vis Sci 1997;74:963-969.

96.     Tan B, Baker K, Chen YL, Lewis JWL, Shi L, Swartz T, Wang M. How keratoconus influences optical performance of the eye. J Vis 2008;8:

97.     Tang M, Shekhar R, Huang D. Mean curvature mapping for detection of corneal shape abnormality. IEEE Trans Med Imaging 2005;24:424-428.

98.     González-Méijome JM, Queirós A, Jorge J, Fernandes P, Cerviño A, De Almeida JB. External factors affecting data acquisition during corneal topography examination. Eye Contact Lens 2007;33:91-97.

99.     Shankar H, Taranath D, Santhirathelagan CT, Pesudovs K. Anterior segment biometry with the Pentacam: Comprehensive assessment of repeatability of automated measurements. J Cataract Refract Surg 2008;34:103-113.

100.    Salmon TO, Horner DG. Comparison of elevation, curvature, and power descriptors for corneal topographic mapping. Optom Vis Sci 1995;72:800-808.

**References for Chapter 5**

1.      Tan DTH, Pullum KW, Buckley RJ. Medical applications of scleral contact lenses: 2. Gas-permeable scleral contact lenses. Cornea 1995;14:130-137.

2.      Severinsky B, Millodot M. Current applications and efficacy of scleral contact lenses - A retrospective study. J Optom 2010;3:158-163.

3.      Schornack MM, Patel SV. Scleral lenses in the management of keratoconus. Eye Contact Lens 2010;36:39-44.

4.      Dalton K, Sorbara L. Fitting an MSD (Mini Scleral Design) rigid contact lens in advanced keratoconus with INTACS. Cont Lens Anterior Eye 2011;34:274-281.

5.      Pullum KW, Whiting MA, Buckley RJ. Scleral contact lenses: The expanding role. Cornea 2005;24:269-277.

6.      Barnett M, Mannis MJ. Contact lenses in the management of keratoconus. Cornea 2011;30:1510-1516.

7.      Jhanji V, Sharma N, Vajpayee RB. Management of keratoconus: Current scenario. Br J Ophthalmol 2011;95:1044-1050.

8.      Gould HL. Management of keratoconus with corneal and scleral lenses. Am J Ophthalmol 1970;70:624-629.

9.      Jinabhai A, Radhakrishnan H, O'Donnell C. Pellucid corneal marginal degeneration: A review. Cont Lens Anterior Eye 2011;34:56-63.

10.     Visser ES, Visser R, Van Lier HJJ, Otten HM. Modern scleral lenses part I: Clinical features. Eye Contact Lens 2007;33:13-20.

11.     Schornack MM, Baratz KH, Patel SV, Maguire LJ. Jupiter scleral lenses in the management of chronic graft versus host disease. Eye Contact Lens 2008;34:302-305.

12.     Tappin MJ, Pullum KW, Buckley RJ. Scleral contact lenses for overnight wear in the management of ocular surface disorders. Eye 2001;15:168-172.

13.     Smiddy WE, Hamburg TR, Kracher GP, Gottsch JD, Stark WJ. Therapeutic contact lenses. Ophthalmology 1990;97:291-295.

14.     Foss AJE, Trodd TC, Dart JKG. Current indications for scleral contact lenses. CLAO J 1994;20:115-118.

15. Pullum KW, Buckley RJ. A study of 530 patients referred for rigid gas permeable scleral contact lens assessment. Cornea 1997;16:612-622.

16. Tan DTH, Pullum KW, Buckley RJ. Medical applications of scleral contact lenses: 1. A retrospective analysis of 343 cases. Cornea 1995;14:121-129.

17. Kok JHC, Visser R. Treatment of Ocular Surface Disorders and Dry Eyes with High Gas-Permeable Scleral Lenses. Cornea 1992;11:518-522.

18. Sorbara L MJ, Mueller K. Use of the Visante™ OCT anterior segment image to measure the saggital depth of keratoconus corneae compared to normal's at a 15mm chord length. Bri Contact Lens Assoc 2011;

19. Sorbara L, Maram J, Fonn D, Woods C, Simpson T. Metrics of the normal cornea: Anterior segment imaging with the Visante OCT. Clin Exp Optom 2010;93:150-156.

20. Stephen, P.B: A simple technique to measure the sagittal depth of a scleral GP contact lens, in GSLS. 2012: Las Vegas NV.

21. Shneor E, Millodot M, Blumberg S, Ortenberg I, Behrman S, Gordon-Shaag A. Characteristics of 244 patients with keratoconus seen in an optometric contact lens practice. Clin Exp Optom 2012;

22. Michaud L. Modern designs of contact lenses as a way to improve vision of keratoconus and pellucid marginal degeneration (PMD) patients. Optometry 2009;80:295.

23. Michaud L, van der Worp E, Brazeau D, Warde R, Giasson CJ. Predicting estimates of oxygen transmissibility for scleral lenses. Cont Lens Anterior Eye 2012;35:266-271.

24. Gemoules G. A novel method of fitting scleral lenses using high resolution optical coherence tomography. Eye Contact Lens 2008;34:80-83.

25. Schornack MM, Patel SV. Relationship between corneal topographic indices and scleral lens base curve. Eye Contact Lens 2010;36:330-333.

26. Segal O, Barkana Y, Hourovitz D, Behrman S, Kamun Y, Avni I, Zadok D. Scleral contact lenses may help where other modalities fail. Cornea 2003;22:308-310.

27. Visser ES, Visser R, Van Lier HJJ, Otten HM. Modern scleral lenses part II: Patient satisfaction. Eye Contact Lens 2007;33:21-25.

28. Jackson WB. Management of dysfunctional tear syndrome: A Canadian consensus. Canadian Journal of Ophthalmology 2009;44:385-394.

29.    Jacobs DS. Update on scleral lenses. Curr Opin Ophthalmol 2008;19:298-301.

30.    Schornack MM. Limbal stem cell disease: Management with scleral lenses. Clin Exp Optom 2011;94:592-594.

31.    Bamrolia NR, Arora R, Yadava U. Unusual presentation of a case of Sjogren's syndrome with neurological and ocular manifestation. Cont Lens Anterior Eye 2012;35:85-88.

32.    Schornack MM, Baratz KH. Ocular cicatricial pemphigoid: the role of scleral lenses in disease management. Cornea 2009;28:1170-1172.

33.    Tanhehco T, Jacobs DS. Technological advances shaping scleral lenses: The boston ocular surface prosthesis in patients with glaucoma tubes and trabeculectomies. Semin Ophthalmology 2010;25:233-238.

34.    Organization IS. Ophthalmic optics–Contact lenses and contact lens care products-Guidance for clinical investigations. 1997.

35.    Caroline, P et al. Scleral lens settling. Contact Lens Spectrum May 2012;27:56.

36.    Mountford, J. Scleral lens settling. Contact Lens Spectrum 2012;27:56.

# References for Chapter 6

1.      Otchere H, Sorbara L, Jones L. Repeatability and accuracy of the Oculus Pentacam HR® corneal topographer in measuring radius of curvature and shape factor. Global specialty lens symposium 2013;Abstract

2.      Kawamorita T, Nakayama N, Uozato H. Repeatability and reproducibility of corneal curvature measurements using the Pentacam and Keratron topography systems. Journal of Refractive Surgery 2009;25:539-544.

3.      Lackner B, Schmidinger G, Pieh S, Funovics MA, Skorpik C. Repeatability and reproducibility of central corneal thickness measurement with pentacam, orbscan, and ultrasound. Optometry and Vision Science 2005;82:892-899.

4.      O'Donnell C, Maldonado-Codina C. Agreement and repeatability of central thickness measurement in normal corneas using ultrasound pachymetry and the OCULUS Pentacam. Cornea 2005;24:920-4.

5.      de Sanctis U, Missolungi A, Mutani B, Richiardi L, Grignolo FM. Reproducibility and Repeatability of Central Corneal Thickness Measurement in Keratoconus Using the Rotating Scheimpflug Camera and Ultrasound Pachymetry. Am J Ophthalmol. 2007;144:712-718.e1.

6.      Doors M, Cruysberg LPJ, Berendschot TTJM, Brabander J, Verbakel F, Webers CAB, Nuijts RMMA. Comparison of central corneal thickness and anterior chamber depth measurements using three imaging technologies in normal eyes and after phakic intraocular lens implantation. Graefes Arch Clin Exp Ophthalmol 2009;247:1139-1146.

7.      Ho T, Cheng ACK, Rao SK, Lau S, Leung CKS, Lam DSC. Central corneal thickness measurements using Orbscan II, Visante, ultrasound, and Pentacam pachymetry after laser in situ keratomileusis for myopia. J Cataract Refract Surg 2007;33:1177-1182.

8.      Uçakhan OO, Çetinkor V, Özkan M, Kanpolat A. Evaluation of Scheimpflug imaging parameters in subclinical keratoconus, keratoconus, and normal eyes. J Cataract Refract Surg 2011;37:1116-1124.

9.      Sedaghat MR, Daneshvar R, Kargozar A, Derakhshan A, Daraei M. Comparison of central corneal thickness measurement using ultrasonic pachymetry, rotating scheimpflug camera, and scanning-slit topography. Am J Ophthalmol 2010;150:780-789.

10.     Al-Mezaine HS, Al-Amro SA, Kangave D, Al-Obeidan S, Al-Jubair KM. Comparison of central corneal thickness measurements using Pentacam and ultrasonic pachymetry in post-LASIK eyes for myopia. Euro J Ophthalmol. 2010;20:852-857.

11. Ciolino JB, Khachikian SS, Belin MW. Comparison of corneal thickness measurements by ultrasound and Scheimpflug photography in eyes that have undergone laser in situ keratomileusis. Am J Ophthalmol. 2008;145:75-80.e2.

12. Read SA, Collins MJ, Iskander DR, Davis BA. Corneal topography with Scheimpflug imaging and videokeratography: Comparative study of normal eyes. J Cataract Refract Surg 2009;35:1072-1081.

13. Mattioli R, Tripoli NK. Corneal geometry reconstruction with the Keratron videokeratographer. Optom Vis Sci 1997;74:881-894.

14. Chen D, Lam AKC. Reliability and repeatability of the Pentacam on corneal curvatures. Clin Exp Optom. 2009;92:110-118.

15. Hara S, Kojima T, Dogru M, Uchino Y, Goto E, Matsumoto Y, Kawakita T, Tsubota K, Shimazaki J. The impact of tear functions on visual outcome following keratoplasty in eyes with keratoconus. Graefes Arch Clin Exp Ophthalmol 2013;1-8.

16. Vanathi M. Keratoconus: Prevalence and associations. Expert Rev Ophthalmol 2012;7:529-531.

17. De Paiva CS, Harris LD, Pflugfelder SC. Keratoconus-like topographic changes in keratoconjunctivitis sicca. Cornea 2003;22:22-24.

18. Dogru M, Karakaya H, Özçetin H, Ertürk H, Yücel A, Özmen A, Baykara M, Tsubota K. Tear function and ocular surface changes in keratoconus. Ophthalmology 2003;110:1110-1118.

19. Roberts C. Analysis of the inherent error of the TMS-1 topographic modeling system in mapping a radially aspheric surface. Cornea 1995;14:258-265.

20. Shankar H, Taranath D, Santhirathelagan CT, Pesudovs K. Anterior segment biometry with the Pentacam: Comprehensive assessment of repeatability of automated measurements. J Cataract Refract Surg 2008;34:103-113.

21. Salmon TO, Horner DG. Comparison of elevation, curvature, and power descriptors for corneal topographic mapping. Optometry and Vision Science 1995;72:800-808.

22. Sorbara L MJ, Mueller K. Use of the Visante™ OCT anterior segment image to measure the saggital depth of keratoconus corneae compared to normal's at a 15mm chord length. Bri Contact Lens Assoc 2011;

23.     Vanathi M, Bypareddy R, Panda A. Corneal collagen crosslinking using UVA light and riboflavin for keratoconus. Expert Rev Ophthalmol 2012;7:33-44.

24.     Jinabhai A, Radhakrishnan H, O'Donnell C. Pellucid corneal marginal degeneration: A review. Cont Lens Anterior Eye 2011;34:56-63.

25.     Dalton K, Sorbara L. Fitting an MSD (Mini Scleral Design) rigid contact lens in advanced keratoconus with INTACS. Cont Lens Anterior Eye 2011;34:274-281.

26.     Schornack MM, Patel SV. Relationship between corneal topographic indices and scleral lens base curve. Eye Contact Lens 2010;36:330-333.

27.     Hostetter TA. Learning the "numbers game" of today's contact lens fitting: clinical and business pearls. J Ophthalmic Nurs Technol 1996;15:148-152.

28.     Caroline, P, J, et, al. Scleral lens settling. Contact Lens Spectrum 2012;27.

29.     Visser ES, Visser R, Van Lier HJJ, Otten HM. Modern scleral lenses part II: Patient satisfaction. Eye Contact Lens 2007;33:21-25.